Hybrid inorganic – organic membranes: Tuning pore properties by sequential grafting

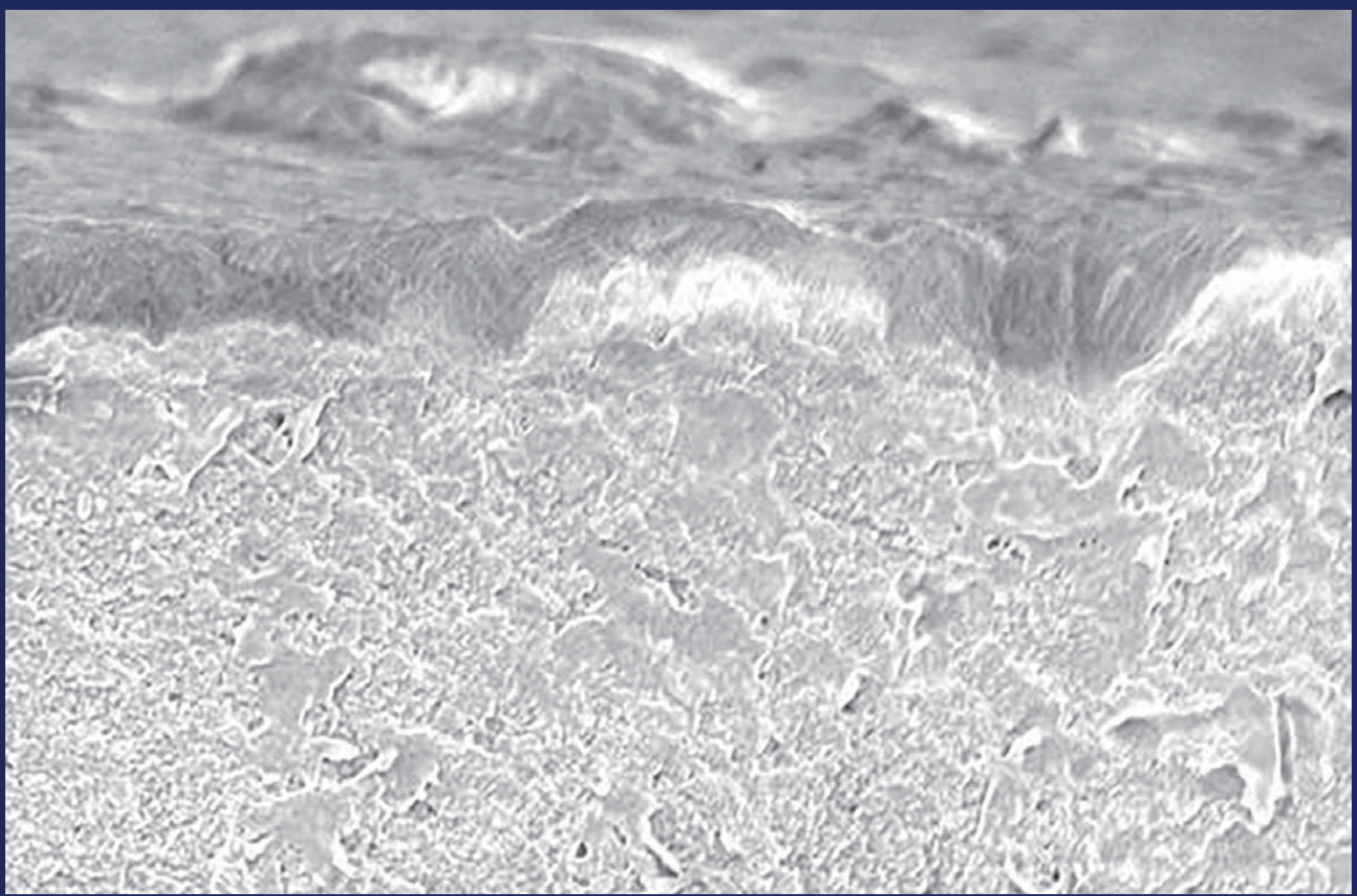

V.G.P. Sripathi

Hybrid inorganic - organic membranes: Tuning pore properties by sequential grafting

This is an Institute for Sustainable Process Technology (ISPT) project

Promotion committee

Prof. Dr. Ir. A. Nijmeijer (promotor)	University of Twente
Prof. Dr. Ir. N.E. Benes (co-promotor)	University of Twente
Prof. Dr. Ir. J.W.M. Hilgenkamp (chairperson)	University of Twente
Prof. Dr. Ir. R.G.H. Lammertink	University of Twente
Prof. Dr. Ir. D.C. Nijmeijer	University of Twente
Prof. Dr. Ir. E.J.M. Hensen	Eindhoven University of Technology
Dr. Ir. J.F. Vente	Energy Research Centre of the Netherlands
Prof. Dr. S.R.A. Kersten	University of Twente

Hybrid inorganic – organic membranes: Tuning pore properties by sequential grafting

PhD thesis, University of Twente, The Netherlands

ISBN: 978-90-365-3747-6

DOI: 10.3990/1.9789036537476

URL: http://dx.doi.org/10.3990/1.9789036537476

Printed by Gildeprint Drukkerijen, Enschede, The Netherlands

© 2014 Venkata Giri Prasad Sripathi, Enschede, The Netherlands

HYBRID INORGANIC – ORGANIC MEMBRANES: TUNING PORE PROPERTIES BY SEQUENTIAL GRAFTING

DISSERTATION

to obtain

the degree of doctor at the University of Twente,

on the authority of the rector magnificus,

Prof. Dr. H. Brinksma,

on account of the decision of the graduation committee,

to be publicly defended on

Thursday the 16th of October, 2014, at 16:45

by

Venkata Giri Prasad Sripathi

born on August 1st , 1980

in Boenpally, India

This dissertation has been approved by:

Prof. Dr. Ir. A. Nijmeijer (promotor)

Prof. Dr. Ir. N.E. Benes (co-promotor)

To my son, wife and parents

Contents

1

General Introduction

This chapter gives an introduction into Membrane Science and Technology. General concepts are introduced and discussed within the context of developing hybrid membranes by post-synthetic grafting for CO_2/CH_4 gas separation. Finally, the aim and outline of this thesis are presented.

1.1 Introduction

Separation of species from a gas mixture is a key issue in various industrial fields. Examples include: hydrogen recovery in petroleum refinery processes, oxygen recovery from air, carbon dioxide (*1-5*) from natural gas, and hydrogen sulfide separation in a desulphurisation process. Traditional technologies, such as pressure swing adsorption (PSA), solvent absorption, and cryogenic distillation, are well established for gas separation. However, in the past four decades, membrane based gas separation processes have been rapidly adopted by the industry, because of their advantages over conventional separation processes (*1, 4*). Membrane separation processes generally consume a relatively low amount of energy compared to distillation, and absorption or adsorption processes. The concept of membrane based gas separation was originally proposed by Thomas Graham in 1866 (*1*). Large scale industrial applications were only established after Loeb and Sourirajan developed a method for the fabrication of asymmetric membranes in 1961 (*1, 4*). Currently, membrane gas separation is utilized worldwide on industrial scale for hydrogen recovery from ammonia purge streams, air separation (>99.5 % nitrogen production and oxygen enrichment), hydrocarbon/light gas separation, CO_2 removal from natural gas and hydrogen from various refinery streams (e.g. fuel gas) (*2, 4-9*). Particularly in natural gas processing, the composition of raw natural gas can vary considerably, depending on the reservoir source. Generally raw natural gas is composed of methane, along with other hydrocarbons, such as ethane, propane and heavier hydrocarbons (*1, 4*). In addition, natural gas can contain water, carbon dioxide, hydrogen sulfide, helium and nitrogen, in varying

concentrations (*10*). It is necessary to process raw natural gas to meet pipeline specifications and regulatory standards on calorific value.

1.1.1 Membrane technology

A membrane can be defined as a semi permeable barrier between two phases that are not in thermodynamic equilibrium. The membrane distinctly influences the transport rates of different species, hence allowing molecular separation. Membranes are widespread in biological systems where they control the transport of various components in and out of living cells. Such membranes are generally referred to as biological membranes. In this thesis focus is on synthetic or artificial membranes, i.e., not of natural origin.

Artificial membranes are applied in life sciences, for instance haemodialysis (*11, 12*), as well as in various industries, including the oil and gas industry (*13, 14*) pharmaceutical industry (*15*), chemical industry (*16*) and water treatment (*17, 18*). Most of the industrial applications are energy and environmentally related, and often membranes are applied in combination with conventional separation technologies. In this thesis the focus is on membranes for gas separation, in particular for the separation of carbon dioxide from light gases. Membranes for gas separation can be classified in many ways. A common distinction is based on the materials the membranes consist of: organic and/or inorganic membranes. Organic membranes can consist of a variety of polymers. Inorganic membranes include ceramic membranes and metal membranes. Hybrid membranes combine organic and inorganic materials in a single membrane material, as can be seen in the schematic representation in Figure 1. In this thesis, a brief description is given about polymeric membranes and

inorganic membranes, but the main focus is on the synthesis of novel hybrid membranes by sequential grafting of organic species inside a porous ceramic material. This approach allows length-scale confinement of organic species within the nano-scale pores, which will further reduce the tendency for swelling and plasticization.

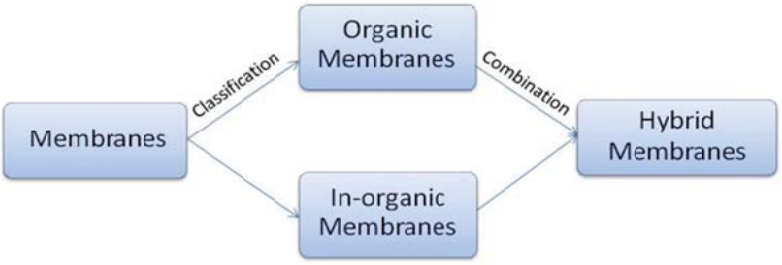

Figure 1: Schematic representation showing an overview of types of membranes.

1.1.2 Organic membranes

Organic membranes typically consist of polymers and have been proven successful in many industrial applications (*11-13, 15*). The versatile chemistry and ease of processing of organic polymers are auspicious for optimizing membranes. In addition, organic polymers and their derived membrane technology are relatively inexpensive. Drawbacks of organic membranes include their limited thermal, mechanical, and chemical stability. The limited stability prohibits application of organic membranes at elevated temperatures, in chemically demanding environments, and at elevated pressures. In high-pressure applications organic membranes can exhibit swelling and plasticization, amplifying the transport rates of all species and hence reducing molecular selectivity. For more information the interested reader is referred to (*19, 20*). Particularly in CO_2/CH_4 separation, many types of polymers have been considered as membrane materials, such as polyamides, polyimides,

polyacetylenes, polycarbonates, poly(phenylene oxides), poly(ethylene oxides) and polysulfones.

Plasticization occurs when the CO_2 concentration in the polymer is high enough to drastically increase mobility of polymer segments (*19, 21-23*). As a result polymeric membranes lose their separation efficiency by allowing all components of the gaseous mixture to pass the membrane. Although many research groups have reported extensively about the plasticization phenomena in literature (*3, 20-40*), it seems hard to identify a fundamental definition of plasticization. Previous studies (*23, 35*) indicated that, at low pressures of CO_2 (purity: >99.99%), most glassy polymers show a decrease in permeability with increasing pressure, followed by an increase in permeance at higher pressures. The pressure corresponding to the minimum in permeance versus pressure is often referred to as plasticization pressure, as shown in Figure 2. Bos *et al*. (*23*) reported a fundamental investigation on relationships between plasticization pressure of pure (>99.99%) CO_2 and chemical structure of the polymer, with a series of 11 glassy polymers. Polysulfone (PSF), polyethersulfone (PES) and polyetherimide (PEI) exhibited plasticization pressures as high as 34, 27 and 28 bar respectively, at 22±1 ^{o}C. Zhang and Handa *et al*. (*41*) reported plasticization of polymers at high pressure by an in-situ high pressure differential scanning calorimetric (DSC) technique. They found that thicker samples (>200 µm) showed a relatively broad transition in glass transition temperature (T_g) compared to thin samples with a thickness of 100 – 200 µm. Several attempts have been conducted to develop plasticization resistant polymeric membranes by several approaches for polymer modification, such as covalent cross-linking with different types of polymeric segments (*3,*

29, 30, 32-34, 42-51), cross-linking by diamino compounds (*52, 53*), co-polymerization (*54, 55*), annealing or heat treatment (*21, 34, 56*), surface modification by plasma treatment (*57*), polymer blending (*21, 55, 58, 59*), mixed matrix membranes (*53, 60*), and grafting of the polymer backbone (*61-63*). In this thesis we propose a novel approach to reduce the plasticization, by confining the organic monomers or oligomers inside a meso-porous γ-alumina structure by covalent grafting. Length-scale confinement of covalently cross-linked oligomeric/polymeric segments inside the pores of the rigid ceramic support potentially limit the movement of polymeric segments, at conditions where organic membranes undergo plasticization.

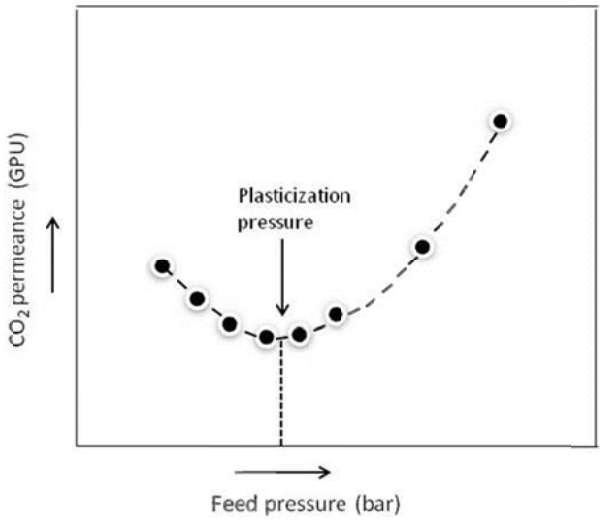

Figure 2: Schematic representation showing general trend for CO_2 induced plasticization as a function of feed pressure, considering pure CO_2.

1.1.3 Inorganic membranes

Compared to organic membranes, inorganic membranes have superior thermo-chemical stability. They do not decompose at elevated temperatures and are not prone to swelling and plasticization. Inorganic materials, used for fabrication of membranes, include ceramics and metals. Ceramic membranes are predominantly metal oxides and can be porous as well as dense. Dense ceramic membranes include for instance ion conducting perovskites for high temperature removal of oxygen (*64*). Metal membranes include palladium alloys, and typically are used for very selective separation of hydrogen. These membranes are already applied at pilot plant scale (*65*).

Porous inorganic membranes can be micro porous (pore size < 2 nm) meso porous (2 < pore size <50 nm) and macro porous (pore size >50 nm) (*66, 67*). Micro-porous membranes allow separation of gases based on the molecular size. To allow permeation at an appreciable rate, very thin micro-porous layers (~10^{-7} m) are required. To provide mechanical strength to such thin layers, they are often supported on a stack of macro-porous and meso-porous layers. Micro-porous membranes are further subdivided in to crystalline (e.g. zeolites (*68-70*)) and amorphous (e.g., silica (*71*)).

Several procedures have been proposed for the fabrication of silica membranes: the most important are the sol-gel technique (*72-74*) and chemical vapor deposition (*75, 76*). In the past decades, sol-gel derived micro-porous silica membranes have been studied extensively for hydrogen separation. The motivation for this involves the mild and adaptive synthesis conditions, and the availability of different types of inorganic precursors (*77*). The

combination of small pore size and minute thickness of these membranes allows for high fluxes for small molecules like hydrogen and helium, and high selectivity for these molecules with respect to larger gas molecules such as sulphur hexafluoride and hydrocarbons (*77*). Main drawbacks of silica-based membranes are related to their limited hydro-thermal stability.

1.1.4 Hybrid membranes

1.1.4.1 Sol-gel derived organo-silica membranes

To improve hydrothermal stability, studies have been aimed at fabrication of hybrid organic-inorganic membranes. De Vos *et al.* (*73*) synthesized hybrid silica membranes by incorporating methyl triethoxysilane (MTES) into a tetraethyl orthosilicate (TEOS) sol during sol preparation, aiming at a porous silica structure with "methyl" groups replacing part of the surface hydroxyl groups. Castricum *et al*. reported on bis(triethoxy)silane (BTESE) – MTES microporous membranes by replacing TEOS with BTESE (*78*). In the dehydration of alcohol by pervaporation, the BTESE-MTES membranes showed stable water permeation at 150 ^{o}C, up to 500 days, whereas methylated silica membranes showed declined performance after 50 days at 95 ^{o}C. These observations indicate a superior hydrothermal stability of the membranes containing alkyl groups within the chains of the inorganic polymer, as compared to the state-of-the-art silica and methylated silica microporous membranes. In subsequent work, Castricum *et al*. synthesized various hybrid organic – inorganic HybSi membranes by introducing different organic fragment or bridge in the silica network, by using "bridged silsesquioxane" precursors. Authors adjusted the size, flexibility,

shape and electronic structure of the organic fragment or bridging group (*78-82*). Membranes comprising short alkylene (CH_2/C_2H_4) bridging groups showed H_2/N_2 permeance ratios of about 16, at 250 ^oC, suggesting selectivity is based on difference in the mobility of the gases. Membranes with longer alkylene (C_8H_{16}) and aryl bridges showed CO_2/H_2 permeation ratios around 5, at 50 ^oC. Here, the selectivity for the large molecule (in this case CO_2) cannot be due to diffusion selectivity; it originates from solubility selectivity.

In recent attempts, a new class of membranes has been synthesized by introducing organic functional groups in the porous structure. These functional groups are intended to have affinity for one or more components of the mixture that must be separated. Paradis *et al.* (*83*) reported amino functionalized BTESE membranes, obtained by incorporating amine functionalized precursors in the BTESE during sol preparation. These membranes show increased adsorption of water molecules with increasing concentration of amino-functional groups. Other strategies have focused on so-called metal organic frameworks; for more information the interested reader is referred to reviews by Caro *et al*. (*7, 8, 84, 85*) and Gascon *et al*. (*86, 87*).

1.1.4.2 Post-synthetic grafting

Although versatile, sol-gel chemistry has limitations for the synthesis of functionalized inorganic – organic hybrid membranes. The composition of the sol not only dictates the materials chemistry of the derived membranes, it also affects too a large extent the pore morphology. A promising alternative approach for synthesizing hybrid inorganic – organic membranes is “post-synthetic grafting”. In this approach inorganic porous membranes or

powders are synthesized and, subsequently, their pore surface is functionalized with selected organic species.

The surface chemistry of porous inorganic membranes can be modified via a reaction of surface chemical groups with organic precursors. The result is that the pore surface is covered with covalently attached organic molecules. This approach allows tuning of the pore morphology and of the pore surface chemistry, in a controlled manner. Various precursors are available for functionalization. Functional silanes have been used for depositing functional groups onto inorganic materials, because of the stable covalent bond formation between the hydrolysable groups (for instace an alkoxy- or chloro- group) of the functional silane and the hydroxyl groups located on the inorganic materials surface (*88-96*). However, functional silanes are highly sensitive to moisture (*89, 91, 97-104*). Their hydrolysable groups undergo self-condensation in presence of water. This occurs even in the presence of traces of water in the solvent, or due to humidity in the atmosphere.

The moisture sensitivity of silanes makes their controlled use very challenging. Various covalently attached organic structures can be produced, depending on the reaction conditions (temperature, reaction time), the nature of the functional silanes (number of hydrolysable groups, alkyl chain length), and the chemistry of the pore surface. The chemistry of silanization reactions is illustrated in Figure 3. Formation of only one single bond is possible if the functional silane contains only one single hydrolysable group (R_3SiX; X= OR, Cl), i.e., reaction I in Figure 3. Surface functionalization with such silanes requires a longer reaction time. Wettability studies of silicon wafers, grafted with silanes with for

instance alkyldimethylchlorosilane, showed a non-homogeneous and incomplete monolayer formation (*88*). Long reaction times (several hours to days) are necessary to achieve maximum surface coverage with monofunctional silanes (*96*). Typically, for these systems the kinetics of the grafting reaction slow down in the later stages of the surface functionalization (~after 1 hour). This is a result of a reducing number of available reactive groups on the surface, as the reaction progresses. This is in contrast to functionalization with silanes containing two or three hydrolysable groups (e.g., alkyltrichlorosilanes). During grafting with such precursors self-assembly can occur, allowing for enhanced surface coverage (*88, 96*).

In the case of difunctional silanes, siloxy bond formation with the surface hydroxyl groups is accompanied by condensation of hydrolysable groups of adjacent silane molecules. This is referred to as vertical oligomerization, and is depicted in Figure 3, reaction II (*96*). Oligomerization of surface attached silanes is also observed for trifunctional silanes. For these precursors two free hydrolysable groups remain after attachment to the surface. These remaining groups can react with other surface hydroxyl goups, but also with other precursor molecule. This allows horizontal and vertical oligomerization, in particular in the presence of water. Resulting structures can vary from randomly connected polymers to a chain like self-assembled structures, as is shown in reaction III in Figure 3 (*88, 96*). Silanes with three hydrolysable groups react much faster as compared to their analogues with less condensable groups. This makes their use for controlled grafting, permitting controlled morphology and chemistry of the grafted layer, more challenging.

The morphology of surface layer, obtained via grafting, is strongly dependent on the chosen reaction conditions, including the selected solvent, the reaction temperature, the type and number of hydrolysable groups, the length of alkyl chain, the reaction time, and the water activity. McGovern *et al*. (*89*) investigated the influence of solvents used for deposition of octadecyltrichlorosilane (OTS) on a glass surface. The authors proposed a new approach, involving the extraction of the moisture present on the substrate surface into the bulk solvent, followed by OTS hydrolysis and deposition on the substrate surface. Solvents with a high capacity for mixing with water, for instance 1-4 dioxane, are not preferable for generating self-assembled monolayers (SAM) of OTS, as these over-solubilize the alkyltrisilanol species and prevent deposition onto the substrate surface.

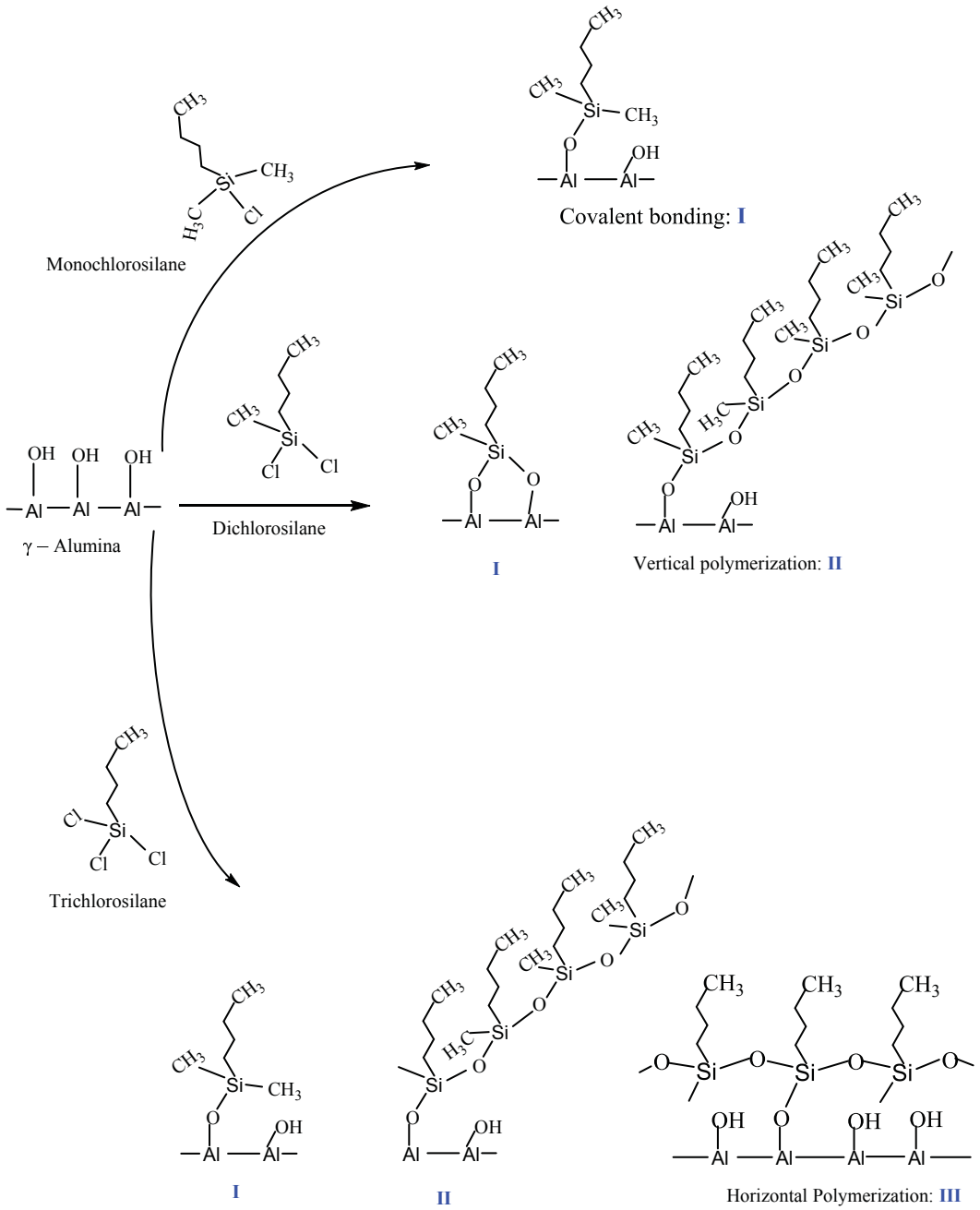

Figure 3: Schematic representation of the chemistry of silanes with varying number of hydrolysable groups present in the functional silane.

Solvents with a very low capacity for mixing with water, such as *n*-pentane, cannot accommodate much moisture in the bulk phase. This results in incomplete hydrolysis of

hydrolysable groups of OTS. Aromatic solvents, such as toluene and benzene, can take up a small quantity of water that appears to be the optimum for the formation of alkyltrisilanol and the subsequent polycondensation thereof. Formation of dense films of OTS on the substrate surface was observed when toluene was used as solvent, which was attributed to the hydrolysis of OTS in the bulk phase followed by deposition on the substrate surface. The authors suggested that a water quantity of 0.15 mg/100 ml of solvent is optimal for the formation of closely packed monolayers.

The significance of water in self-assembly was first proposed by Sagiv *et al*. (*103*). They proposed that traces of water are needed for covalent attachment of silanes to surface hybdroxyl groups. Later Finklea *et al.* (*104*) discovered that organised OTS SAMs can also be formed on substrate surfaces without hydroxyl groups. They proposed that self-assembly occurs on the water film adsorbed on the gold surface, where silanes form a 2D network of Si-O-Si bonds. This proposition of Finklea *et al.* has been supported by several authors (*98, 99, 101, 105*). Britt *et al.* (*102*) reported on the influence of the degree of hydration of a mica surface on layer formation with OTS. Deposition of 200 nm thick clusters, or islands, of OTS oligomers was observed after less than 10 seconds reaction time. As the reaction time prolonged to 40 seconds the thickness of the islands increased to 1 µm. Finally, in 300 seconds the surface was completely covered. In partially hydrated mica, the formation of uniformly distributed OTS clusters on the surface was observed from the beginning of the reaction and no large islands were observed.

Tripp and Hair (*98*) reported that the adsorption of OTS species on silica is sensitive to the amount of water present on the silica surface, or in the solvent. They used in-situ infrared spectroscopy to show that in the absence of water molecules there is no reaction between the OTS and surface hydroxyl groups. In contrast, in the case of hydrated silica surface grafting is observed. They showed that dried silica adsorbs water from the solvent. This is in contrast to the conclusions of McGovern *et al*. (*89*), who suggested extraction of water from the substrate surface into the solvent. Despite this contradiction, both groups claim that the equilibrium between surface water and molecular water dictates the nature of the adsorbed OTS species on the substrate. Alexy *et al.* (*100*) reported a ingenious method to utilize the water sensitivity of functional silanes to enlarge the extent of surface grafting. They showed an increased concentration of surface grafted silanes, after washing silanized samples with water before followed by a second silane treatement at identical experimental conditions. In this way the unhydrolyzed alkoxy groups were hydrolyzed during water washing. These newly generated silanol groups on silanes were used for grafting more functional silanes.

1.1.4.3 Grafting on porous membranes

Shah et al. (*106*) reported the functionalization of meso-porous γ-alumina membranes with mono-, di- and trichloromethylsilanes. Monochlorosilanes were able to diffuse inside the meso-pores. In case of di- and trichloromethylsilanes grafting of silanes was observed to occur predominantly at the entrances of the pores, and blocking of small pores was also observed. This can be explained by self-condensation or cross-linking of adjacent silanes. Supporting the above observations, Hendren *et al.* (*107*) reported that surface modification of alumina membranes with trichloromethylsilane resulted in blocked pore entrances. Zang

et al. (*92*) reported patching of defects in zeolite membranes. In principle zeolite membranes are micro-porous membranes, but it is difficult to synthesize defect-free zeolite membranes. Generally, defects consist of gaps between zeolite crystals. These gaps constitute mesopores and macropores. The authors proposed a systematic approach for reducing the defects in silicalite-1 membranes, by post-synthetic sequential grafting of 3-chloropropyltryethoxysilane (CPTES) and tetraethoxysilane (TEOS). The meso- and macro-porous defects were filled with an amorphous network of CPTES-TEOS oligomers, referred to as a silsesquioxane/silicate hybrid. The approach resulted in an increase in CO_2/N_2 selectivity from 1 to 15. Hong *et al.* (*108*) reported healing the non-zeolitic pores of silicalite microporous membranes by grafting three different types of silane precursors: TEOS, tetramethoxysilane (TMOS) and dimethoxydimethylsilane (DMDS). They found that DMDS is relatively more suitable for blocking or filling the non-zeolitic pores, as compared to TEOS and TMOS. After grafting with DMDS the p-/o-xylene separation factor was increased from 2 to 10, with the p-xylene flux reduced by only 12.6 %.

Javaid *et al.* (*95, 109-111*) reported solubility selective separation of C_3H_8/N_2 by tuning the surface chemistry and pore volume of γ-alumina membranes by grafting alkyltrichorosilanes with varying alkyl chain length (C_4 - C_{22}) on the porous surface. The permeation rates in the modified membranes decreased by three orders of magnitude as compared to the untreated membranes. Concurrently, the propane/nitrogen selectivity increased significantly from 1.9 up to 35. The performance of the membranes was strongly dependent on variations in the synthesis conditions (hydration state, number of hydrolysable groups of silane, length of alkyl chain of silane). This suggests the possibility for controlling the

hydrophobic characteristics of the membrane surface, by optimizing the grafting experimental conditions. Sakamoto (*112*) reported grafting of aminopropyltrimethoxysilane (APTMS) onto meso-porous MCM-48 membranes, with a pore diameter of about 2 nm. After grafting with APTMS, the average pore diameter was reduced from 2 nm to 1.2 nm, suggesting that the pores are functionalized with aminopropyl groups. The performance of the membranes was evaluated with gas permeation. Before APTMS grafting, the membranes showed Knudsen selectivity for CO_2/N_2. This is expected because the pores are significantly larger than CO_2 and N_2. After grafting, the membranes showed significant increase in CO_2/N_2 selectivity, up to 800, accompanied by a decrease in permeability of two orders of magnitude. These observations are consistent with those of Javaid *et al.* (*95*).

Hyun *et al.* (*113*) investigated the influence of grafting phenyltriethoxysilane (PTES) on γ-alumina membranes. After grafting PTES on TiO_2 supported membranes ($dp_{TIO2\ support}$: 0.3 μm) the authors observed an increase in CO_2/N_2 selectivity to 1.7 (at 90 ^{o}C, a transmembrane pressure of 2 bar, and for a binary mixture containing 50 vol% CO_2), This change in selectivity was attributed to enhanced surface diffusion. An increase in selectivity was not observed for α-alumina supported membranes ($dp_{\alpha-alumina}$: 0.1 μm).

Abidi *et al.* (*114*) reported CO_2 selective membranes by grafting fluorinated alkylsilane ($C_8F_{17}C_2H_4Si(OCH_3)_3$) on TiO_2 and γ-alumina meso-porous membranes, both with an average *dp* of 4 nm. After grafting fluorosilane, the permeabilities of the membranes decreased about 2-3 orders of magnitude compared with untreated membranes. However, an increase in permselectivity of CO_2/N_2 to around 10 is observed for TiO_2 membranes and to around 4

for γ-alumina membranes suggesting the favourable interactions between the organic groups and CO_2. The authors hypothesized that the transport mechanism involves a combination of surface diffusion and solution diffusion, depending on the pore filling. The major contribution is from surface diffusion.

Sah *et al.* (*91*) reported grafting of supported γ-alumina meso-porous membranes with mono-, di- and trichlorosilanes. These authors performed pore morphology analysis with permporometry, before and after grafting. In permporometry all pores are filled with a condensable vapor and no diffusion of a non-condensable gas through the pores will be possible. When the partial pressure of the vapor is reduced, pores with a radius larger than the so-called Kelvin radius (determined by Kelvin equation) will open and allow the diffusion non-condensable gas. In this way, the flux of non-condensable gas versus vapor partial pressure provides the size distribution of active pores. For further details see (*91, 115*). Sah *et al*. observed a reduction in Kelvin radius from 2.3 to 2 nm after grafting with monochlorosilane, implying penetration of alkylsilanes inside the mesopores. In contrast, after grafting with dichloroalkylsilane and trichloroalkylsilanes an increased Kelvin radius was observed, to 2.5 nm and 3.4 nm respectively. The authors proposed that smaller pores are completely blocked while larger pores remain open, resulting in a larger average pore diamter. X-ray photo electron spectroscopy (XPS) analysis showed a high concentration of silicon on the external surface of the supported membranes, after grafting with of di- and trichloroalkylsilanes. This indicates vertical and horizontal polymerization, resulting in blocking of pore entrances, which is consistent with the permporometry analysis. After grafting with monochloroalkylsilanes, silicon was observed deep inside the mesopores. At

the surface the silicon concentration was low. These observations suggest the penetration of alkylsilanes inside the pores, which is consistent with the permporometry analysis.

Hendren *et al.* (*107*) reported on surface modification of porous alumina anodisks with trichloromethylsilane (TCMS) and perfluorotrichlorosilane (PFTCMS). They showed skin layer formation over the pore entrances with TCMS, which resulted in blocking a few pores. In the case of PFTCMS no layer formation was observed, despite the large number of hydrolysable groups of this precursor. This suggests a low reactivity of PFTCMS compared to TCMS.

1.1.4.4 Grafting via vapor phase

Vapor phase grafting (VPG) is a chemical process in which precursors from a vapor phase react with the surface of a solid substrate. In solution phase grafting (SPG) the precursor is provided in a liquid solution. Theoretically, VPG comprises the following steps:

1. Diffusion of the precursor vapors towards the substrate surface
2. Adsorption of vapors on to the substrate surface
3. Chemical reaction between precursor and reactive groups on substrate surface

In the case of a porous solid material there is an additional mass transfer resistance: the transport of precursors into the pores. It should be noted that in VPG, due to capillary condensation, the pores of a porous material can be filled with condensable solvent that is in a vapor state outside the pores.

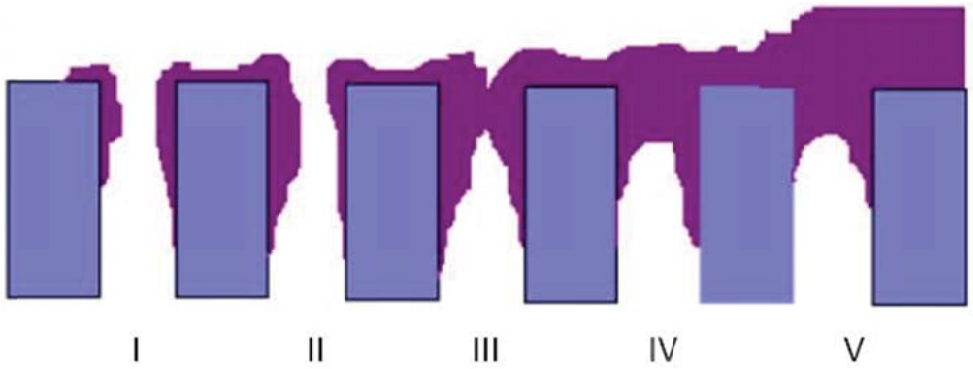

Figure 4: Over-view of various stages in the vapor deposition process (*116*).

As shown in Figure 4, several stages can be involved in the deposition of functional precursors inside porous structure. Particularly, at stage II, pores are narrowing and further deposition can result in localized pore closure (stage III). In the last stages (stage IV & V) the pore will be blocked completely. In this thesis the aim is to achieve stage III

VPG allows variation of various parameters, such as the selection of reactants, pore size and morphology of the substrate, temperature, precursor partial pressure, and the solvent partial pressure.

Several research groups have reported efficient deposition of functional silanes by vapour phase deposition, using the atomic layer deposition technique (ALD) (*93, 94, 117-121*). Ek *et al.* (*121*) reported ALD modification of porous silica with mono-, di- and trialkoxysilanes containing a primary amino group. They found a linear correlation between surface densities of amino groups and the number of isolated silanol groups on the silica surface. The pretreatment temperature (200 – 800 ^{o}C) of the silica showed a significant influence on the density of the amino groups grafted onto the surface, as this temperature affects the

amount of surface water and hydroxyl groups on the surface. The surface density of amino groups decreased when the pretreatment temperature was increased. The most dense molecular layers were achieved with difunctional and trifunctional silanes at the lowest pretreatment temperature, 200 ^{o}C.

Ritter *et al.* (*118*) reported the difference between solution phase and vapor phase post-synthetic grafting of meso-porous silica, MCM-41 by ALD. They showed the possibility of eliminating the influence of trace water, by using VPG: a narrow pore size distribution curves was obtained by VPG as compared to SPG. Introducing water into the reactor caused an increase in the width of the pore size distribution curves. These observations suggest oligomerization of functional silanes in presence of trace water, which block the pore entrances. This results in incomplete or partial grafting of the porous materials.

Ek *et al.* (*117*) reported a solid state 29 CP/MAS NMR investigation on the influence of the reaction temperature on the surface species after gas phase grafting of aminopropyltri*methoxy*silane (APTMS), aminopropyltri*ethoxy*silane (APTES), and aminopropyl*diethoxymethyl*silane (APDMS) by ALD. The investigations showed that ≤150 ^{0}C amino ends of APTS and APTMS molecules did not react with surface hydroxyl groups and other precursors. At temperatures > 150 ^{0}C, the amino ends of the APTS and APTMS react with surface silanol groups, forming Si-N bonds. At even higher deposition temperatures, particularly at 300 ^{0}C, decomposition of aminoalkyl groups was observed. The same group reported a simple method to increase the density of the aiminosilanes grafted by vapor phase deposition on to the silica surface, by consecutive reactions of

aminopropylalkoxysilanes and water vapor (*120*). First a heat-treated silica surface was saturated with trifunctional alkoxysilanes by ALD. In the consecutive step, the surface was treated with water vapor in order to hydrolyse the free alkoxy groups of the grafted aminosilane molecules. These hydrolysed groups, and remaining silanol groups, could react with with precursor molecules during a next cycle. In this way, the authors increased the density of aminosilane groups from about 2 molecules/nm^2 to 3 molecules/nm^2. After four cycles the surface was found to be saturated with aminosilanes, and no further increase in density was observed. In the case of APDMS, repetition of aminosilane/water cycles did not increase the amino group content. The authors explained this by a lack of free and reactive ethoxy groups on the aminosilylated silica surface, due to vertical polymerization of APDMS on silica.

Kurth *et al.* (*93*) reported thin layer formation of APTES by vapor phase deposition on aluminum and gold substrates. The authors investigated the difference between SPG and VPG. They concluded that thin mono layers with a thickness in the range of the length of the precursor molecule (10 - 20 Å) (*122*) were obtained by VPG, and multi-layers by SPG. The authors used ellipsometry and quartz crystal micro-balance techniques to quantify the amount of APS grafted on the substrates. They found 5±1 Å and 11±1 Å thick layers by VPG, in dry and wet conditions respectively. However, in case of SPG the average thickness was 21±4 Å, suggesting multiple layers. The same research group (*94*) successfully performed subsequent grafting of multiple-layers with chlorodimethylsilane (CDMS) on a thin-layer of APTES by using the chemistry between NH_2 groups of APTES and Chlorine groups of CDMS.

Lowe *et al.* (*119*) demonstrated the influence of a hydrated salt, $MgSO_4.7H_2O$ on vapor phase grafting (VPG) of tetradecyltri(deuteromethoxy)silane on silicon wafers. VPG was performed in a closed desiccator. $MgSO_4.7H_2O$ was placed beside to the silicon wafers at the bottom of the desiccator as a water source. Ellipsometry measurements showed a layer thickness of 14.1±1 Å without salt, and 18.1±1 Å with salt. During the first 5 hours of the reaction, the thickness of the layer increased drastically. From 5 up to 12 hour reaction time a very slow increase in the layer thickness was observed, No further change in thickness was observed after 12 hr. Water contact angles were always lower on wafers grafted without salt (~104°±1), as compared to with salt (~109°±1).

As reviewed above, the ALD technique has been successfully used in deposition of functional silane layers on various types of substrates. However, ALD requires very expensive equipment, and is not readily available in many laboratories. In this thesis, novel, facile, and robust set-ups are presented for simultaneous SPG and VPG on flat ceramic membranes (Figure 5, upper), and powders (Figure 5, lower). The set-ups require simple laboratory glassware.

In this thesis, we used in particular 3APTMS and CPTES as precursors (boiling point, 90 ^{o}C), and toluene (boiling point, 110 ^{o}C) as solvent. The use of a solvent is chosen to be able to perform simultaneous vapor phase grafting and solution phase grafting, in a single experiment, with a set-up as depicted in Figure 5.

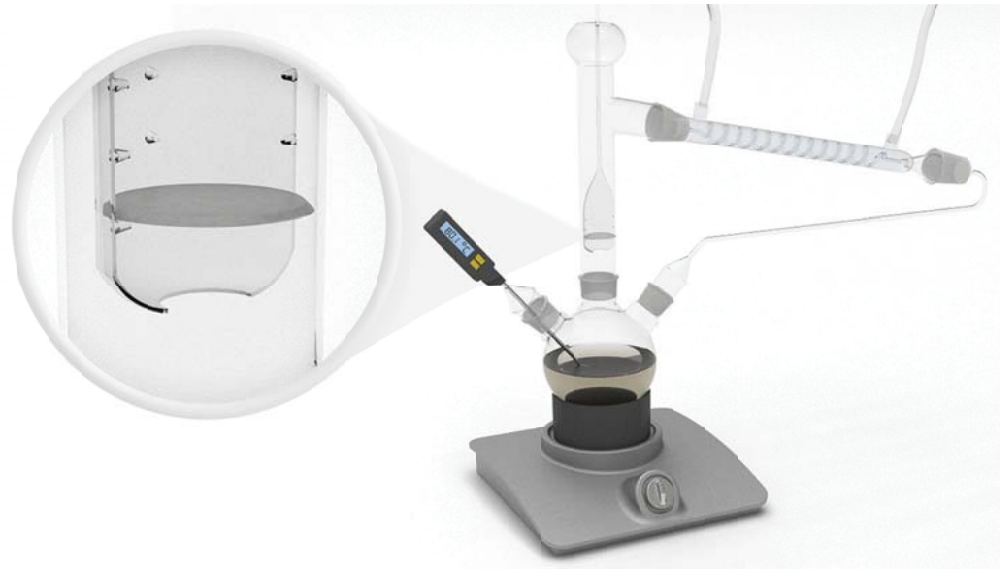


SPG
RBI
VPG
RBII
Powder

Figure 5: Set-ups for simultaneous vapor phase grafting and solution phase grafting, for disk shaped membranes (upper) and powders (lower).

1.1.5 Transport in porous membranes

The study of gas permeation through porous membranes has a long history dating back to Graham`s contribution in 1866 (*1*). If the pores of a micro-porous membranes are 0.1 μm or larger, gas permeation will generally take place by viscous flow, for instance described by Poiseuille`s law. As the pore radius (*r*) decreases, the pore radius can become comparable to, or less than, the mean free path (λ) of the gas molecules. At atmospheric pressure and room temperature the free mean path of small gases is in the range 50 – 200 (nm) (*1*). When the ratio of the radius to the gas mean free path (r/λ) is less than one, diffusing gas molecules have more collisions with the pore walls than with other gas molecules. Gas permeation in this region occurs by Knudsen diffusion. At every collision with the pore walls, the gas molecules are momentarily adsorbed and then reflected in a random direction. Molecule-molecule collisions are rare, so each gas molecule moves independently of all others. Different gas species move at different average velocities, depending on their molecular or atomic mass. This allows separation of a gas containing different species. The gas flow in a porous membrane made of cylindrical shaped pores for Knudsen diffusion is:

$$N = \frac{4r\varepsilon}{3} \left(\frac{2RT}{\pi m}\right)^{1/2} \frac{P_0 - P_x}{x\,RT} \qquad [1]$$

Where *m* is the molecular weight of the gas, *N* is the flux in g mol $cm^{-2}s^{-1}$, ε is the porosity of the membrane, *r* is the pore radius, *x* is the pore length and P_0 *and* P_x are the partial pressures of the gas species at the beginning of the pore (P_0) and at the end (P_x).

The permeance of a gas exhibiting Knudsen diffusion is proportional to $m_i^{-0.5}$. The permselectivity for Knudsen diffusion ($F_{\alpha i/j}$, ratio of gas permeances) is given by $(m_j/m_i)^{-0.5}$.

Surface adsorption and diffusion can also contribute to gas permeation in small-pore-diameter membranes. Adsorption onto the walls of the small pores becomes noticeable when the pore diameter drops below about 50-100 Å (*1*). For this pore diameter, the total pore surface area of the material is in the range 100 m^2 cm^{-3}. Significant amounts of gas may absorb onto the pore walls, particularly if the gas is condensable. Sorbed gas molecules are mobile and can move by surface diffusion through the membrane. For not too high surface concentrations this can be described with a Fick`s law type of expression,

$$N_s = -D_s \frac{dc_s}{dx} \qquad [2]$$

Where N_s is the flux by surface diffusion, c_s is the surface concentration, and D_s is surface diffusion coefficient.

1.1.5.1 Transport in non-porous, dense, organic membranes

In non-porous, dense, organic membranes the gases dissolve in the membrane material and diffuse through the membrane, down their concentration gradient. According to Fick's law, the gas diffusion can be described by similar type of expression as equation [2] (*123*),

$$N = -D \frac{dc}{dx} \qquad [3]$$

Where *N* is the gas flux through the membrane (mol $m^{-2}s^{-1}$), *D* is the diffusion coefficient (m^2s^{-1}) and d*c*/d*x* is the concentration gradient over the membrane (mol m^{-2}). Assuming steady-state conditions, Equation [3] can be integrated and results in the following equation:

$$N = \frac{D\,(c_0 - c_x)}{l} \qquad [4]$$

Where the subscripts *0* and *x* refer to the feed and permeate side of the membrane, and *l* is the thickness (m) of the membrane.

According to Henry's law the concentration of the gas component is linearly proportional to its partial pressure *p* (*124*):

$$c = s \cdot p \qquad [5]$$

Where *S* is the solubility coefficient of the gas component (mol $m^{-3}Pa^{-1}$).

Combining equations [4] and [5] results in

$$N = \frac{P\,(p_0 - p_x)}{l} \qquad [6]$$

Where *P* is the permeance of the gas component (mol $m^{-2}s^{-1}Pa^{-1}$), given by

$$P = D \,.\, S \qquad [7]$$

Equation [7] is often used to describe transport of gases through dense organic membranes (*19, 125*). According to this model, transport occurs in three successive steps: sorption of the penetrant at the feed side of the membrane followed by diffusion through the membrane and desorption at the permeate side of the membrane. From this equation the permselectivity of a membrane for two gas components *i* and *j* can be calculated with the following equation.

$$\alpha_{i/j} = \frac{P_i}{P_j} = \frac{D_i}{D_j} \cdot \frac{S_i}{S_j} \qquad [8]$$

The diffusion coefficient (D_i) reflects the mobility of the individual molecules in the membrane material (*1*). It is a kinetic parameter and predominantly influenced by the shape and size of the gas molecules under consideration. In general, D_i decreases with increasing kinetic diameter of the gas molecule (*125*) because large molecules interact with more segments of the polymer chain compared to small molecules. Particularly in view of the CO_2/CH_4 separation, CO_2 has two to six times higher diffusion coefficient than CH_4 in glassy polymers, calculated by molecular dynamics simulation of glassy polymers (*1*). As shown in Figure 6, CH_4 is more or less spherical with a kinetic diameter of 3.72 Å, while CO_2 is an oblate ellipsoid. Viewed from the top, the CO_2 molecule is 5.25 Å long, but seen end-on, the molecule's diameter is only 3.03 Å (*1*). This means that CO_2 molecules that bouncing around in a micro cavity may occasionally become oriented so they can pass a gaps are as narrow as 3.03 Å to another micro cavity. Such gaps reject CH_4 molecules (*1*).

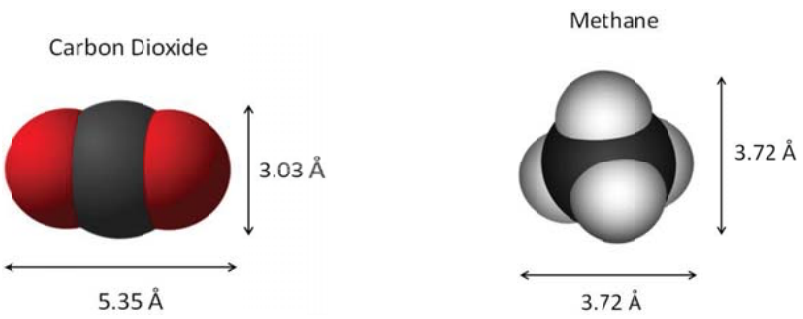

Figure 6: Illustration showing the approximate molecular dimensions of CO_2, CH_4 (*1*).

The solubility coefficient (S_i) is a thermodynamic factor which reflects the number of molecules dissolved in the membrane material (*1, 125*). S_i is dependent on: (1) condensability of the penetrant gas, (2) nature of interactions between the penetrant and polymer, and (3) chain packing density in glassy polymers. The S_i of gases increases with increasing condensability of the penetrant. This means that the solubility coefficient also increases with molecular diameter, because large molecules are normally more condensable than small ones (*1*). Particularly, for the separation of CO_2 from CH_4, CO_2 is more condensable (CO_2: T_c=304 K, CH_4: T_c=191 K) (*126*). Thus, a higher CO_2 solubility can be expected in polymeric membranes (*125*). Combined, a higher diffusion coefficient and solubility of CO_2 as compared to CH_4 is expected to result in a higher permeance of CO_2, and hence molecular separation.

1.1.5.2 Transport behaviour in glassy polymer membranes upon plasticization

This section describes changes in gas transport upon plasticization in glassy polymers, particularly polyimides, in natural gas processing. At relatively low pressures, the gas

permeability of the polyimide membrane decreases with increasing pressure. This behaviour is attributed to the exclusion effects in sorption and diffusion when the concentration of penentrant in the polymer increases (*31, 35, 126*). In the sorption process the exclusion effects are related to the excess free volume (EFV) that becomes increasingly filled with increasing penetrant concentration. When this EFV is filled, sorption can only occur if the polymer is dilated by the penentrant, which occurs at the cost of a higher energy penalty. Exclusion effects in diffusion are related to the inaccessibility of a adjacent open micro cavity, when it is already occupied by a penentrant molecule. These effects are likely minor for most polymer-penetrant systems. Further increasing the pressure results in upward inflection in gas permeability. This is due to plasticization of the polymer matrix (*127*) and the pressure at which this occurs is referred to as the plasticization pressure. Due to plasticization, the mobility of the polymer chains increases dramatically, allowing higher penetrant diffusion as well as higher penetrant uptake. Above the plasticization pressure, the gas permeability becomes highly time dependent due to irreversible relaxation of the glassy polymer chains (*31*).

In CO_2/CH_4 separation using glassy polymeric membranes, CO_2-induced plasticization accelerates the CH_4 permeation, thus deteriorates the CO_2/CH_4 selectivity. CO_2-induced plasticization in gas transport properties of glassy polymeric membranes depends on pressure, temperature and thickness of the membrane. Several approaches have been performed to suppress the plasticization of organic membranes. Here, an attempt is aspired where length-scale confinement of the organic material in the pores of a rigid ceramic host will moderate chain mobility, and hence plasticization.

1.2 Project description and objectives

The works described in this thesis is aimed at developing methodology for synthesis of hybrid membranes via sequential grafting. The approach is to functionalize the pore surface of a meso-porous ceramic with linker molecules that provide anchoring sites for subsequent grafting steps. In the subsequent grafting steps other organic species are covalently attached to the functionalized pore surface of the ceramic material. This approach allows molecular design of the organic species, combined with length-scale confinement on a nanometer scale. The choice of suitable precursors permits tuning of the affinity for specific molecules. The length-scale confinement aids moderating the molecular (oligomer) dynamics, in turn reducing the propensity to swelling and plasticization. The combination of these advantages may be beneficial for membrane applications involving the presence of a plasticizing penetrant (e.g., an organic solvent), at elevated pressure, or at high temperatures. In this thesis, the target application is gas separation of CO_2 and CH_4, at elevated pressures. In particular, this thesis demonstrates the synthesis of organic-inorganic hybrid membranes, by sequential grafting of organic precursors on the pore surface of meso-porous membranes, resulting in confined oligomers of fluoroimides and etheroxides.

1.3 Thesis out-line

This thesis focuses on fabrication of hybrid inorganic – polymeric hybrid membranes by sequential grafting.

The initial step in the sequential grafting process is functionalization of a meso-porous ceramic with a linker molecule. This is commonly done by wet chemical methods, or

solution phase grafting, using functional silanes. However, functional silanes are sensitive to moisture and undergo self condensation, resulting in non-homogeneous and dense structures. In case of grafting porous materials this may result in uncontrolled filling, or even blocking, of the pores. **Chapter 2** presents extensive investigation on difference between solution phase grafting (SPG) and vapor phase grafting (VPG) of meso-porous γ-alumina with aminosilanes. It is shown that thin layers inside the pores of the ceramic can readily be obtained via VPG, and that this method is relatively insensitive to the presence of water. In contrast, SPG is found sensitive for presence of water and reaction conditions, resulting in less controlled functionalization of the pore surface. The observations are rationalized by the low vapor pressure of oligomers, formed by the self-condensation reactions of the precursors. **Chapter 3** demonstrates the possibility to obtain polyimide-alumina hybrid membranes via the sequential grafting approach. Particular emphasis is on the influence of linker morphology (VPG or SPG functionalization materials) on effectiveness of pore filling. **Chapter 4** explores the influence of proliferation of the surface functionality, by introducing linker molecules containing multi (eight) functional groups, on subsequent grafting of polyimides. Introduction of such a linker molecule (octa aminophenyl silsesquioxane) is shown to allow more effective filling of the pores, until the meso-porous characteristics no longer persist. **Chapter 5** presents sequential grafting strategies for synthesis of polyether-alumina membranes. The length-scale confinement of ether oxides is shown to effect gas permeation performance of the membranes, an increase of selectivity of carbon dioxide over nitrogen and methane is observed. **Chapter 6** explores possibilities of functionalization

of meso-porous hybrid silica. It is shown that water is required for the surface functionalization, in particular when grafting is conducted from the vapor phase.

References

1. R. W. Baker, *Membrane Technology and Applications,* . (A John Wiley & Sons, Ltd., Publications, ed. 3, 2012).

2. H. Lin, E. V. Wagner, R. Raharjo, B. D. Freeman, I. Roman, High Performance Polymer Membranes for Natural-Gas Sweetening. *Advanced Materials* **18**, 39 (2006).

3. H. Lin, B. D. Freeman, Materials selection guidelines for membranes that remove CO2 from gas mixtures. *Journal of Molecular Structure* **739**, 57 (2005).

4. R. W. Baker, Future directions of membrane gas separation technology. *Ind. Eng. Chem. Res.* **41**, 1393 (2002).

5. R. W. Baker, K. Lokhandwala, Natural gas processing with membranes. *Ind. Eng. Chem. Res.* **47**, 2109 (2008).

6. W. J. Koros, R. Mahajan, Pushing the limits on possibilities for large scale gas separation: which strategies ? *Journal of Membrane Science* **175**, 181 (2000).

7. J. Caro, Are MOF membranes better in gas separation than those made of zeolites? *Current Opinion in Chemical Engineering* **1**, 77 (2011).

8. J. Caro, M. Noack, Zeolite membranes - Recent developments and progress. *Microporous and Mesoporous Materials* **115**, 215 (2008).

9. H. Lin, B. D. Freeman, Materials selection guidelines for membranes that remove CO_2 from gas mixture. *Journal of Molecular Structure* **739**, 57 (2005).

10. C. A. Scholes, G. W. Stevens, S. E. Kentish, Membrane gas separation applications in natural gas processing. *Fuel* **96**, 15 (2012).

11. K.-V. Peinemann, S. Pereira-Nunes, *Membranes for Life Sciences*. K.-V. Peinemann, Ed., (WILEY-VCH Verlag GmbH & Co. , Deutsche Nationalbibiliothek, 2008), vol. 1.

12. N. N. Li, A. G. Fane, W. S. W. Ho, T. Matsuura, *Advanced Membrane Technology and Applications*. (John Wiley & Sons, Inc., 2008).

13. Y. Yampolskii, I. Pinnau, B. Freeman., *Materials Science of Membranes for Gas and Vapor Separation*. (John Wiley & Sons, Inc. , 2006).

14. N. K. Kanellopoulos, *Recent advances in gas separation by microporus ceramic membranes, vol. 6*, (2000).

15. A. K. Pabby, S. S. H. Rizvi, A. M. Sastre, *Hand book of Membrane Separations: Chemical, Pharmaceutical, Food and Biotechnological Applications*. (Taylor & Francis Group, LLC., 2009).

16. N. S. Pereira, K.-V. Pieneman, *Membrane Technology: in the Chemical Industry, 2nd, Revised and Enlarged Edition*. Membrane technology in the chemical industry (2000 - 2014 by John Wiley & Sons, Inc., 2006).

17. S. P. N. Klaus-Viktor Peinemann, *Membrane technology: Membranes for water treatment*, (2010).

18. P. Hillis, *Membrane Technology in Water and Waste Water Treatment*. (The Royal Society of Chemistry, 2000).

19. A. Bos, High pressure CO_2/CH_4 separation with glassy polymer membranes. *Ph.D. thesis, University of twente, The Netherlands*, (1996).

20. M. Wessling, Relaxation phenomena in dense gas separation membranes. *Ph.D. thesis, University of twente, The Netherlands*, (1993).

21. A. Bos, I. Pünt, H. Strathmann, M. Wessling, Suppression of gas separation membrane plasticization by homogeneous polymer blending. *AIChE Journal* **47**, 1088 (2001).

22. A. Bos, I. G. M. Pünt, M. Wessling, H. Strathmann, Plasticization-resistant glassy polyimide membranes for CO_2/CH_4 separations. *Separation and Purification Technology* **14**, 27 (1998).

23. A. Bos, I. G. M. Pünt, M. Wessling, H. Strathmann, CO_2-induced plasticization phenomena in glassy polymers. *Journal of Membrane Science* **155**, 67 (1999).

24. S. R. Reijerkerk, K. Nijmeijer, C. P. Ribeiro, B. D. Freeman, M. Wessling, On the effects of plasticization in CO_2/light gas separation using polymeric solubility selective membranes. *Journal of Membrane Science* **367**, 33 (2011).

25. S. R. Reijerkerk, A. Arun, R. J. Gaymans, K. Nijmeijer, M. Wessling, Tuning of mass transport properties of multi-block copolymers for CO_2 capture applications. *Journal of Membrane Science* **359**, 54 (2010).

26. A. C. Ijzer *et al.*, Synthesis and properties of hydrophilic segmented block copolymers based on poly(ethylene oxide)- ran-poly(propylene oxide). *Journal of Applied Polymer Science* **117**, 1394 (2010).

27. S. R. Reijerkerk, M. Wessling, K. Nijmeijer, Pushing the limits of block copolymer membranes for CO 2 separation. *Journal of Membrane Science* **378**, 479 (2011).

28. S. R. Reijerkerk, Polyether based block copolymer membranes for CO_2 separation. *Ph.D. thesis*, pg. 51 (2010).

29. S. R. Reijerkerk, M. H. Knoef, K. Nijmeijer, M. Wessling, Poly(ethylene glycol) and poly(dimethyl siloxane): Combining their advantages into efficient CO_2 gas separation membranes. *Journal of Membrane Science* **352**, 126 (2010).

30. S. R. Reijerkerk, K. Nijmeijer, C. P. Ribeiro, B. D. Freeman, M. Wessling, On the effects of plasticization in CO 2/light gas separation using polymeric solubility selective membranes. *Journal of Membrane Science* **367**, 33 (2011).

31. T. Visser, Mixed gas plasticization phenomena in asymmetric membranes. *Ph.D. thesis, University of twente, The Netherlands*, (2006).

32. J. D. Wind *et al.*, Relaxation dynamics of CO_2 diffusion, sorption, and polymer swelling for plasticized polyimide membranes. *Macromolecules* **36**, 6442 (2003).

33. J. D. Wind, C. Staudt-Bickel, D. R. Paul, W. J. Koros, The effects of crosslinking chemistry on CO_2 plasticization of polyimide gas separation membranes. *Industrial and Engineering Chemistry Research* **41**, 6139 (2002).

34. J. D. Wind *et al.*, Carbon dioxide-induced plasticization of polyimide membranes: Pseudo-equilibrium relationships of diffusion, sorption, and swelling. *Macromolecules* **36**, 6433 (2003).

35. A. F. Ismail, W. Lorna, Penetrant-induced plasticization phenomenon in glassy polymers for gas separation membrane. *Separation and Purification Technology* **27**, 173 (2002).

36. S. G. Kazarian, M. F. Vincent, F. V. Bright, C. L. Liotta, C. A. Eckert, Specific intermolecular interaction of carbon dioxide with polymers. *Journal of the American Chemical Society* **118**, 1729 (1996).

37. N. E. Benes, Mass transport in thin supported membranes. *Ph.D. thesis, University of twente, The Netherlands*, (2000).

38. J. N. Barsema, G. C. Kapantaidakis, N. F. A. Van Der Vegt, G. H. Koops, M. Wessling, Preparation and characterization of highly selective dense and hollow fiber asymmetric membranes based on BTDA-TDI/MDI co-polyimide. *Journal of Membrane Science* **216**, 195 (2003).

39. B. Krause, R. Mettinkhof, N. F. A. Van Der Vegt, M. Wessling, Microcellular foaming of amorphous high-T_g polymers using carbon dioxide. *Macromolecules* **34**, 874 (2001).

40. M. Wessling, M. Lidon Lopez, H. Strathmann, Accelerated plasticization of thin-film composite membranes used in gas separation. *Separation and Purification Technology* **24**, 223 (2001).

41. Z. Zhang, Y. P. Handa, An in situ study of plasticization of polymers by high-pressure gases. *Journal of Polymer Science, Part B: Polymer Physics* **36**, 977 (1998).

42. H. Lin *et al.*, Transport and structural characteristics of crosslinked poly(ethylene oxide) rubbers. *Journal of Membrane Science* **276**, 145 (2006).

43. J. J. Richards *et al.*, Relation between structure and gas transport properties of polyethylene oxide networks based on crosslinked bisphenol A ethoxylate diacrylate. *Chemical Engineering Science* **64**, 4707 (2009).

44. V. A. Kusuma, B. D. Freeman, S. L. Smith, A. L. Heilman, D. S. Kalika, Influence of TRIS-based co-monomer on structure and gas transport properties of cross-linked poly(ethylene oxide). *Journal of Membrane Science* **359**, 25 (2010).

45. V. A. Kusuma, S. Matteucci, B. D. Freeman, M. K. Danquah, D. S. Kalika, Influence of phenoxy-terminated short-chain pendant groups on gas transport properties of cross-linked poly(ethylene oxide) copolymers. *Journal of Membrane Science* **341**, 84 (2009).

46. V. A. Kusuma, B. D. Freeman, M. A. Borns, D. S. Kalika, Influence of chemical structure of short chain pendant groups on gas transport properties of cross-linked poly(ethylene oxide) copolymers. *Journal of Membrane Science* **327**, 195 (2009).

47. V. I. Bondar, B. D. Freeman, I. Pinnau, Gas transport properties of poly(ether-b-amide) segmented block copolymers. *Journal of Polymer Science Part B: Polymer Physics* **38**, 2051 (2000).

48. V. I. Bondar, B. D. Freeman, I. Pinnau, Gas sorption and characterization of poly(ether-b-amide) segmented block copolymers. *Journal of Polymer Science Part B: Polymer Physics* **37**, 2463 (1999).

49. G. Chatterjee, A. A. Houde, S. A. Stern, Poly(ether urethane) and poly(ether urethane urea) membranes with high H2S/CH4 selectivity. *Journal of Membrane Science* **135**, 99 (1997).

50. K.-i. Okamoto *et al.*, Gas permeation properties of poly(ether imide) segmented copolymers. *Macromolecules* **28**, 6950 (1995/09/01, 1995).

51. H. B. Park, C. K. Kim, Y. M. Lee, Gas separation properties of polysiloxane/polyether mixed soft segment urethane urea membranes. *Journal of Membrane Science* **204**, 257 (2002).

52. X. Chen, D. Rodrigue, S. Kaliaguine, Diamino-organosilicone APTMDS: A new cross-linking agent for polyimides membranes. *Separation and Purification Technology* **86**, 221 (2012).

53. J. K. Adewole, A. L. Ahmad, S. Ismail, C. P. Leo, Current challenges in membrane separation of CO2 from natural gas: A review. *International Journal of Greenhouse Gas Control* **17**, 46 (2013).

54. T. Nakagawa, T. Nishimura, A. Higuchi, Morphology and gas permeability in copolyimides containing polydimethylsiloxane block. *Journal of Membrane Science* **206**, 149 (2002).

55. Y. Xiao, B. T. Low, S. S. Hosseini, T. S. Chung, D. R. Paul, The strategies of molecular architecture and modification of polyimide-based membranes for CO2 removal from natural gas-A review. *Progress in Polymer Science (Oxford)* **34**, 561 (2009).

56. A. F. Ismail, W. Lorna, Suppression of plasticization in polysulfone membranes for gas separations by heat-treatment technique. *Separation and Purification Technology* **30**, 37 (2003).

57. C. C. Hu *et al.*, Effects of plasma treatment on CO_2 plasticization of poly(methyl methacrylate) gas-separation membranes. *Journal of Applied Polymer Science* **93**, 395 (2004).

58. S. S. Hosseini, N. Peng, T. S. Chung, Gas separation membranes developed through integration of polymer blending and dual-layer hollow fiber spinning process for hydrogen and natural gas enrichments. *Journal of Membrane Science* **349**, 156 (2010).

59. P. Iyer, G. Iyer, M. Coleman, Gas transport properties of polyimide-POSS nanocomposites. *Journal of Membrane Science* **358**, 26 (2010).

60. T.-S. Chung, L. Y. Jiang, Y. Li, S. Kulprathipanja, Mixed matrix membranes (MMMs) comprising organic polymers with dispersed inorganic fillers for gas separation. *Progress in Polymer Science* **32**, 483 (2007).

61. A. Bhattacharya, B. N. Misra, Grafting: a versatile means to modify polymers: Techniques, factors and applications. *Progress in Polymer Science* **29**, 767 (2004).

62. M. R. Pixton, D. R. Paul, Gas transport properties of adamantane-based polysulfones. *Polymer* **36**, 3165 (1995).

63. C. A. Scholes, G. Q. Chen, G. W. Stevens, S. E. Kentish, Plasticization of ultra-thin polysulfone membranes by carbon dioxide. *Journal of Membrane Science* **346**, 208 (2010).

64. H. J. M. Bouwmeester, M. W. Den Otter, B. A. Boukamp, Oxygen transport in La0.6Sr0.4Co1-yFe yO3-δ. *Journal of Solid State Electrochemistry* **8**, 599 (2004).

65. H. Hamilton, Palladium-based membranes for hydrogen separation. *Platinum Metals Review* **56**, 117 (2012).

66. L. B. McCusker, F. Liebau, G. Engelhardt, Nomenclature of structural and compositional characteristics of ordered microporous and mesoporous materials with inorganic hosts: (IUPAC recommendations 2001). *Pure and Applied Chemistry* **73**, 381 (2001).

67. L. B. McCusker, F. Liebau, G. Englehardt, Nomenclature of structural and compositional characteristics of ordered microporous and mesoporous materials with inorganic hosts (IUPAC recommendations 2001): Physical chemistry Division commision on colloid and surface chemistry including catalysis. *Microporous and Mesoporous Materials* **58**, 3 (2003).

68. E. E. McLeary, J. C. Jansen, F. Kapteijn, Zeolite based films, membranes and membrane reactors: Progress and prospects. *Microporous and Mesoporous Materials* **90**, 198 (2006).

69. M. A. Snyder, M. Tsapatsis, Hierarchical nanomanufacturing: From shaped zeolite nanoparticles to high-performance separation membranes. *Angewandte Chemie - International Edition* **46**, 7560 (2007).

70. H. Bux *et al.*, Zeolitic Imidazolate Framework Membrane with Molecular Sieving Properties by Microwave-Assisted Solvothermal Synthesis. *Journal of the American Chemical Society* **131**, 16000 (2009/11/11, 2009).

71. M. Asaeda, S. Yamasaki, Separation of inorganic/organic gas mixtures by porous silica membranes. *Separation and Purification Technology* **25**, 151 (2001).

72. A. Nijmeijer, *Hydrogen - selective silica membranes for use in membrane steam reforming*. Ph.D. thesis, University of twente, The Netherlands (1999).

73. R. M. De Vos, H. Verweij, High-selectivity, high-flux silica membranes for gas separation. *Science* **279**, 1710 (1998).

74. R. S. A. de Lange, J. H. A. Hekkink, K. Keizer, A. J. Burggraaf, Formation and characterization of supported microporous ceramic membranes prepared by sol-gel modification techniques. *Journal of Membrane Science* **99**, 57 (1995).

75. S. J. Khatib, S. T. Oyama, K. R. de Souza, F. B. Noronha, in *Membrane Science and Technology,* S. T. Oyama, M. S.-W. Susan, Eds. (Elsevier, 2011), vol. Volume 14, pp. 25-60.

76. K. Kuraoka, T. Kakitani, T. Suetsugu, T. Yazawa, Methanol vapor separation through the silica membrane prepared by the CVD method with the aid of evacuation. *Separation and Purification Technology* **25**, 161 (2001).

77. C. Casado Coterillo, A. María Urtiaga Mendia, I. Ortiz Uribe. (2008), vol. 13, pp. 217-253.

78. H. L. Castricum *et al.*, Hybrid ceramic nanosieves: Stabilizing nanopores with organic links. *Chemical Communications*, 1103 (2008).

79. H. L. Castricum *et al.*, Tailoring the separation behavior of hybrid organosilica membranes by adjusting the structure of the organic bridging group. *Advanced Functional Materials* **21**, 2319 (2011).

80. H. L. Castricum *et al.*, Structure of hybrid organic-inorganic sols for the preparation of hydrothermally stable membranes. *Journal of Sol-Gel Science and Technology* **48**, 11 (2008).

81. H. L. Castricum, A. Sah, M. C. Mittelmeijer-Hazeleger, C. Huiskes, J. E. Ten Elshof, Microporous structure and enhanced hydrophobicity in methylated SiO 2 for molecular separation. *Journal of Materials Chemistry* **17**, 1509 (2007).

82. H. L. Castricum *et al.*, High-performance hybrid pervaporation membranes with superior hydrothermal and acid stability. *Journal of Membrane Science* **324**, 111 (2008).

83. G. G. Paradis, R. Kreiter, M. M. A. Van Tuel, A. Nijmeijer, J. F. Vente, Amino-functionalized microporous hybrid silica membranes. *Journal of Materials Chemistry* **22**, 7258 (2012).

84. Y.-S. Li *et al.*, Molecular Sieve Membrane: Supported Metal–Organic Framework with High Hydrogen Selectivity. *Angewandte Chemie International Edition* **49**, 548 (2010).

85. J. Caro, M. Noack, Zeolite membranes - Recent developments and progress. *Microporous and Mesoporous Materials* **115**, 215 (2008).

86. J. Gascon, F. Kapteijn, Metal-organic framework membranes-high potential, bright future? *Angewandte Chemie - International Edition* **49**, 1530 (2010).

87. J. Gascon, U. Aktay, M. D. Hernandez-Alonso, G. P. M. van Klink, F. Kapteijn, Amino-based metal-organic frameworks as stable, highly active basic catalysts. *Journal of Catalysis* **261**, 75 (2009).

88. A. Y. Fadeev, T. J. McCarthy, Trialkylsilane Monolayers Covalently Attached to Silicon Surfaces: Wettability Studies Indicating that Molecular Topography Contributes to Contact Angle Hysteresis. *Langmuir* **15**, 3759 (1999/05/01, 1999).

89. M. E. McGovern, K. M. R. Kallury, M. Thompson, Role of Solvent on the Silanization of Glass with Octadecyltrichlorosilane. *Langmuir* **10**, 3607 (1994/10/01, 1994).

90. H. L. Castricum, M. C. Mittelmeijer-Hazeleger, A. Sah, J. E. Ten Elshof, Increasing the hydrothermal stability of mesoporous SiO_2 with methylchlorosilanes - a 'structural' study. *Microporous and Mesoporous Materials* **88**, 63 (2006).

91. A. Sah, H. L. Castricum, A. Bliek, D. H. A. Blank, J. E. Ten Elshof, Hydrophobic modification of γ-alumina membranes with organochlorosilanes. *Journal of Membrane Science* **243**, 125 (2004).

92. B. Zhang, C. Wang, L. Lang, R. Cui, X. Liu, Selective defect-patching of zeolite mmebranes using chemical liquid deposition at organic/aqueous interfaces. *Advanced Functional Materials* **18**, 3434 (2008).

93. D. G. Kurth, T. Bein, Thin Films of (3-Aminopropyl)triethoxysilane on Aluminum Oxide and Gold Substrates. *Langmuir* **11**, 3061 (1995/08/01, 1995).

94. D. G. Kurth, T. Bein, Surface reactions on thin layers of silane coupling agents. *Langmuir* **9**, 2965 (1993/11/01, 1993).

95. A. Javaid, D. A. Krapchetov, D. M. Ford, Solubility-based gas separation with oligomer-modified inorganic membranes: Part III. Effects of synthesis conditions. *Journal of Membrane Science* **246**, 181 (2005).

96. A. Y. Fadeev, T. J. McCarthy, Self-Assembly Is Not the Only Reaction Possible between Alkyltrichlorosilanes and Surfaces: Monomolecular and Oligomeric Covalently Attached Layers of Dichloro- and Trichloroalkylsilanes on Silicon. *Langmuir* **16**, 7268 (2000/09/01, 2000).

97. D. H. Flinn, D. A. Guzonas, R. H. Yoon, Characterization of silica surfaces hydrophobized by octadecyltrichlorosilane. *Colloids and Surfaces A: Physicochemical and Engineering Aspects* **87**, 163 (1994).

98. C. P. Tripp, M. L. Hair, Direct Observation of the Surface Bonds between Self-Assembled Monolayers of Octadecyltrichlorosilane and Silica Surfaces: A Low-Frequency IR Study at the Solid/Liquid Interface. *Langmuir* **11**, 1215 (1995/04/01, 1995).

99. C. P. Tripp, M. L. Hair, An infrared study of the reaction of octadecyltrichlorosilane with silica. *Langmuir* **8**, 1120 (1992/04/01, 1992).

100. A. V. Krasnoslobodtsev, S. N. Smirnov, Effect of water on silanization os silica by trimethoxysilanes. *Langmuir* **18**, 3181 (2002).

101. D. L. Allara, A. N. Parikh, F. Rondelez, Evidence for a Unique Chain Organization in Long Chain Silane Monolayers Deposited on Two Widely Different Solid Substrates. *Langmuir* **11**, 2357 (1995/07/01, 1995).

102. D. W. Britt, V. Hlady, An AFM Study of the Effects of Silanization Temperature, Hydration, and Annealing on the Nucleation and Aggregation of Condensed OTS Domains on Mica. *Journal of Colloid and Interface Science* **178**, 775 (1996).

103. J. Sagiv, Organized monolayers by adsorption. 1. Formation and structure of oleophobic mixed monolayers on solid surfaces. *Journal of the American Chemical Society* **102**, 92 (1980/01/01, 1980).

104. H. O. Finklea *et al.*, Formation of an organized monolayer by solution adsorption of octadecyltrichlorosilane on gold: electrochemical properties and structural characterization. *Langmuir* **2**, 239 (1986/03/01, 1986).

105. P. Silberzan, L. Leger, D. Ausserre, J. J. Benattar, Silanation of silica surfaces. A new method of constructing pure or mixed monolayers. *Langmuir* **7**, 1647 (1991/08/01, 1991).

106. A. shah, Chemically modified ceramic membranes: study of structural and transport properties. *University of twente*, PhD thesis (2006).

107. Z. D. Hendren, J. Brant, M. R. Wiesner, Surface modification of nanostructured ceramic membranes for direct contact membrane distillation. *Journal of Membrane Science* **331**, 1 (2009).

108. Z. Hong, C. Zhang, X. Gu, W. Jin, N. Xu, A simple method for healing nonzeolitic pores of MFI membranes by hydrolysis of silanes. *Journal of Membrane Science* **366**, 427 (2011).

109. A. Javaid, S. O. Gonzalez, E. E. Simanek, D. M. Ford, Nanocomposite membranes of chemisorbed and physisorbed molecules on porous alumina for environmentally important separations. *Journal of Membrane Science* **275**, 255 (2006).

110. A. Javaid, D. M. Ford, Solubility-based gas separation with oligomer-modified inorganic membranes: Part II. Mixed gas permeation of 5 nm alumina membranes modified with octadecyltrichlorosilane. *Journal of Membrane Science* **215**, 157 (2003).

111. A. Javaid, M. P. Hughey, V. Varutbangkul, D. M. Ford, Solubility-based gas separation with oligomer-modified inorganic membranes. *Journal of Membrane Science* **187**, 141 (2001).

112. Y. Sakamoto, K. Nagata, K. Yogo, K. Yamada, Preparation and CO_2 separation properties of amine-modified mesoporous silica membranes. *Microporous and Mesoporous Materials* **101**, 303 (2007).

113. S. H. Hyun, S. Y. Jo, B. S. Kang, Surface modification of γ-alumina membranes by silane coupling for CO_2 separation. *Journal of Membrane Science* **120**, 197 (1996).

114. N. Abidi *et al.*, Surface modification of mesoporous membranes by fluoro-silane coupling reagent for CO_2 separation. *Journal of Membrane Science* **270**, 101 (2006).

115. G. Z. Cao, J. Meijernik, H. W. Brinkman, A. J. Burggraaf, Permporometry study on the size distribution of active pores in porous ceramic membranes. *Journal of Membrane Science* **83**, 221 (1993).

116. Y.-S. Lin, Chemical and electrochemical vapor deposition of zirconia - yitria solid solutions in porous ceramic media, chemical engineering, university of twente. *PhD thesis*, p. 219 (1992).

117. S. Ek *et al.*, A 29Si and 13C CP/MAS NMR Study on the Surface Species of Gas-Phase-Deposited γ-Aminopropylalkoxysilanes on Heat-Treated Silica. *The Journal of Physical Chemistry B* **108**, 11454 (2004/08/01, 2004).

118. H. Ritter, M. Nieminen, M. Karppinen, D. Brühwiler, A comparative study of the functionalization of mesoporous silica MCM-41 by deposition of 3-aminopropyltrimethoxysilane from toluene and from the vapor phase. *Microporous and Mesoporous Materials* **121**, 79 (2009).

119. R. D. Lowe, M. A. Pellow, T. D. P. Stack, C. E. D. Chidsey, Deposition of dense siloxane monolayers from water and trimethoxyorganosilane vapor. *Langmuir* **27**, 9928 (2011).

120. S. Ek *et al.*, Atomic layer deposition of a high-density aminopropylsiloxane network on silica through sequential reactions of γ-aminopropyltrialkoxysilanes and water. *Langmuir* **19**, 10601 (2003).

121. S. Ek, E. I. Iiskola, L. Niinistö, Gas-Phase Deposition of Aminopropylalkoxysilanes on Porous Silica. *Langmuir* **19**, 3461 (2003/04/01, 2003).

122. G. Demirel, M. Çakmak, T. Çaykara, Ş. Ellialtıoğlu, Chemisorption of 3-Aminopropyltrimethoxysilane on Si(001)-(2 × 2). *The Journal of Physical Chemistry C* **111**, 15020 (2007/10/01, 2007).

123. M. H. V. Mulder, Basic principles of membrane technology, Kluwer Academic publishers. (1996).

124. N. Du, H. B. Park, M. M. Dal-Cin, M. D. Guiver, Advances in high permeability polymeric membrane materials for CO_2 separations. *Energy and Environmental Science* **5**, 7306 (2012).

125. K. Simons, Membrane technologies for CO_2 capture. *Ph.D. thesis, University of twente, The Netherlands*, (2010).

126. Y. Xiao, B. T. Low, S. S. osseini, T. S. Chung, D. R. Paul, The strategies of molecular architecture and modification of polyimide-based membranes for CO_2 removal from natural gas - A review. *Progress in Polymer Science* **34**, 561 (2009).

127. M.Wessling, S. Schoeman, T. V. d. Boomgaard, C. A. Smolders, Plasticization of gas separation membranes. *Gas separation & Purification* **5**, 222 (1991).

2

Vapor phase versus liquid phase grafting of meso-porous alumina

This chapter is adapted from:

V.G.P. Sripathi, Barbara L. Mojet, Arian Nijmeijer, Nieck E. Benes, 'Vapor phase versus liquid phase grafting of meso-porous alumina,' *Microporous and Mesoporous Materials* **172** 1 (2013).

Abstract

Functionalization of meso-porous γ-alumina has been performed by grafting of 3-Aminopropyltrimethoxysilane (3APTMS) from either the liquid phase or from the vapor phase. In both cases, after grafting nitrogen physisorption indicates that the materials remain meso porous with significant differences in pore morphology, and infrared spectroscopy analysis reveals the presence of adsorbed APTMS in different quantities. Grafting from the liquid phase is affected by pronounced oligomerization of the precursor molecules, resulting in relatively non-homogeneous grafting and ultimately in pore blocking. In contrast, grafting via the vapor phase results in a homogeneous monolayer of grafted molecules, with a thickness similar to the length of the 3APTMS molecule. Grafting via the vapor phase is relatively insensitive to the reaction temperature and the presence of water. This is explained by the low concentration of oligomers in the vapor phase, due to their low vapor pressure. This study clearly shows that for thin mono-layer functionalization vapor phase grafting is highly preferable.

2.1 Introduction

Surface modification of inorganic materials by organic groups is a topic of interest in numerous fields, including separation technology, catalysis, bio-medical applications, surface coating, and surface engineering (*1-4*). Advantages of these materials derive from the combination of versatile chemistry provided by the organic groups and the thermo-mechanical stability of the inorganic matrix. For instance, in organic-inorganic hybrid membranes confinement of a polymer, with desired molecular selectivity, in the nanometer size pores of an inorganic material affects the undesired effects of polymer swelling and plasticization.

Different approaches allow the accommodation of organic moieties on the internal pore surface of an inorganic material. One approach is via "sol-gel", in which organic groups can be introduced directly into the matrix of the inorganic material, by using precursors such as bridged polysilsesquioxanes (*5-7*). Another approach is "grafting", which involves covalent attachment of organic functional groups to the pore walls of the inorganic material.

A large number of grafting agents exists for functionalizing the surface of porous inorganic materials. In particular, amino-functionalized silanes have been studied extensively because of their advantages in a broad range of applications, such as CO_2 capture in power plants (*8*), adsorption of metal ions (*6*), catalysts (*7*), and drug delivery (*9*). Amino-functionalized grafted groups allow for subsequent coupling of a variety of functional organic species (*5, 10*). In addition to the amino-functionalized group, the silane can contain one to three hydrolysable groups (e.g., Si-OCH_3, Si-OC_2H_5). Grafting of the silane precursors involves hydrolysis and subsequent condensation of these hydrolysable groups with residual OH

groups on the pore surface of the inorganic material (*11*). In the case of a single hydrolysable group a covalent bond (Si– O) between silane and the oxide leaves no possibility for oligomerization with other silane molecules. In the case of two or three hydrolysable groups, oligomerization of silane molecules is more difficult to avoid (*12*) and can for instance result in pore blocking (*13*).

Two methods of grafting are used in literature; grafting from the liquid or solution phase (in the remainder denoted "solution phase grafting", SPG) and grafting from the vapor phase (in the remainder denoted "vapor phase grafting", VPG)". In SPG the liquid precursor solution is in direct contact with the substrate and, in addition to single precursor molecules, larger oligomers in the solution can also react with surface hydroxyl groups. The extent of precursor oligomerization is strongly affected by the presence of water (*14-17*). Onclin *et al.* and Wang *et al.* (*18, 19*) have observed that in wet conditions octadecyltrichlorosilane (OTS) molecules undergo hydrolysis and subsequent polycondensation before they reach the substrate surface. Consequently, in wet conditions the grafting of OTS is fast and generates inhomogeneous layers. Strong effects of the presence of trace water on grafting density, and even pore blocking, have been observed for 3-Aminopropyltrimethoxysilane (3APTMS) modified porous MCM-41 (*8, 11*). Even for dry solvents the presence of trace water appears to influence the pore size distribution of MCM-41 functionalized with 3APTMS (*20*). These observations substantiate that it is difficult to avoid oligomerization of tri-functional silanes in SPG.

In VPG, only molecules in the vapor phase can be in contact with the substrate. The vapor pressure of dimers and oligomers is much lower as compared to that of single precursor

molecules. Consequently, reactions between single precursor molecules and the surface hydroxyl groups will predominate, allowing for homogeneous surface coverage. In VPG the effects of trace water are expected to be less pronounced and the use of non-benign solvents can be avoided, in turn circumventing operations such as solvent removal. A number of studies have been performed on vapor phase deposition using alkoxysilanes (*21-24*) and chlorosilanes (*25-27*). Well-defined silylated surfaces have been obtained by VPG for chromatographic applications (*28*). Song *et al.* (*29*) have reproducibly produced smooth and homogeneous self-assembled monolayers of 3-APTMS on silicon wafers, via VPG. Haller *et al.* (*30*) have demonstrated differences between solution phase deposition and vapor phase deposition of aminosilanes on a semiconductor surface. For SPG, they obtained amorphous polymeric globules in the order of 100 nm due to the poly-condensation of tri-alkoxysilanes; in VPG, the formation of polymeric globules was prevented. Sugimura *et al.* (*31*) demonstrated the possibility to avoid competitive cross-linking of tri-functional silanes by using vapor phase deposition where the authors obtained thin homogeneous layers in the order of 1–2 nm thickness.

In the present study we investigate the benefits of VPG as compared to SPG for grafting of the internal pore surface of meso-porous alumina with an aminosilane. In particular, we investigate the relations between pore morphology of the material after grafting, and the molecular characteristics and aggregation state of the grafting agent. In this respect, we consider morphology to include the intrusion depth of molecules into the pores, and the grafting density of the functional groups on the surface.

2.2 Experimental

2.2.1 Materials

3-Aminopropyltrimethoxysilane (3APTMS, 97 % purity) and toluene (anhydrous 99.8 %) were obtained from sigma-Aldrich. Ethanol (~98 % purity) was obtained from Merck.

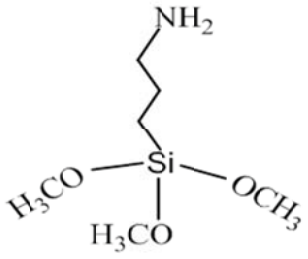

Figure 1: Chemical structure of 3-amonipropyltrimethoxysilane (3APTMS).

2.2.2 Synthesis of meso-porous alumina

Meso-porous γ-alumina flakes were prepared from a boehmite sol that was dried and subsequently calcined at 600 ^{o}C in air, as described in detail elsewhere (*32*).

2.2.3 Grafting on un-supported γ-alumina powders

The γ-alumina powders were pre-treated or cleaned by soaking in a 2:1 ethanol-water mixture for 24 hrs at ambient temperature, as reported in literature (2), followed by vacuum drying at 150 ^{o}C for 60 minutes. Equal amounts of pre-treated γ-alumina powders were placed in two round bottom (33) flasks, connected to each other by a horizontal glass tube (chapter 1, Figure 4, lower). Toluene and 3APTMS (3 wt %) were added to one round bottom flask (denoted as RB I). No liquid was added to the second round bottom flask (denoted as RB II). The powder in RB I was in direct contact with the liquid solution, the powder placed in RB II was only in contact with the toluene / aminosilane vapor allowed to pass through the

horizontal tube. Equal temperatures (50 or 80 ^{o}C) were maintained in the two RB flasks and the reaction was carried out for 3 hrs. All chemicals were added to the RB flasks inside the glove box prior to the start of the reaction.

After the reaction, the powder present in RB I (SPG sample) was separated from the solution by using a filter paper, in air.

2.2.4 Grafting on supported γ-alumina disk shaped membranes

Two γ-alumina membranes were pretreated by soaking in a 2:1 ethanol-water mixture for 24 hrs at ambient temperature as reported in literature (2), followed by vacuum drying at 150 ^{o}C for 60 minutes, similar to the un-supported γ-alumina powders. One pretreated membrane was placed inside a round bottom flask (RB) and a second membrane was placed upside down in a rack at the top of the round bottom flask (see the upper schematic in Figure 4 in Chapter 1). Toluene and 3APTMS (3 wt %) were added to RB flask. The membrane in RB flask was in direct contact with the liquid solution, the second membrane placed in the rack was only in contact with the toluene / aminosilane vapors produced in RB flask. The reaction was carried out at identical experimental conditions used above for powders: 3 hrs reaction time at controlled temperature (50, 80, or 120 ^{o}C).

2.2.5 Post-treatment

Subsequently, the powders and membranes were soaked in toluene (~10 hrs) and then in ethanol (~10 hrs), to remove physically adsorbed aminosilanes. Finally, the aminosilylated γ-alumina porous materials were annealed at 100 ^{o}C for 2 hrs in air. All experiments were repeated more than three times to check the reproducibility of the methods. The vapor

phase grafting method developed in this chapter has recently been used by several colleagues in the group Inorganic Membranes of the University of Twente, without any reproducibility problems (*34, 35*).

2.2.6 Materials characterization

The samples were characterized with transmission Fourier Transform Infrared Spectroscopy (FT-IR), using a Bruker Tensor 27 infrared spectrometer. Self-supporting pellets were measured at room temperature in ambient atmosphere. Pellets were prepared with KBr in 50:50 proportion with the sample. The morphology of the material was investigated with nitrogen gas physisorption at -196 ^{o}C on a Quantachrome Autosorb 1MP apparatus. Prior to the sorption experiments, all samples were degassed under vacuum at 200 ^{o}C for 12 hrs. The pore size distributions were estimated from the desorption branch of the isotherm by the Barret-Joyner-Halenda (BJH) method (*36, 37*). The total surface area (S_{BET}) was obtained using the standard Brunauer-Emmett-Teller (BET) method for adsorption data (*38*). The total pore volume (V_p) was calculated from the amount of nitrogen adsorbed at a relative pressure of 0.95.

The elemental characterization of 3APTMS functionalized meso-porous (~5 nm) disk shaped, supported γ-alumina membranes by vapor phase grafting and solution phase grafting are investigated by X-ray photoelectron spectroscopy (XPS). XPS analysis was carried out on grafted γ-alumina membranes using a PHI Quantera Scanning ESCA microprobe at a spatial resolution < 10 µm. Al-Kα monochromatic X-rays (1486.6 ev) have been generated at an accelerating voltage of 25 V and a 2.6 mA emission current. The atomic percentages of Si, Al, N and C were determined by the atomic concentrations calculated from energy bands of

respective atoms. The sum of Al, Si, C and N is considered as 100 %. Pore intrusion of aiminosilanes was analyzed through depth profiles by sputtering with an Ar^+ beam (3 kV) on a 2×2 mm area, with an estimated sputter rate of 20 nm/min.

2.3 Results & Discussion

2.3.1 Un-supported γ-alumina powders

2.3.1.1 N_2-physisorption Characterization

Figure 2a depicts the N_2-physisorption isotherms of γ-alumina grafted with 3APTMS by SPG and VPG. The corresponding pore size distribution curves are shown in Figure 2b. The specific BET surface area, pore volumes and pore sizes of original and grafted γ-alumina materials are summarized in Table 1.

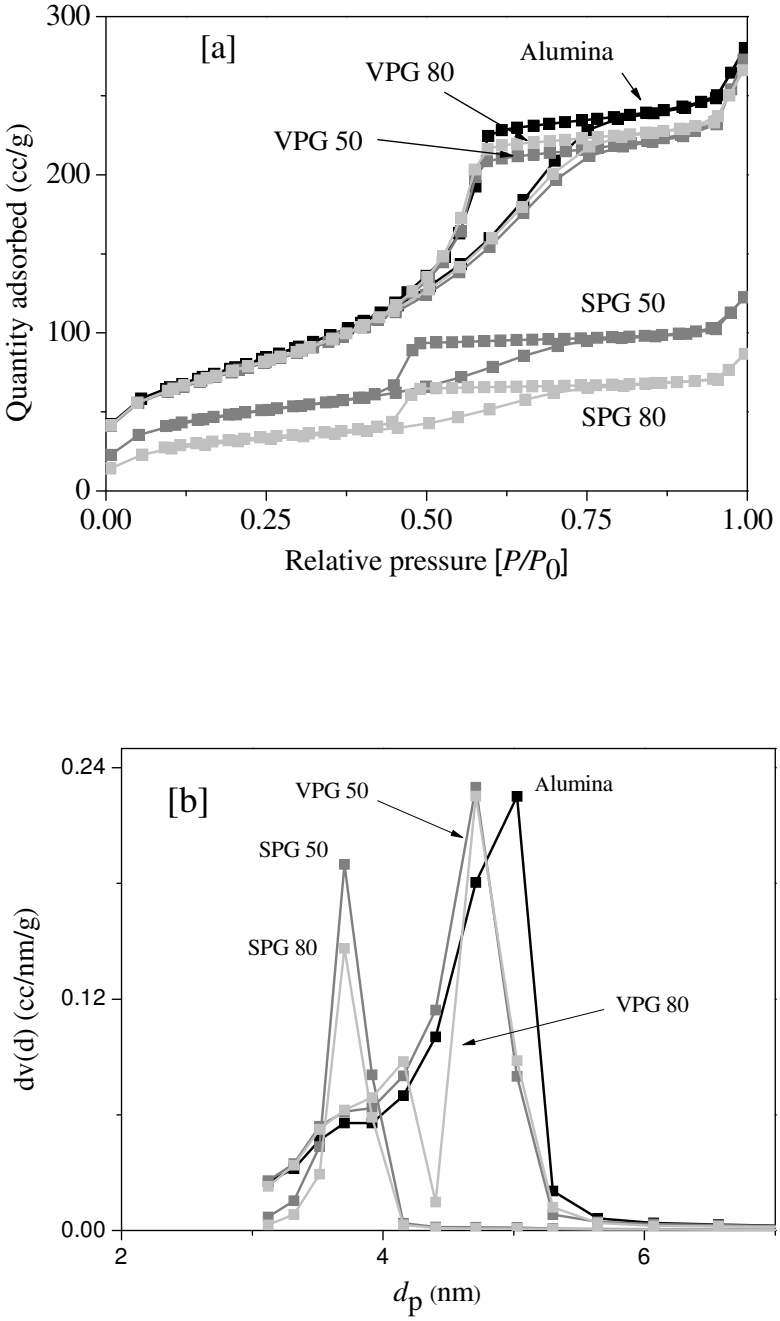

Figure 2: N_2-physisorption analysis of γ-alumina before and after grafting with 3APTMS, from either the vapor or liquid phase (a) sorption isotherms (b) corresponding pore size distribution curves.

All the obtained sorption isotherms are Type IV, indicating that the materials remain meso-porous after grafting. This is in agreement with the earlier study of Van Castricum *et al.* (*32*). After grafting, sorption of N_2 has decreased. This effect is more pronounced for SPG than for VPG.

For VPG, no significant change in pore volume was observed. However, the BET surface area decreases slightly from 320 to 300 m^2/g and the average pore diameter reduces from 5.0 to 4.6 nm. The ~0.4 nm reduction in mode of the pore size distribution is small but significant given the resolution of nitrogen sorption characterization (*20, 36-39*). The reduction in pore size is comparable to the length of the aminosilane molecule, ~0.5±0.1 nm (*40-45*), which is consistent with the uniform formation of a thin layer of grafted molecules on the pore surface with a thickness in the range of the molecular size of the precursor. The uniform film formation originates from prevalence of reactions of silanes with surface reactive groups, instead of oligomerization reactions. The thicknesses of the grafted layers, obtained by our VPG method, are in good agreement with the observations of Kurth *et al*. (*40, 41*), who obtained very thin aminosilane films on dry (0.5±0.1 nm) and wet (1.1±0.1 nm) silicon wafers by the vapor phase method. Crampton *et al.* (*45*) reported deposition of aminopropyltriethoxysilane (APTES) on mica in the presence of a base catalyst under 7% and 60% humidity. This resulted in 0.54 nm thick APTES films at 7% humidity and 1.6 nm thick films at 60% humidity. Fiorilli *et al.* (*43*) compared vapor phase grafting and solution phase grafting of aminosilanes self assembled monolayers (SAMs) on silicon substrates. For grafting from the vapor phase, using AFM they observed the formation of smooth and uniform layers formed with very few aggregates of APTES. This was attributed to the low

concentration of APTES oligomers in the vapor phase, which is in agreement with our investigations. Zhang *et al.* (*46*) reported the similar investigations of vapor phase grafting of APTES on dehydrated silicon surface at 150 ^{o}C. They found the thickness of the aminosilane film is 0.81±0.02 nm even after 6 months storage of samples, attributing to the stability of the aminosilanized substrates.

The formation of a thin film on the surface, with thickness in the range of the molecular size of the precursor, is contrary to observations from extensive investigations reported on pore blocking by solution phase grafting (*13, 20, 47*). For SPG, the strong reduction in nitrogen sorption results from filling of the pores with the aminosilane precursor, and from partial blocking of the pores impeding N_2 transport (*47, 48*). The reduction of the mode of the pore size distribution from 5 to 3.7 nm (Table 1) suggests formation of relatively thick layers of aminosilanes by oligomerization of adjacent aminosilanes (*22, 40, 43, 45*) as depicted schematically in Figure 3.

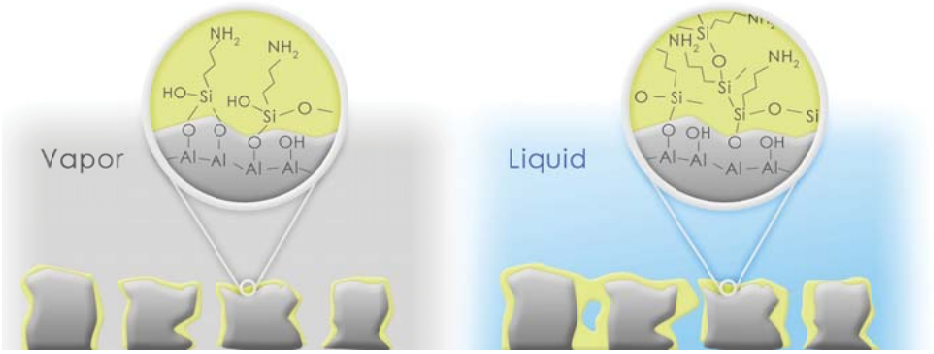

Figure 3: Graphical representation showing monolayer formation with vapor phase grafting (vapor) and multi-layer formation by solution phase grafting (liquid).

The effect of temperature on grafting is more pronounced for SPG as compared to VPG. For both methods an increase in reaction temperature from 50 ^{o}C to 80 ^{o}C has no significant effect on the mode of the pore size distribution (Figure 2b). For SPG the increase in temperature is accompanied by a stronger reduction in the total amount of nitrogen sorption (Figure 2a), a reduction in pore volume (Figure 2b), and a reduction in the BET surface area (Table 1). This can be attributed to a higher rate of oligomerization at higher temperature (*49*). The higher rate of oligomerization has minor effect on the monolayer formation in VPG. This is attributed to the low concentration of oligomers in the vapor phase, due to their relatively low vapor pressure.

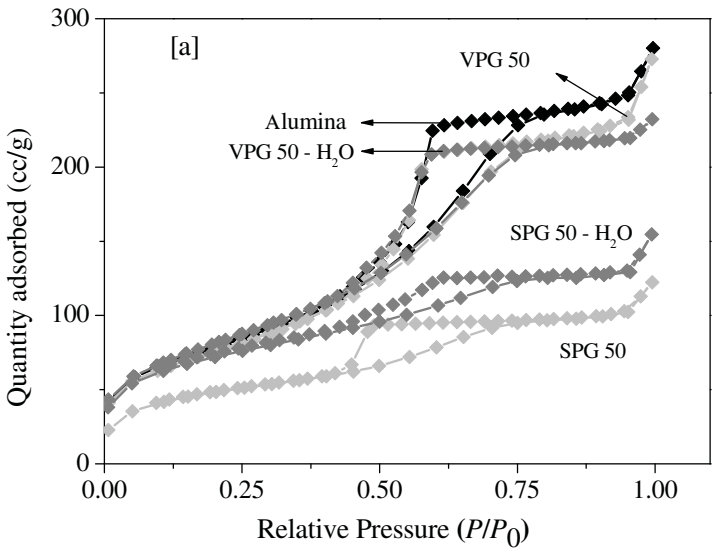

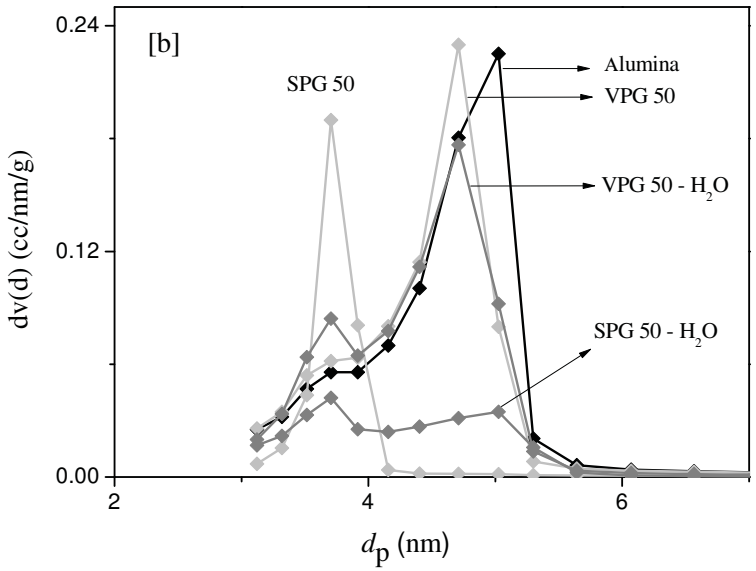

Figure 4: N_2-physisorption analysis of γ-alumina before and after grafting with 3APTMS, in the absence and presence of water (a) sorption isotherms (b) corresponding pore size distribution curves.

Figure 4 depicts the effect of water in the reaction mixture on the nitrogen isotherms obtained after grafting. The effect of water is much more pronounced in the case of SPG as compared to VPG. For VPG the shape of the isotherm is not significantly affected. For SPG, the amount of nitrogen sorption decreases and the shape, in particular the hysteresis, of the isotherm changes. The addition of water is expected to result in a higher rate of oligomerziation (*15, 50-52*). In contrast, after the grafting in the presence of water the amount of nitrogen sorption is higher and the mode of the pore size distribution is larger. This indicates less effective and non-homogeneous grafting, and is probably due to pore blocking of entrances during grafting in the presence of water. Pore blocking substantially reduces the transport of precursor molecules into the pore structure of the alumina (*13, 20,*

47). The influence of water was extensively investigated by Britt *et al.* (*51*), who reported AFM investigations on octadecyltrichlorosilane (OTS) self-assembled layer formation on a mica surface. In the presence of excess water on mica, deposition of 200 nm thick clusters or islands, of OTS oligomers in less than 10 seconds reaction time was observed. As the reaction time was prolonged to 40 seconds, the thickness of the islands increased to 1 µm. After 300 seconds the surface was completely covered. In partially hydrated mica, the formation of uniformly distributed OTS clusters on the surface was observed from the beginning of the reaction and no large islands were observed. For more literature on water/moisture influence on silanization of various silane precursors, see chapter 1.

Method	Reaction *T* [^{o}C]	Water [ppm]	S_{BET} [m^2/g]	d_p, BJH [nm]	V_p, BJH [cc/g]	Ref.
Unmodified	-----	----	320	5.0	0.43	PS
SPG	50	----	130	3.7	0.16	PS
VPG	50	----	300	4.6	0.42	PS
SPG	80	----	95	3.7	0.12	PS
VPG	80	----	295	4.8	0.42	PS
SPG	50	50	107	3.7	0.16	PS
VPG	50	50	285	4.8	0.33	PS
SPG		----	215	3.8	0.22	34

Table 1: Structural properties of 3APTMS grafted meso-porous γ-alumina (PS: present study). The same batch of γ-alumina powder is used for all experiments in this chapter in order to minimize the error

contribution from powder synthesis. S_{BET}: BET-surface area obtained between 0.05 – 0.2 P/P_0. V_p and d_p: Meso-pore volume and pore diameter respectively, calculated by BJH method.

2.3.1.2 FT-IR characterization

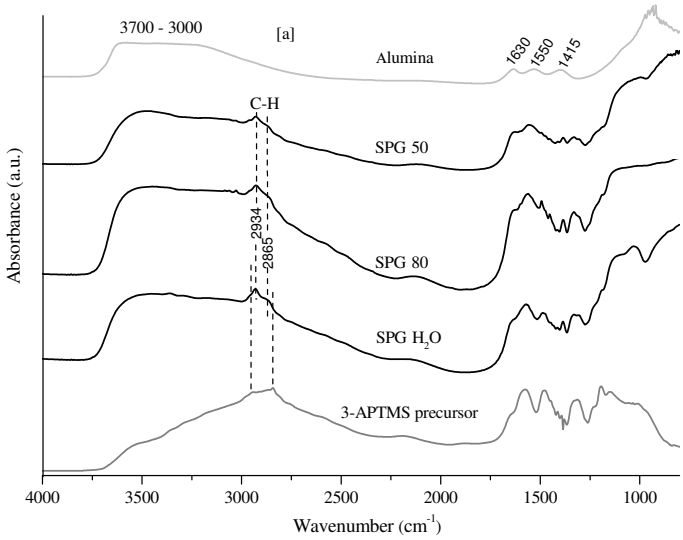

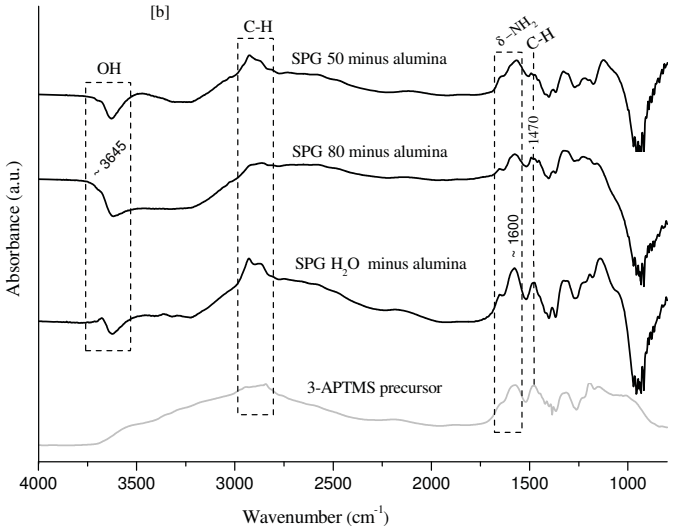

Figure 5: a) FTIR spectra of SPG grafted samples. The spectra of the pure support and 3APTMS on KBr have been added for reference. The spectra have been shifted along the *y*-axis for clarity. b) Difference FTIR spectra for SPG treated samples: original spectrum minus the γ-alumina contribution.

Figure 5a shows the FT-IR spectra of meso-porous γ-alumina before and after grafting with 3APTMS at different temperatures via SPG. The support γ-alumina is characterized by a broad band between 3700 and 3000 cm^{-1} that can be attributed to the presence of physisorbed water on the alumina hydroxyls. This is confirmed by a sharp band at 1630 cm^{-1}, representing the bending mode in adsorbed water (*53*). The additional broad band at 1550 cm^{-1} has been attributed in literature to stretching vibrations of the Al-OH bond and the band at 1415 cm^{-1} might be because of residual nitrates (*54*) or organic groups, such as PVA (*55*) used in the sol preparation of the γ-alumina. The steep increase below 1200 cm^{-1} is due to extensive framework vibrations that are not well resolved. SPG-grafting of the γ-alumina leads to additional bands in the FTIR spectra as can be seen in Figure 5a. Grafting results in a decrease in the intensity of band at 3400 cm^{-1}, indicating part of the hydroxyl groups react with the aminosilane. The persistence of a broad band at 3400 cm^{-1} suggests that some of the surface hydroxyl groups are still present. It is known that only single and geminal hydroxyl groups are able to react with silanes, whereas hydrogen bonded hydroxyl groups are inaccessible for such a reaction (*48, 56*).

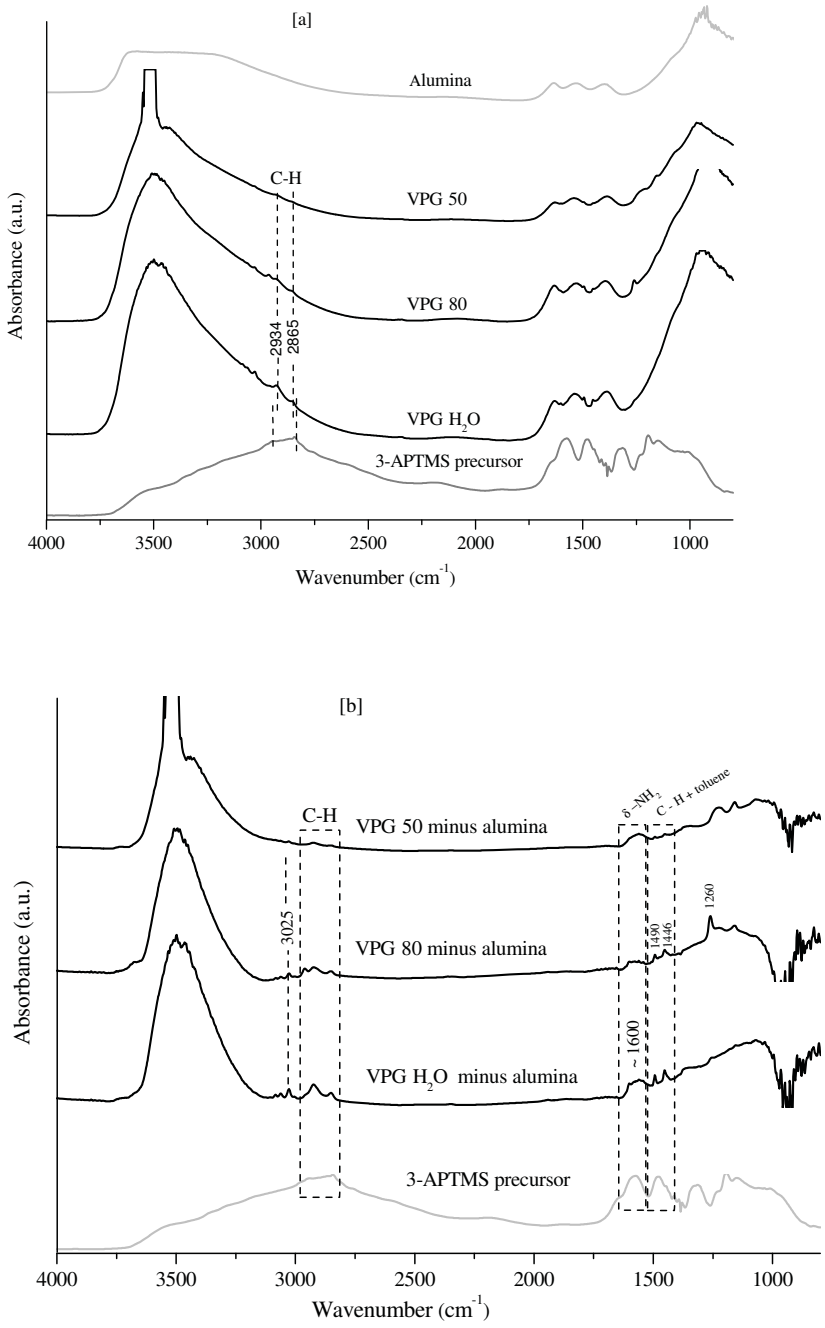

Figure 6: a) FTIR spectra of VPG grafted samples. The spectra of the pure support and 3APTMS on KBr have been added for reference. The spectra have been shifted along the *y*-axis for clarity. b) Difference FTIR

spectra for VPG treated samples: original spectrum minus the γ-alumina contribution (which was minimized between 1700 – 1200 cm^{-1}).

Figure 5b shows the difference spectra for the SPG samples after subtraction of the γ-alumina spectrum. A clear negative peak at 3645 cm^{-1} can be seen after grafting, which confirms the reaction between alumina hydroxyls and APTMS. In addition, between 3000 and 2800 cm^{-1} bands are observed that can be assigned to C-H stretching of the propyl-chains present in APTMS. Between 1700 and 1200 cm^{-1} the difference spectra for all three samples very much resemble the pure APTMS spectra, suggesting the presence of large oligomers on the surface of the γ-alumina.

The FT-IR data provide no direct indication of the presence of Al-O-Si bonds. The symmetric and asymmetric stretching modes of Si-O bonds are located between 1100 - 990 cm^{-1} (*57-59*) and the region 1100 – 800 cm^{-1} is obscured by Al-O-Al bonds of γ-alumina (*60*). However, the covalent attachment of silanes on γ-alumina substrate has been confirmed by NMR investigations (*60*).

Figure 6a shows the FTIR data for the VPG samples together with the pure γ-alumina support for comparison. Clearly after the VPG treatment only minor changes are observed in the spectra. Still a broad band due to water adsorption on the surface is observed, suggesting a low coverage of adsorbed APTMS after the VPG treatment. For a better comparison the spectrum of the γ-alumina support has been subtracted and the resulting difference spectra are shown in Figure 6b together with the spectrum of APTMS. For all three samples distinct bands are visible at 2934 and 2865 cm^{-1} that represent the CH_2-sym and CH_2-as vibrations from the propyl chains in APTMS. These bands are much better

resolved than for the SPG samples, pointing to their isolated presence in the VPG-samples. It is obvious that the bulk APTMS structure cannot be found in the VPG samples. However, a shoulder is observed at 1600 cm^{-1} that can be assigned to the δ-NH_2 (*8, 57, 61*). Both the intensities of the C-H and N-H vibrations increase in the order VPG-50 < VPG-80 < VPG-H_20.

The small vibrations between 3100 – 3000 cm^{-1} and at 1490 and 1446 cm^{-1} are due to residual toluene in the samples. The peak at 1260 cm^{-1} is assigned to methyl stretching of a trace contaminant, probably methyltrichlorosilane. For VPG the concentration of 3-APTMS on the surface is relatively low and the presence of this contaminant becomes apparent.

The samples treated via VPG reveal only weak bands associated with the Si-O bond, suggesting grafting of a thin layer. More extensive oligomerization of the aminosilane precursor molecules is expected for SPG, because the oligomeric molecules formed in the liquid water can participate in the surface reaction. In contrast, in VPG the larger oligomer molecules will remain in the liquid phase due to their relatively low vapor pressure. This indicates SPG is more sensitive of to the presence of trace water. This is further substantiated by varying the water concentration during grafting. For VPG no significant effect of water observed. In SPG the addition of water has a pronounced effect; the water enhances the degree of oligomerization. The effect of temperature on the FT-IR data is not significant for SPG and VPG.

In summary, for VPG a homogeneous monolayer of grafted aminosilanes can be obtained, heedless of the reaction temperature and the presence of trace water. For SPG oligomerization of the aminosilanes results in less homogeneous grafting inside the meso-porous structure and possibly in partial pore blocking, in particular at higher temperature

and in the presence of water. This implies VPG is the preferable approach for controlled functionalizing of the internal pore surface with a thin layer of molecules, e.g., with linker groups, without pore blocking.

2.3.2 Supported γ-alumina membranes

2.3.2.1 X-ray photo electron spectroscopy (XPS)

Figure 7 depicts elemental survey scans by XPS on the external top surface of γ-alumina membranes, after 3APTMS treatment. The survey scans show no other elements than the expected Al, Si, C, O and N. The presence of Si (~150 eV) in all 3APTMS treated samples suggests the successful grafting of aminosilanes, by both SPG and VPG. For membranes treated by SPG, no elemental band for aluminum (Al) (Figure 7a) was observed, indicating that the external surface is completely covered with an aminosilane layer. This can be explained by the deposition of oligomerized aminopropylsilanes; the trifunctional silanes undergo self-condensation (*26, 47*). In contrast, the elemental band for Al is apparent (Figure 7b) for VPG treated membranes, indicating a low concentration of aminosilanes on the external surface of the membrane.

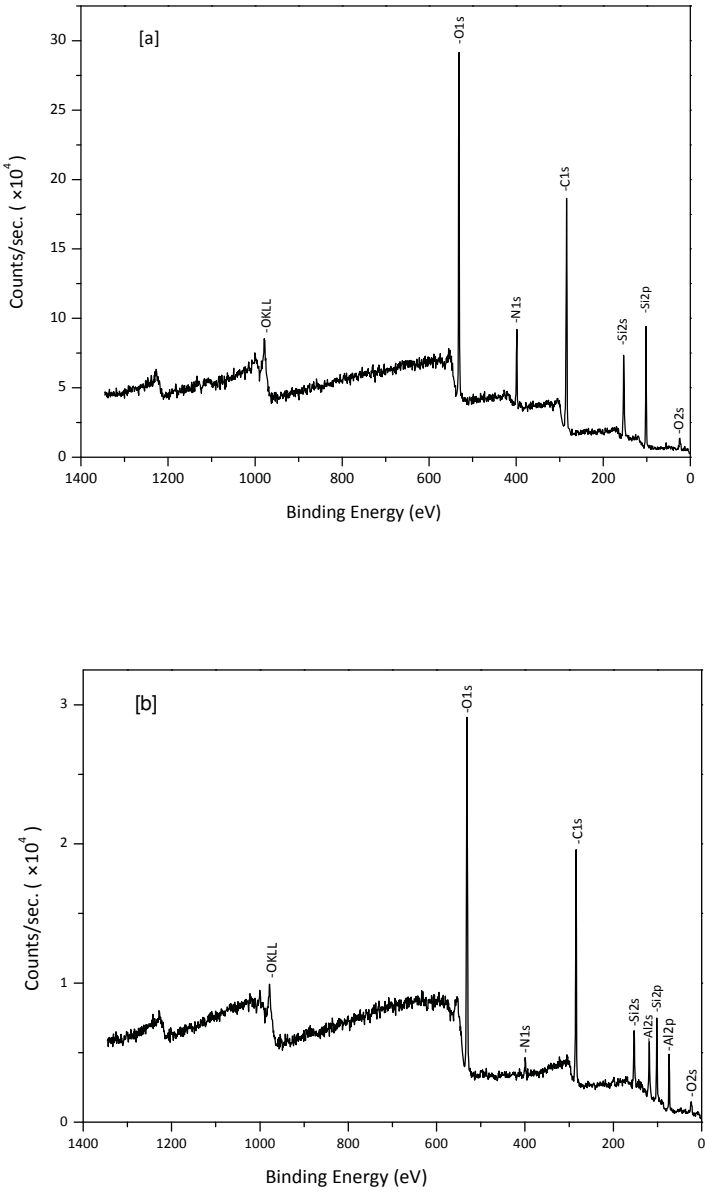

Figure 7: XPS survey scans of the external top surface of γ-alumina membranes obtained after 3APTMS grafting at 80 °C by (a) SPG and (b) VPG.

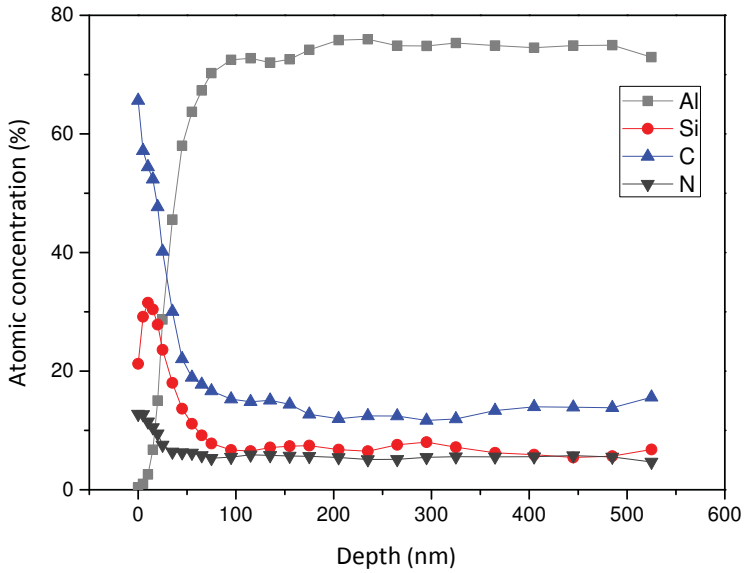

Figure 8: XPS depth profiles showing Al, Si, C and N atomic concentrations on/in the γ-alumina membrane functionalized with 3APTMS by SPG at 80 °C as a function of pore depth.

Figure 8 depicts atomic concentration profiles of Al, Si, C and N as a function of pore depth (up to 500 nm) in the γ-alumina layer treated with 3APTMS by solution phase grafting (SPG). At zero depth, i.e., on the external surface of the membrane, no Al is observed, and the atomic concentration of Si is around 20 %. Assuming that experimental inaccuracy is the cause for deviations between in elemental ratios of Si, C and N from XPS and APTES, this is in agreement with the presence of a polymerized aminopropylsilane layer completely covering the external surface of the membrane.

This is also in agreement with the results obtained for powders (Figure 2 and Figure 5) as well with as the reported depth profiles of trichloromethylsilane by Sah *et al.* (*47*). For

increasing depth, the elemental concentration of the silicon reduces; this is due to a limited transport rate of, in particular oligomerized, aminosilanes into and inside the pores.

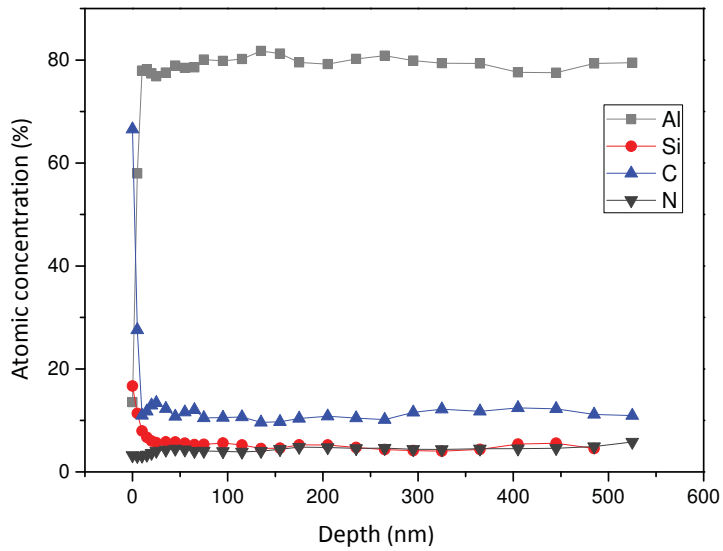

Figure 9: XPS depth profiles showing Al, Si, C and N atomic concentrations on/in the γ-alumina membrane functionalized with 3APTMS by VPG at 80 °C as a function of pore depth.

In case of 3APTMS treated γ-alumina membranes by VPG a significant concentration (~12 %) of Al is observed on the membrane surface, combined with a lower Si concentration as compared to the SPG method. This indicates a low concentration of aminosilanes on the membrane surface, which can be explained by the low deposition of oligomers, due to their low vapor pressure (*40*).

The XPS data are consistent with the FT-IR and nitrogen sorption data and suggest a thin layer of 3APTMS is grafted onto the pore surface of the γ-alumina. The grafting of aiminosilanes by VPG is further confirmed by successful subsequent grafting with (hexafluoroisopropylidene) diphthalic anhydride (6FDA), see chapter 3 for more

information. The formation of a thin film in VPG, without blocking of pores by polymerized 3APTMS as occurs with SPG, can be considered beneficial for such a sequential grafting approach. This will be investigated further in this thesis.

2.4 Conclusions

Functionalization of meso-porous γ-alumina powders and supported membranes was performed by grafting 3APTMS from the liquid phase and from the vapor phase. After grafting, the material remains meso-porous. Depending on the grafting conditions, significant differences in pore morphology are observed. FT-IR characterization confirms the presence of Si-O and -NH_2 bonds after grafting. Grafting from the liquid phase is affected by oligomerization of the precursor molecules. The presence of oligomers in the liquid phase results in relatively non-homogeneous grafting, and ultimately in pore blocking. This is more pronounced at higher reaction temperature and, especially, in the presence of water. A higher reaction temperature and presence of water cause the rate of oligomerization to increase. In contrast, when grafting occurs in the vapor phase a homogeneous monolayer of grafted molecules is obtained, with a thickness similar to the length of the grafting molecule. Grafting in the vapor phase is relatively insensitive to the reaction temperature and the presence of water. This is explained by the low concentration of oligomers in the vapor phase, due to their low vapor pressure. A higher rate of oligomeriziation results in more and larger oligomers in the liquid phase, but in the vapor phase the presence of unreacted precursor molecules prevails. As such, vapor phase grafting is preferable when the aim is to achieve thin mono-layer functionalization, allowing effective further sequential

grafting inside the porous structure. Grafting from the liquid phase is more suitable when the aim is to obtain thick multi-layers.

Acknowledgements

This is an Institute of Sustainable Process Technology (ISPT) project. We acknowledge the help of Koteswara Rao Nidadavolu with IR experiments.

References

1. A. Javaid, D. A. Krapchetov, D. M. Ford, Solubility-based gas separation with oligomer-modified inorganic membranes: Part III. Effects of synthesis conditions. *Journal of Membrane Science* **246**, 181 (2005).

2. A. Javaid, D. M. Ford, Solubility-based gas separation with oligomer-modified inorganic membranes: Part II. Mixed gas permeation of 5 nm alumina membranes modified with octadecyltrichlorosilane. *Journal of Membrane Science* **215**, 157 (2003).

3. J. Salonen, V. P. Lehto, Fabrication and chemical surface modification of mesoporous silicon for biomedical applications. *Chemical Engineering Journal* **137**, 162 (2008).

4. D. F. Stamatialis *et al.*, Medical applications of membranes: Drug delivery, artificial organs and tissue engineering. *Journal of Membrane Science* **308**, 1 (2008).

5. C. Li, T. Glass, G. L. Wilkes, NMR Studies of Sol-Gel Derived Hybrid Materials Based on Triethoxysilylated Diethylenetriamine and Tetramethoxysilane. *Journal of Inorganic and Organometallic Polymers* **9**, 79 (1999).

6. K. J. Shea, D. A. Loy, Bridged polysilsesquioxanes. Molecular-engineered hybrid organic-inorganic materials. *Chemistry of Materials* **13**, 3306 (2001).

7. D. A. Loy *et al.*, Dialkylene carbonate-bridged polysilsesquioxanes. Hybrid organic-inorganic sol-gels with a thermally labile bridging group. *Chemistry of Materials* **11**, 3333 (1999).

8. F.-Y. Chang, K.-J. Chao, H.-H. Cheng, C.-S. Tan, Adsorption of CO2 onto amine-grafted mesoporous silicas. *Separation and Purification Technology* **70**, 87 (2009).

9. F. Balas, M. Manzano, P. Horcajada, M. Vallet-Regí, Confinement and Controlled Release of Bisphosphonates on Ordered Mesoporous Silica-Based Materials. *Journal of the American Chemical Society* **128**, 8116 (2006/06/01, 2006).

10. S. Sawamoto *et al.*, Nanotechnological method to control pore diameter of organic–inorganic composite membrane: Part II. Molecular-wise vapor polymerization (MVP). *Journal of Membrane Science* **174**, 151 (2000).

11. K. K. Sharma, T. Asefa, Efficient bifunctional nanocatalysts by simple postgrafting of spatially isolated catalytic groups on mesoporous materials. *Angewandte Chemie - International Edition* **46**, 2879 (2007).

12. H. Salmio, D. Brühwiler, Distribution of Amino Groups on a Mesoporous Silica Surface after Submonolayer Deposition of Aminopropylsilanes from an Anhydrous Liquid Phase. *The Journal of Physical Chemistry C* **111**, 923 (2007/01/01, 2006).

13. Z. D. Hendren, J. Brant, M. R. Wiesner, Surface modification of nanostructured ceramic membranes for direct contact membrane distillation. *Journal of Membrane Science* **331**, 1 (2009).

14. A. V. Krasnoslobodtsev, S. N. Smirnov, Effect of Water on Silanization of Silica by Trimethoxysilanes. *Langmuir* **18**, 3181 (2002/04/01, 2002).

15. C. P. Tripp, M. L. Hair, Direct Observation of the Surface Bonds between Self-Assembled Monolayers of Octadecyltrichlorosilane and Silica Surfaces: A Low-Frequency IR Study at the Solid/Liquid Interface. *Langmuir* **11**, 1215 (1995/04/01, 1995).

16. D. L. Angst, G. W. Simmons, Moisture absorption characteristics of organosiloxane self-assembled monolayers. *Langmuir* **7**, 2236 (1991/10/01, 1991).

17. P. Silberzan, L. Leger, D. Ausserre, J. J. Benattar, Silanation of silica surfaces. A new method of constructing pure or mixed monolayers. *Langmuir* **7**, 1647 (1991/08/01, 1991).

18. S. Onclin, B. J. Ravoo, D. N. Reinhoudt, Engineering Silicon Oxide Surfaces Using Self-Assembled Monolayers. *Angewandte Chemie International Edition* **44**, 6282 (2005).

19. Y. Wang, M. Lieberman, Growth of Ultrasmooth Octadecyltrichlorosilane Self-Assembled Monolayers on SiO2. *Langmuir* **19**, 1159 (2003/02/01, 2003).

20. H. Ritter, M. Nieminen, M. Karppinen, D. Brühwiler, A comparative study of the functionalization of mesoporous silica MCM-41 by deposition of 3-aminopropyltrimethoxysilane from toluene and from the vapor phase. *Microporous and Mesoporous Materials* **121**, 79 (2009).

21. S. Ek, E. I. Iiskola, L. Niinistö, Gas-Phase Deposition of Aminopropylalkoxysilanes on Porous Silica. *Langmuir* **19**, 3461 (2003/04/01, 2003).

22. W. Yoshida, R. P. Castro, J.-D. Jou, Y. Cohen, Multilayer Alkoxysilane Silylation of Oxide Surfaces. *Langmuir* **17**, 5882 (2001/09/01, 2001).

23. L. D. White, C. P. Tripp, Reaction of (3-Aminopropyl)dimethylethoxysilane with Amine Catalysts on Silica Surfaces. *Journal of Colloid and Interface Science* **232**, 400 (2000).

24. C. P. Tripp, M. L. Hair, Reaction of chloromethylsilanes with silica: a low-frequency infrared study. *Langmuir* **7**, 923 (1991/05/22, 1991).

25. A. Y. Fadeev, T. J. McCarthy, Trialkylsilane Monolayers Covalently Attached to Silicon Surfaces: Wettability Studies Indicating that Molecular Topography Contributes to Contact Angle Hysteresis. *Langmuir* **15**, 3759 (1999/05/01, 1999).

26. A. Y. Fadeev, T. J. McCarthy, Self-Assembly Is Not the Only Reaction Possible between Alkyltrichlorosilanes and Surfaces: Monomolecular and Oligomeric Covalently Attached Layers of Dichloro- and Trichloroalkylsilanes on Silicon. *Langmuir* **16**, 7268 (2000/09/01, 2000).

27. C. M. Stafford, A. Y. Fadeev, T. P. Russell, T. J. McCarthy, Controlled Adsorption of End-Functionalized Polystyrene to Silicon-Supported Tris(trimethylsiloxy)silyl Monolayers. *Langmuir* **17**, 6547 (2001/10/01, 2001).

28. P. Wikström, C. F. Mandenius, P.-o. Larsson, Gas phase silylation, a rapid method for preparation of high-performance liquid chromatography supports. *Journal of Chromatography A* **455**, 105 (1988).

29. X. Song, J. Zhai, Y. Wang, L. Jiang, Self-assembly of amino-functionalized monolayers on silicon surfaces and preparation of superhydrophobic surfaces based on alkanoic acid dual layers and surface roughening. *Journal of Colloid and Interface Science* **298**, 267 (2006).

30. I. Haller, Covalently attached organic monolayers on semiconductor surfaces. *Journal of the American Chemical Society* **100**, 8050 (1978/12/01, 1978).

31. H. Sugimura, A. Hozumi, T. Kameyama, O. Takai, Organosilane self-assembled monolayers formed at the vapour/solid interface. *Surface and Interface Analysis* **34**, 550 (2002).

32. H. L. Castricum, A. Sah, M. C. Mittelmeijer-Hazeleger, J. E. ten Elshof, Hydrophobisation of mesoporous γ-Al_2O_3 with organochlorosilanes—efficiency and structure. *Microporous and Mesoporous Materials* **83**, 1 (2005).

33. N. Abidi *et al.*, Surface modification of mesoporous membranes by fluoro-silane coupling reagent for CO_2 separation. *Journal of Membrane Science* **270**, 101 (2006).

34. A. F. d. M. Pinheiro, Development and charecterization of polymer-grafted ceramic membranes for solvent nanofiltration. *Ph.D. thesis, University of Twente*, (2013).

35. Velianti, M. Sc. thesis, Inorganic Membranes Group, University of Twente (2010).

36. E. P. Barrett, L. G. Joyner, P. P. Halenda, The Determination of Pore Volume and Area Distributions in Porous Substances. I. Computations from Nitrogen Isotherms. *Journal of the American Chemical Society* **73**, 373 (1951/01/01, 1951).

37. N. Gartmann, C. Schütze, H. Ritter, D. Brühwiler, The Effect of Water on the Functionalization of Mesoporous Silica with 3-Aminopropyltriethoxysilane. *The Journal of Physical Chemistry Letters* **1**, 379 (2010/01/07, 2009).

38. S. Brunauer, P. H. Emmett, E. Teller, Adsorption of Gases in Multimolecular Layers. *Journal of the American Chemical Society* **60**, 309 (1938/02/01, 1938).

39. H. Ritter, D. Brühwiler, Accessibility of Amino Groups in Postsynthetically Modified Mesoporous Silica. *The Journal of Physical Chemistry C* **113**, 10667 (2009/06/18, 2009).

40. D. G. Kurth, T. Bein, Thin Films of (3-Aminopropyl)triethoxysilane on Aluminum Oxide and Gold Substrates. *Langmuir* **11**, 3061 (1995/08/01, 1995).

41. D. G. Kurth, T. Bein, Monomolecular layers and thin films of silane coupling agents by vapor-phase adsorption on oxidized aluminum. *The Journal of Physical Chemistry* **96**, 6707 (1992/08/01, 1992).

42. F. Zhang *et al.*, Chemical vapor deposition of three aminosilanes on silicon dioxide: surface characterization, stability, effects of silane concentration, and cyanine dye adsorption. *Langmuir* **26**, 14648 (Sep 21, 2010).

43. S. Fiorilli *et al.*, Vapor-phase self-assembled monolayers of aminosilane on plasma-activated silicon substrates. *Journal of Colloid and Interface Science* **321**, 235 (2008).

44. E. Asenath Smith, W. Chen, How To Prevent the Loss of Surface Functionality Derived from Aminosilanes. *Langmuir* **24**, 12405 (2008/11/04, 2008).

45. N. Crampton, W. A. Bonass, J. Kirkham, N. H. Thomson, Formation of Aminosilane-Functionalized Mica for Atomic Force Microscopy Imaging of DNA. *Langmuir* **21**, 7884 (2005/08/01, 2005).

46. F. Zhang *et al.*, Chemical Vapor Deposition of Three Aminosilanes on Silicon Dioxide: Surface Characterization, Stability, Effects of Silane Concentration, and Cyanine Dye Adsorption. *Langmuir* **26**, 14648 (2010/09/21, 2010).

47. A. Sah, H. L. Castricum, A. Bliek, D. H. A. Blank, J. E. ten Elshof, Hydrophobic modification of γ-alumina membranes with organochlorosilanes. *Journal of Membrane Science* **243**, 125 (2004).

48. S. Kim, J. Ida, V. V. Guliants, Y. S. Lin, Tailoring Pore Properties of MCM-48 Silica for Selective Adsorption of CO2. *The Journal of Physical Chemistry B* **109**, 6287 (2005).

49. R. M. Pasternack, S. Rivillon Amy, Y. J. Chabal, Attachment of 3-(Aminopropyl)triethoxysilane on Silicon Oxide Surfaces: Dependence on Solution Temperature. *Langmuir* **24**, 12963 (2008/11/18, 2008).

50. J. Sagiv, Organized monolayers by adsorption. 1. Formation and structure of oleophobic mixed monolayers on solid surfaces. *Journal of the American Chemical Society* **102**, 92 (1980/01/01, 1980).

51. D. W. Britt, V. Hlady, An AFM Study of the Effects of Silanization Temperature, Hydration, and Annealing on the Nucleation and Aggregation of Condensed OTS Domains on Mica. *Journal of Colloid and Interface Science* **178**, 775 (1996).

52. H. O. Finklea *et al.*, Formation of an organized monolayer by solution adsorption of octadecyltrichlorosilane on gold: electrochemical properties and structural characterization. *Langmuir* **2**, 239 (1986/03/01, 1986).

53. A. Vázquez *et al.*, X-Ray Diffraction, FTIR, and NMR Characterization of Sol–Gel Alumina Doped with Lanthanum and Cerium. *Journal of Solid State Chemistry* **128**, 161 (1997).

54. M. K. Naskar, Hydrothermal Synthesis of Petal-Like Alumina Flakes. *Journal of the American Ceramic Society* **92**, 2392 (2009).

55. H. Vigué, P. Quintard, T. Merle-Méjean, V. Lorenzelli, An FT–IR Study of the Chlorination of γ-Alumina Surfaces. *Journal of the European Ceramic Society* **18**, 305 (1998).

56. X. S. Zhao, G. Q. Lu, A. K. Whittaker, G. J. Millar, H. Y. Zhu, Comprehensive Study of Surface Chemistry of MCM-41 Using 29Si CP/MAS NMR, FTIR, Pyridine-TPD, and TGA. *The Journal of Physical Chemistry B* **101**, 6525 (1997/08/01, 1997).

57. Y.-F. Chen, Y.-H. Hu, Y.-I. Chou, S.-M. Lai, C.-C. Wang, Surface modification of nano-porous anodic alumina membranes and its use in electroosmotic flow. *Sensors and Actuators B: Chemical* **145**, 575 (2010).

58. S. Barrientos-Ramírez *et al.*, Surface modification of natural halloysite clay nanotubes with aminosilanes. Application as catalyst supports in the atom transfer radical polymerization of methyl methacrylate. *Applied Catalysis A: General* **406**, 22 (2011).

59. P. Yuan *et al.*, Functionalization of Halloysite Clay Nanotubes by Grafting with γ-Aminopropyltriethoxysilane. *The Journal of Physical Chemistry C* **112**, 15742 (2008/10/09, 2008).

60. J. L. Hardin, N. A. Oyler, E. D. Steinle, G. A. Meints, Spectroscopic analysis of interactions between alkylated silanes and alumina nanoporous membranes. *Journal of Colloid and Interface Science* **342**, 614 (2010).

61. J. Kim, P. Seidler, L. S. Wan, C. Fill, Formation, structure, and reactivity of amino-terminated organic films on silicon substrates. *Journal of Colloid and Interface Science* **329**, 114 (2009).

3

Sequential grafting strategy for hybrid meso-porous polyimide-alumina

Abstract

A method is presented for synthesis of hybrid polyimide-alumina materials. The organic species is confined to the nano length scale of the pores of meso-porous alumina, reducing the tendency for plasticization and swelling by moderating macromolecular dynamics. Confinement is achieved by sequential grafting of a di-anhydride (6FDA) and a di-amine (6F*p*DA or DABF) on to aminosilane (3APTMS) functionalized alumina. The obtained hybrid poly(amic acid)-alumina is transformed into a polyimide-alumina by thermal imidization: the cyclization of the amic acid groups by the removal of water at elevated temperature. Hybrid materials, obtained after different numbers of grafting steps, have been analyzed with nitrogen sorption and FTIR. The data indicate filling of the pores and confirm the presence of the imide group in the material. Amino functionalization is done from the vapor phase (VPG) or the solution phase (SPG). VPG results in materials with a monolayer of linker molecules, SPG results in a more random multilayer surface functionalization. As compared to SPG, VPG derived materials show lower imide concentration after the first grafting step, with 6FDA, and more pronounced increase in imide concentration in the second grafting step. This is due to the lower concentration of linker groups and larger available pore volume in VPG.

Keywords: hybrid inorganic-organic, surface modification, polyimide, meso-porous alumina

3.1 Introduction

Inorganic-organic hybrid materials may combine the advantages of their inorganic and organic species. In general, inorganic materials have superior thermal and mechanical stability, while organic materials provide broader chemical versatility. The combination of these distinct materials properties can be beneficial for various applications in many fields such as catalysis (*1*), sensors (*2, 3*), biology (*3*) optics (*4*), electronic (*5*), tissue regeneration (*6*), drug delivery (*6*). For example, television screens are coated with hybrid materials made of indigo dyes embedded in a silica-zirconia matrix (*3*), and sol-gel entrapped enzymes are produced on industrial scale (*3*). In particular, in hybrid inorganic-organic membranes confining the polymer in an inorganic host may inhibit disadvantages of organic polymers, such as swelling and plasticization. Such a strategy potentially allows the use of high performance polymers under conditions where normally their performance would deteriorate (*7*).

In the present study, we aim to construct a hybrid material by confining a fluoropolyimide organic polymer in the meso-pores of γ-alumina. Polyimides have been identified as interesting materials for, e.g., membrane separation of carbon dioxide and methane. The relationship between chemical structure and gas permeability of polyimides has been investigated extensively by several groups (*8-11*). Particularly, it has been observed that the presence of the hexafluoroisopropylidene group in a polyimide can increase carbon dioxide permeability without significant loss of molecular selectivity in its separation from methane

(*12, 13*). Yet, at higher pressures extensive sorption of carbon dioxide in the polymer results in enhanced macromolecular dynamics, manifested by swelling and plasticization and a corresponding decline in the molecular selectivity. Nano-scale confinement of the polyimide in the pores of a porous ceramic material may inhibit this increase in macromolecular dynamics.

Different approaches allow the accommodation of organic moieties within the pores of an inorganic material. One approach is via “sol-gel”, in which organic groups are introduced directly into the matrix of the inorganic material by using precursors such as bridged polysilsesquioxanes (*14, 15*). Another approach is “post-synthetic grafting”, which involves covalent attachment of organic functional groups to the pore walls of the inorganic material (*16-18*).

In the present study we focus on post-synthetic grafting. Our approach is based on performing a sequence of individual grafting steps, as is schematically depicted in Figure 1. This allows combined nano length scale confinement of the polymer and controlling its molecular composition. In the first grafting step the pore surface of the ceramic is functionalized with so-called linker molecules, providing nucleophile primary amine groups as anchoring sites. In the second step, fluorinated di-anhydride monomers are covalently attached to the anchoring sites by forming an amic acid. In a third step, a fluorinated diamine is covalently attached to the remaining anhydride groups. Steps two and three can

be repeated. The amic acid groups can be transformed into cyclic imid bonds by thermal imidization.

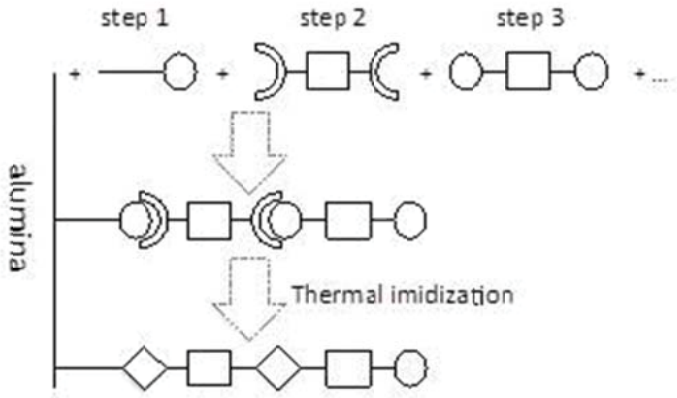

Figure 1: Schematic presentation of the sequential grafting procedure for hybrid polyimide-alumina

In Figure 2 a more detailed reaction scheme is presented, based on the molecular structures of the reactants.

3.1.1 Linker attachment

In step 1, functionalization of the pores in alumina with primary amine groups is achieved by grafting with 3-Aminopropyltrimethoxysilane (3APTMS) (Figure 2). The alkoxy groups of this silane can react with surface hydroxyl groups of the ceramic substrate, forming a covalent Si-O-Al bond and an alcohol as by product (*16*). The functionalization of the ceramic substrate involves preferably the formation of only a single layer of linker molecules,

facilitating subsequent grafting of other molecules. This requires that oligomerization of the precursor molecules should be avoided, as this would result in a thicker layer of cross-linked silane molecules that unnecessarily fills up pore volume or even causes obstruction of pores. It is difficult to avoid oligomerization for silanes containing two or three hydrolysable groups (*18, 19*). In a previous study we have shown that controlled monolayer formation can be achieved in a facile manner by grafting from the vapor phase (VPG), rather than from the liquid solution phase (SPG) (*20*). In short, oligomers formed by self-condensation of the precursor molecules have a low vapor pressure, and hence their concentration in the vapor phase will be relatively low. Just a few research groups (*7, 21, 22*) reported the step-by-step grafting of polymer molecules inside the pores of an inorganic material, all of these attached the linker molecules by solution phase grafting. In the present study we explore the effect of linker attachment via VPG versus SPG on sequential grafting of meso-porous alumina.

3.1.2 Sequential grafting of polyimides

In step 2, the nucleophile primary amine groups of the functionalized ceramic can react with one of the dianhydride groups of 4,4`-hexafluoroisopropylidene diphthalic anhydride (6FDA), at ambient conditions in a dipolar aprotic solvent such as N,N-dimethyleacetamide (DMAc). Nucleophilic attack of the amino group on the carbonyl carbon of the anhydride group yields an amic acid.

In step 3, in order to introduce more fluorinated organic groups, the material obtained in step 2 is grafted by one of the following two diamines: 4,4`-hexafluoroisopropylidene

dianiline (6F*p*DA) or the larger 4,4`-hexafluoroisopropylidene bis *p*-phenyleneoxydianiline (BADF). This again yields amic acid groups.

In a subsequent step, the primary amine groups of 6F*p*DA/BADF, remaining after step 3, can react with the di-anhydride 6FDA. Etcetera.

The amic acid groups, present in materials obtained after a sequence of grafting steps, can be cyclized to form an imide group by chemical or thermal imidization (*23, 24*).

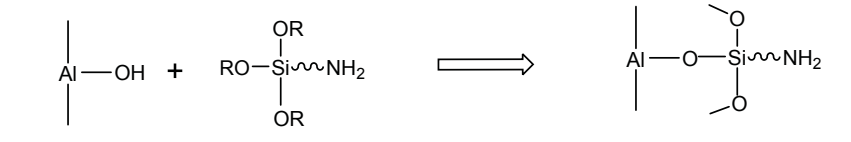

Alumina porous surface: **I** | 3APTMS (R: OCH_3) | Aminosilylated alumina: **II**

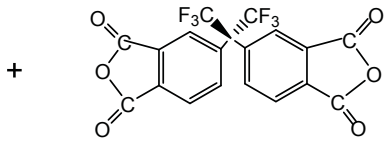

6FDA

25 °C
DMAc

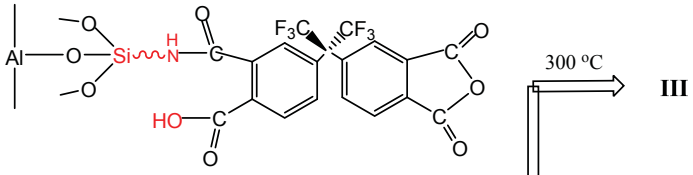

300 °C → **III**

Amic acid formation with one anhydride of 6FDA

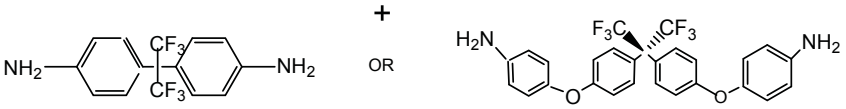

6FpDA | OR | BADF

25 °C
DMAc

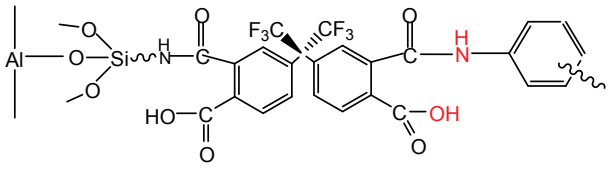

Amic acid formation with second anhydride of 6FDA

Imidization
- H_2O

300 °C
1hr

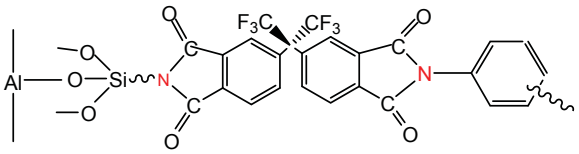

Imide formation on both anhydrides of 6FDA: Polyimide

Figure 2: Schematic representation showing the chemical reaction mechanism of polyimide formation over porous surface of aminosilylated alumina.

3.2 Experimental

3.2.1 Materials

3-Aminopropyltrimethoxysilane (3APTMS, 97 % purity), 4,4-hexafluoroisopropyldiene diphthalic anhydride (6FDA), 4,4-hexafluoroisopropylidene dianiline (6F*p*DA) and 4,4-hexafluoroisopropylidene bis *p*-phenyleneoxydianiline (BADF), toluene (anhydrous, 99.8 %) and N,N-dimethyleacetamide (DMAc) were obtained from Aldrich, and used as received. High purity, 98 % ethanol was obtained from Merck, and used as received. Deionized water was used for pretreatment of alumina powders.

3.2.2 Synthesis of meso-porous γ-alumina

Meso-porous alumina flakes were prepared from a boehmite sol, which was dried and subsequently calcined at 600 ˚C in air for 1 hr at a heating rate of 1 ˚C . min^{-1}. A detailed description can be found in (*16*).

3.2.3 Pre-treatment of alumina flakes

Before grafting, alumina powders were pretreated by soaking in an ethanol/water (2:1) solution for 24 hours at ambient temperature, followed by vacuum drying at 150 ^{o}C overnight, and stored under nitrogen atmosphere until further use. Pretreatment can

remove contaminants located on the material surface that prevent access to surface reactive groups.

3.2.4 3APTMS grafting

Vapor phase grafting (VPG): The method was followed as reported in our previous work (*20*). 100 ml of toluene with 2.5 wt% of 3APTMS were added to a round bottom flask (denoted as RB I). Pre-treated alumina powder was placed in a round bottom flask (denoted as RB II). No liquid was added to RB II. An insulated horizontal glass tube connected the two RB flasks to each other as shown in a schematic in Chapter 1, Figure 5 (lower). Both RB flasks were maintained at 80 ^{o}C. The aminosilane vapors produced in RB I were allowed to pass in to the RB II through the horizontal tube. The reaction was carried out for 3 hrs. All chemicals were added inside the glove box prior to the start of the reaction.

Solution phase grafting (SPG): Porous γ-alumina powder was added in to a RB flask containing 100 ml of toluene with 2.5 wt % of 3APTMS. The RB flask is connected to a reflux cooler and the reaction performed at identical experimental condition as for vapor phase grafting.

After the reaction, the powders were separated from the reactors and soaked in toluene for ~10 hrs, and in ethanol for ~10 hrs, to remove physically adsorbed or unreacted aminosilanes. Finally, the powders were annealed at 100 ^{o}C for 1 hr.

3.2.5 Sequential grafting of polyimides (6FDA-6F*p*DA & 6FDA-BADF)

300 mg of aminosilylated γ-alumina powder was placed in a flask containing 20 ml dimethylacetamide (DMAc). 2.35 g of 6FDA was added to the solution; the reaction was performed at room temperature under nitrogen atmosphere. After 16 hours 0.59 g of 6F*p*DA *or* 4.53 g of BADF was added allowed to react for 16 hrs. Subsequently, the powders were soaked in DMAc over-night, followed by filtering to remove DMAc, and finally dried in air.

3.2.6 Imidization

The amic acid groups in the grafted γ-alumina were converted to their imide form by thermal imidization, allowing ring closure via the removal of water. Grafted flakes were heated to 300 ^{o}C for 1h (heating/cooling rate of 1 ^{o}C . min^{-1}) well above the temperature of onset of imidization (~180 ^{o}C) (*23, 24*).

3.2.7 Materials characterization

Fourier Transform Infrared Spectroscopy

The samples were characterized with transmission Fourier Transform Infrared Spectroscopy (FT-IR), using a Bruker Tensor 27 infrared spectrometer. Self-supporting pellets were measured at room temperature in ambient atmosphere. Pellets were prepared with KBr in 50:50 proportion with the sample. All FT-IR spectra were measured against air background.

N_2-physisorption

The morphology of the material was investigated with nitrogen gas physisorption at 77 K on a Micromeritics apparatus (model Gemini VII). Prior to the sorption experiments, all samples were placed under vacuum at 120 ^{o}C for 12 hrs. The pore size distributions were estimated from the desorption branch of the isotherm by the Barret-Joyner-Halenda (BJH) method (*25-27*). The total surface area (S_{BET}) was obtained using the standard Brunauer-Emmett-Teller (BET) method for adsorption data (*25*). The total pore volume (V_p) was calculated from the amount of nitrogen adsorbed at a relative pressure of 0.95.

3.3 Results and Discussion

3.3.1 Pore morphology: N_2-physisorption

In Figures 3a & 4a nitrogen sorption isotherms are depicted for materials obtained after different grafting steps, after thermal imidization at 300 ^{o}C. The Figures 3b & 4b at the bottom depicts the corresponding pore size distributions. The values of the BET surface area, pore volume and mean pore size are given in Table I.

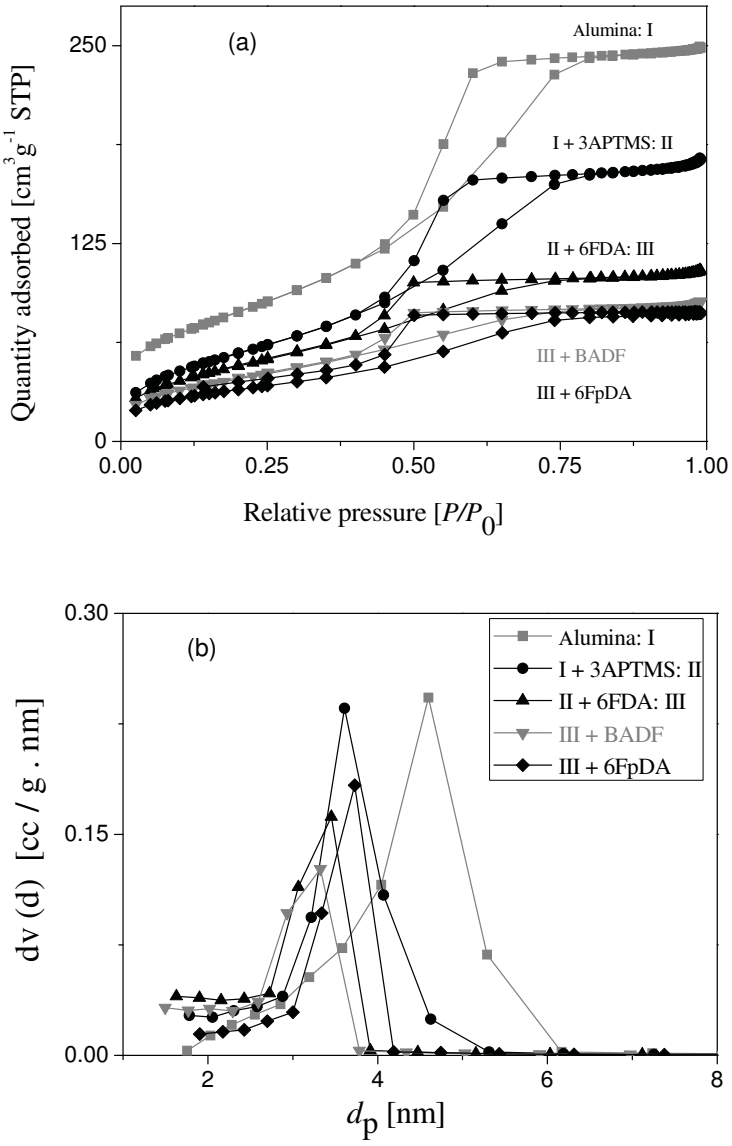

Figure 3: N_2-physisorption analysis of meso-porous γ-alumina after (sequential) grafting with linker 3APTMS via SPG: (a) sorption isotherms (b) corresponding pore size distribution curves

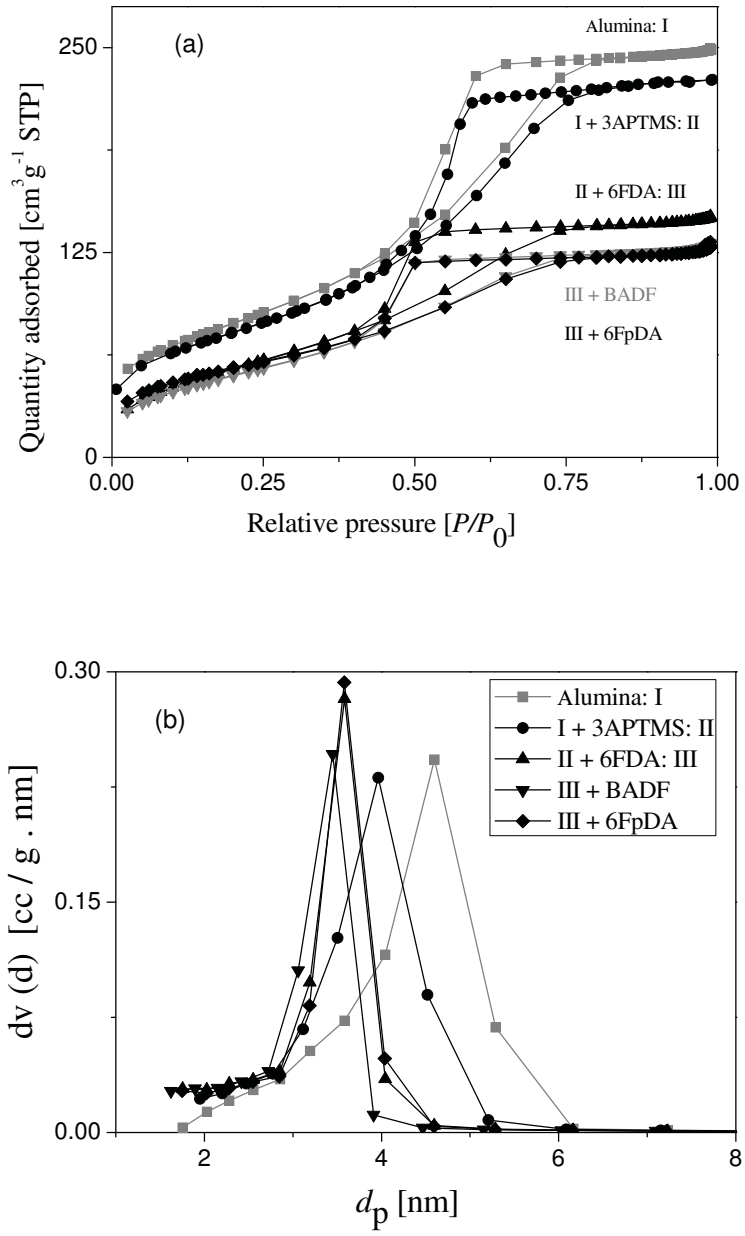

Figure 4: Nitrogen physisorption analysis of meso-porous γ-alumina after (sequential) grafting with linker 3APTMS via by VPG: (a) sorption isotherms (b) corresponding pore size distribution curves.

Grafting of 3APTMS

Prior to functionalization, the sorption isotherm of γ-alumina is Type IV (IUPAC classification) (*28*), indicative of a meso-porous material with an average pore size ~5 nm. After functionalization with 3APTMS the isotherm remains Type IV, irrespective of whether grafting is done by VPG or SPG. As compared to VPG, for SPG a more pronounced change in the amount of nitrogen sorption is observed. This suggests a more pronounced filling of the pores by the silane, perhaps even partial blocking of the pores (*21, 29*). Correspondingly, lower values for the BET surface area and pore size are listed in Table 1. The reduction of the mode of the pore size distribution from 4.7 to 3.7 nm suggests multi-layer formation of aminosilanes, by oligomerization during SPG (*20, 29, 30*). For VPG the sorption of nitrogen reduces less, and the BET surface area decreases only slightly. The ~0.3 nm reduction in the average pore size is in the range of the length of an aminosilane molecule (*29, 31-35*), indicating formation of a monolayer of grafted molecules. A more extensive investigation on difference between grafting γ-alumina with 3APTMS by SPG and VPG has been reported in (*20*) and also chapter 2 in this thesis.

Material	S_{BET} [m^2g^{-1}]	V_p, BJH [cm^3g^{-1}]	d_p, BJH [nm]
I: γ-alumina	250	0.36	4.6
II: I+3APTMS (VPG)	225	0.32	4.0
II: I+3APTMS (SPG)	213	0.25	3.6
III: II(VPG) + 6FDA	206	0.23	3.6
III: II(SPG) + 6FDA	179	0.16	3.5
III(VPG) + 6F*p*DA	189	0.21	3.6
III(SPG) + 6F*p*DA	140	0.13	3.7
III(VPG) + BADF	188	0.21	3.5
III(SPG) + BADF	158	0.14	3.3

Table 1: Structural properties of (modified) meso-porous γ-alumina material. Functionalization was done using 3APTMS as linker, grafted via either VPG or SPG. For all materials (except I and II) after the final grafting step thermal imidization was performed at 300 °C. S_{BET}: BET-surface area obtained between 0.05 – 0.2 P/P_0. V_P and d_p: Meso-pore volume and pore diameter respectively, calculated by BJH method. The same batch of γ-alumina powder was used for all experiments in this chapter in order to minimize the error contribution from powder synthesis.

Grafting of 6FDA

Subsequent grafting of 6FDA results in an additional reduction in the amount of nitrogen sorption (Figure 3a & 4a). This is a clear indication that the dianhydride is present on the materials surface. For the SPG functionalized material no significant change in average pore size is observed (3.6 to 3.5 nm), while the pore volume and BET surface area decrease significantly (from 0.25 to 0.16 cm^3g^{-1}, and from 213 to 179 m^2g^{-1}, respectively). This might be because of blocking of pores, rendering part of the pores inaccessible to nitrogen. For the VPG functionalized material, a shift in the mode of pore size distribution is observed (from 4.0 to 3.6 nm). This change in pore diameter corresponds well with the size of the 6FDA. The pore volume and surface area of the material also reduces (0.32 to 0.23 cm^3g^{-1}, and 225 to 206 m^2g^{-1}, respectively), but these changes are less pronounced as compared to the SPG functionalized material because of limited pore blocking upon VPG. The data suggest a regimented attachment of a monolayer of 6FDA on to the VPG functionalized pore walls

Grafting of 6F*p*DA / BADF

Subsequent grafting of the 6FDA modified hybrid material (III) by either 6F*p*DA or BADF results in a further reduction of the amount of nitrogen sorption.

For the VPG derived material the changes in surface area (from 206 to 189 m^2g^{-1} for 6F*p*DA, and from 206 to 188 $m^2g^{-}$for BADF) and in pore volume (from 0.23 to 0.21 cm^3g^{-1} for 6F*p*DA and BADF) are similar for both diamines. The change in the average pore size (from 3.6 to

3.6 nm for 6F*p*DA, and from 3.6 to 3.5 nm for BADF) is within experimental error. The data suggest a comparable limited amount of grafting of both diamines to the available 6FDA anhydride groups.

In contrast, for the SPG derived material the change in pore size (6F*p*DA: from 3.5 to 3.7 nm, BADF: from 3.5 to 3.3) is not significant, given the experimental error. In contrast to pore size data, as compared to the VPG derived material the changes in BET surface area (6F*p*DA: from 179 to 140 m^2g^{-1}, and BADF: from 179 to 160 m^2g^{-1}) and pore volume (6F*p*DA: from 0.16 to 0.13 cm^3g^{-1}, and BADF from 0.16 to 0.14 cm^3g^{-1}) are more pronounced. These data are indicative of further blocking of pores in the SPG derived materials. The difference in surface area in the case of 6F*p*DA as compared to BADF can be due to the uncontrollable nature of the SPG process, rather than from difference between the diamines.

3.3.2 FT-IR characterization

Figure 5 depicts the FT-IR characterization of meso-porous γ-alumina after different sequential grafting steps, for SPG derived materials. For comparison the FT-IR spectra of the pure precursor compounds are given at the bottom of the Figure.

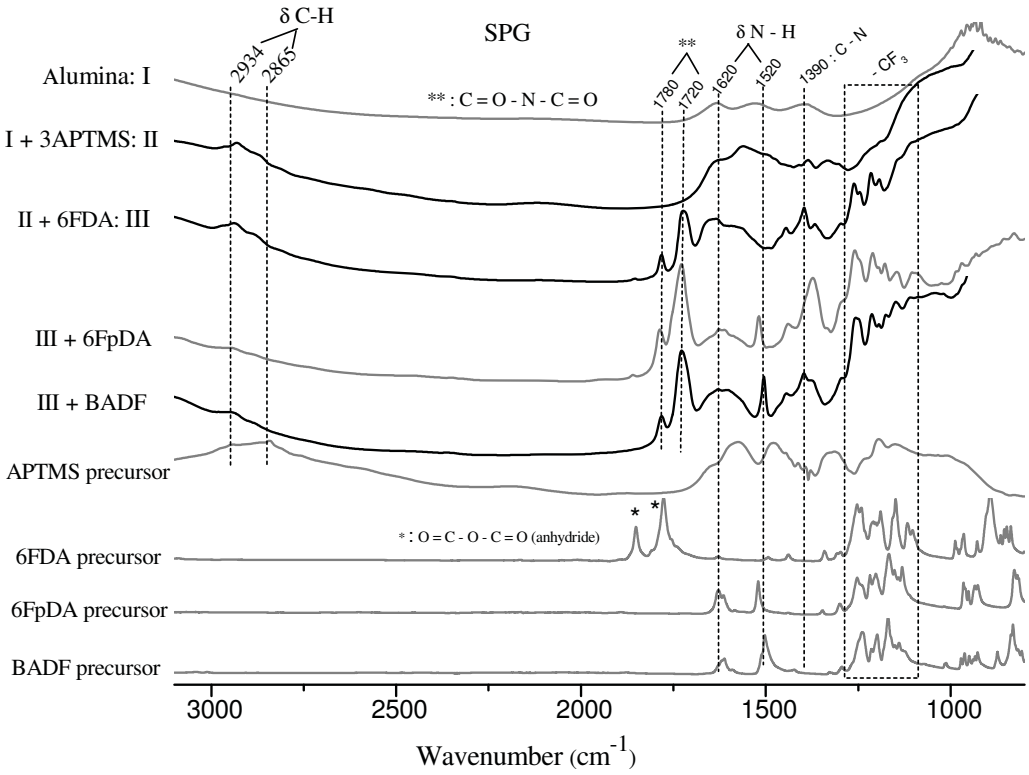

Figure 5: FT-IR spectra of meso-porous γ- alumina after sequential grafting steps and the spectra of the corresponding precursors. The linker molecules were grafted from solution phase (SPG). For the grafted materials, after the final grafting step (with dianhydride or diamine) thermal imidization was performed at 300 °C.

Prior to grafting, the spectrum of γ-alumina is characterized by a broad band between 3700 to 3500 cm^{-1} that can be attributed to the presence of physisorbed water on γ-alumina hydroxyls. Grafting 3APTMS on to porous γ-alumina by SPG results in additional bands in FT-IR spectra; distinctive bands observed between 3000 and 2800 cm^{-1} can be assigned to C-H

stretching of the propyl chain present in 3APTMS. For a more extensive investigation of 3APTMS grafting of meso-porous γ -alumina, readers are referred to (*20*).

After grafting of the SPG amino-functionalized γ-alumina with 6FDA, and subsequent thermal imidization, new bands emerge in the FT-IR spectrum. The bands observed between 1260 to 1190 cm^{-1} represent characteristic peaks of the fluorine groups in 6FDA. The characteristic peaks at 1780 and 1720 cm^{-1} are assigned to the C=O asymmetric and symmetric stretching of the imide group (*23, 24, 36*). In the spectrum of the precursor, 6FDA, these peaks are also visible, at larger wave number. Here, the peaks correspond to C=O asymmetric and symmetric stretching of the anhydride group. The presence of the amine band around 1600 cm^{-1} corresponds to amine groups, which have not participated in the reaction with 6FDA. Incomplete imidization of amic acid groups will be reflected by the presence of a broad band around 1620 cm^{-1}, corresponding to amide groups. The absence of this band and appearance of band at 1780 and 1720 cm^{-1} suggests high conversion of the amic acid groups in to imides (*36, 37*). The band at 1390 cm^{-1} corresponds to C-N stretching of the imide group (*23, 24*). These observations substantiate that after grafting with 6FDA, and subsequent thermal imidization, indeed a hybrid alumina-imide is obtained.

Spectra are shown for the subsequent grafting of two types of diamines (6F*p*DA or BADF) on to 6FDA grafted porous γ-alumina, followed by thermal imidization. The band emerging at around 1500 cm^{-1} corresponds to non-converted amine groups of the diamine precursors, 6F*p*DA & BADF. These peaks, and the pronounced peaks corresponding to imide groups at

1720 cm^{-1} and 1780 cm^{-1} indicate successful third sequential grafting of these diamine precursors over 6FDA, and successful imidization. Supporting the above observation, the peak around 1390 cm^{-1} becomes more pronounced, suggesting an increase in C-N groups upon grafting with 6F*p*DA or BADF.

Figure 6 shows sequential grafting of polyimides on to a VPG amino functionalized porous γ-alumina.

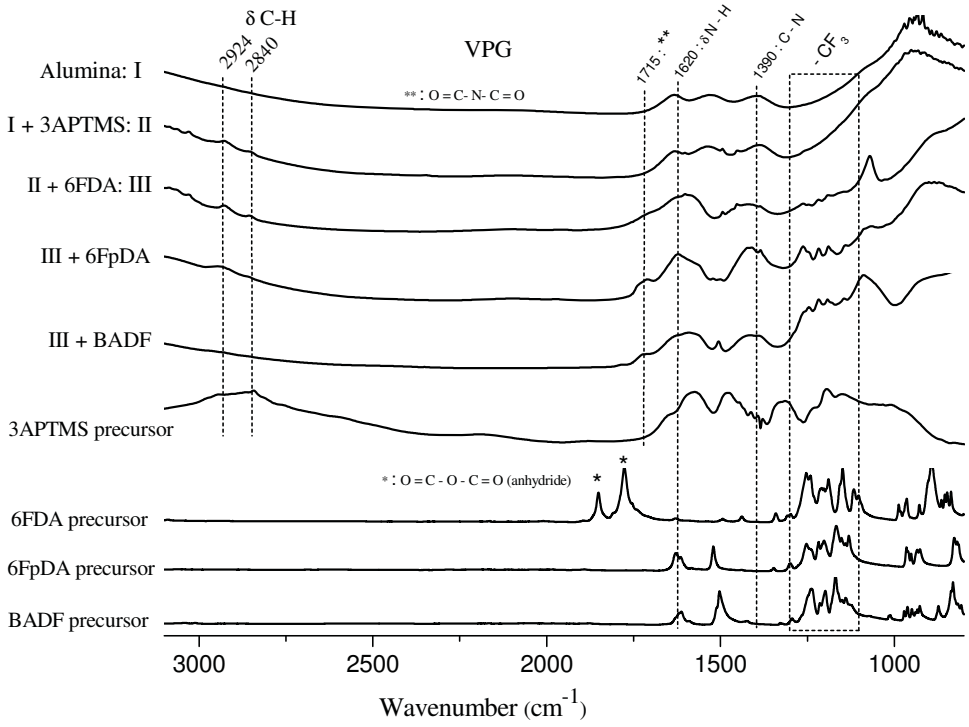

Figure 6: FT-IR spectra of meso-porous γ-alumina after sequential grafting steps and the spectra of the corresponding precursors. The linker molecules are grafted from vapor phase (VPG). After the final grafting step (with dianhydride or diamine) thermal imidization was performed at 300 °C.

After VPG treatment of 3APTMS, a broad band around 3500 cm^{-1} clearly indicates adsorption of water on the surface. New peaks emerge between 3000 and 2800 cm^{-1}, which are assigned to C-H stretching of the propyl chain in 3APTMS. As compared to SPG, these peaks are less pronounced. This is in agreement with the conclusions from the nitrogen sorption data: monolayer coverage of 3APTMS in VPG and multilayer coverage in SPG. A more extensive investigation on VPG of APTMS is given in our previous report (*20*).

Grafting of 6FDA on the VPG aminosilylated γ-alumina, followed by thermal imidization results in bands between 1250 and 1120 cm^{-1}, assigned to fluorine groups present in 6FDA. The shoulder observed at 1715 cm^{-1} corresponds to symmetric stretching of C=O in imide groups (*23, 24*). The low intensity of peaks in Figure 5, as compared to those in Figure 4, supports the premise of a lower coverage of 3APTMS via VPG, and hence a lower amount of primary amine groups that serve as anchoring sites. Spectra are shown for the subsequent grafting of two types of diamines (6F*p*DA or BADF) on to 6FDA grafted porous alumina. A broad low intensive peak is observed around 1720 cm^{-1}. This confirms the formation of additional imide groups after diamine grafting and thermal imidization. As compared to SPG, for VPG the increase in the intensity of the band at 1720 cm^{-1} is more pronounced (compare Figure 5 and Figure 6). This is probably because VPG, in contrast to SPG, allows monolayer functionalization of the porous alumina, providing a befitting surface for subsequent sequential grafting.

3.4 Conclusions

Inorganic – polymeric hybrid materials are synthesized by sequential grafting of a porous alumina. The sequence of steps involves first aminosilane functionalization of the ceramic with 3APTMS, followed by an alternating sequence of grafting steps with an anhydride (6FDA) and a diamine (6F*p*DA or BADF). The obtained hybrid poly(amic acid)-alumina is transformed into a polyimide-alumina by thermal treatment at 300 ^{o}C, where water removal results in cyclization of the amic acid group. The materials are characterized by nitrogen sorption and FT-IR.

A comparison is made between materials in which the linker, 3APTMS, is grafted from the solution or from the vapor phase. Grafting from the vapor phase results in a material with a monolayer of linker molecules, from the solution phase a more random surface functionalization occurs, accompanied by pore blocking.

In the first grafting step, with 6FDA, materials functionalized via SPG show increased pore blocking, while in the VPG derived materials the 6FDA covers the functionalized surface in a layer-by-layer manner. In the subsequent grafting step, with 6F*p*DA or BADF, a larger increment in the concentration of grafted groups is observed for the VPG derived material, as compared to the SPG derived material.

The results indicate that sequential grafting of dianhydrides and diamine onto an aminosilane functionalized meso-porous γ-alumina allows the construction of a hybrid

polyimide-alumina. Sequential grafting is better modulated when the porous material is functionalized via vapor phase grafting, instead of solution phase grafting.

References

1. C. W. Jones, Zeolites go organic. *Science* **300**, 439 (2003).

2. C. Rottman, G. Grader, Y. De Hazan, S. Melchior, D. Avnir, Surfactant-Induced Modification of Dopants Reactivity in Sol−Gel Matrixes. *Journal of the American Chemical Society* **121**, 8533 (1999).

3. C. Sanchez *et al.*, Designed hybrid organic-inorganic nanocomposites from functional nanobuilding blocks. *Chemistry of Materials* **13**, 3061 (2001).

4. B. Lebeau, S. Brasselet, J. Zyss, C. Sanchez, Design, Characterization, and Processing of Hybrid Organic−Inorganic Coatings with Very High Second-Order Optical Nonlinearities. *Chemistry of Materials* **9**, 1012 (1997).

5. T. D. d. Morais, F. Chaput, K. Lahlil, J.-P. Boilot, Hybrid Organic–Inorganic Light-Emitting Diodes. *Advanced Materials* **11**, 107 (1999).

6. F. Balas, M. Manzano, P. Horcajada, M. Vallet-Regí, Confinement and Controlled Release of Bisphosphonates on Ordered Mesoporous Silica-Based Materials. *Journal of the American Chemical Society* **128**, 8116 (2006).

7. I. Okazaki *et al.*, Nanotechnological method to control the molecular weight cut-off and/or pore diameter of organic–inorganic composite membrane. *Journal of Membrane Science* **141**, 65 (1998).

8. K. Tanaka, M. Okano, H. Kita, K.-i. Okamoto, S. Nishi, Effects of trifluoromethyl side groups on gas permeability and permselectivity in polyimides. *Polymer Journal* **26**, 1186 (1994).

9. Y. Hirayama *et al.*, Relation of gas permeability with structure of aromatic polyimides I. *Journal of Membrane Science* **111**, 169 (1996).

10. Y. Hirayama *et al.*, Relation of gas permeability with structure of aromatic polyimides II. *Journal of Membrane Science* **111**, 183 (1996).

11. L. M. Robeson, C. D. Smith, M. Langsam, A group contribution approach to predict permeability and permselectivity of aromatic polymers. *Journal of Membrane Science* **132**, 33 (1997).

12. T.-H. Kim, W. J. Koros, G. R. Husk, Advanced gas separation membrane materials: Rigid aromatic polyimides. *Separation Science and Technology* **23**, 1611 (1988).

13. M. R. Coleman, W. J. Koros, Isomeric polyimides based on fluorinated dianhydrides and diamines for gas separation applications. *Journal of Membrane Science* **50**, 285 (1990).

14. K. J. Shea, D. A. Loy, Bridged Polysilsesquioxanes. Molecular-Engineered Hybrid Organic−Inorganic Materials. *Chemistry of Materials* **13**, 3306 (2001).

15. D. A. Loy *et al.*, Dialkylene Carbonate-Bridged Polysilsesquioxanes. Hybrid Organic−Inorganic Sol−Gels with a Thermally Labile Bridging Group. *Chemistry of Materials* **11**, 3333 (1999).

16. H. L. Castricum, A. Sah, M. C. Mittelmeijer-Hazeleger, J. E. ten Elshof, Hydrophobisation of mesoporous γ-Al_2O_3 with organochlorosilanes—efficiency and structure. *Microporous and Mesoporous Materials* **83**, 1 (2005).

17. A. Stein, B. J. Melde, R. C. Schroden, Hybrid Inorganic–Organic Mesoporous Silicates—Nanoscopic Reactors Coming of Age. *Advanced Materials* **12**, 1403 (2000).

18. A. Sah, H. L. Castricum, A. Bliek, D. H. A. Blank, J. E. ten Elshof, Hydrophobic modification of γ-alumina membranes with organochlorosilanes. *Journal of Membrane Science* **243**, 125 (2004).

19. A. Y. Fadeev, T. J. McCarthy, Self-Assembly Is Not the Only Reaction Possible between Alkyltrichlorosilanes and Surfaces: Monomolecular and Oligomeric Covalently Attached Layers of Dichloro- and Trichloroalkylsilanes on Silicon. *Langmuir* **16**, 7268 (2000).

20. V. G. P. Sripathi, B. L. Mojet, A. Nijmeijer, N. E. Benes, Vapor phase versus liquid phase grafting of alumina. *Microporous and Mesoporous Materials* **172**, 1 (2013).

21. S. Kim, J. Ida, V. V. Guliants, Y. S. Lin, Tailoring Pore Properties of MCM-48 Silica for Selective Adsorption of CO_2. *The Journal of Physical Chemistry B* **109**, 6287 (2005).

22. S. Sawamoto *et al.*, Nanotechnological method to control pore diameter of organic–inorganic composite membrane: Part II. Molecular-wise vapor polymerization (MVP). *Journal of Membrane Science* **174**, 151 (2000).

23. T. Suzuki, Y. Yamada, Characterization of 6FDA-based hyperbranched and linear polyimide–silica hybrid membranes by gas permeation and 129Xe NMR measurements. *Journal of Polymer Science Part B: Polymer Physics* **44**, 291 (2006).

24. J. Ren, R. Wang, T.-S. Chung, D. F. Li, Y. Liu, The effects of chemical modifications on morphology and performance of 6FDA-ODA/NDA hollow fiber membranes for CO_2/CH_4 separation. *Journal of Membrane Science* **222**, 133 (2003).

25. S. Brunauer, P. H. Emmett, E. Teller, Adsorption of Gases in Multimolecular Layers. *Journal of the American Chemical Society* **60**, 309 (1938).

26. N. Gartmann, C. Schütze, H. Ritter, D. Brühwiler, The Effect of Water on the Functionalization of Mesoporous Silica with 3-Aminopropyltriethoxysilane. *The Journal of Physical Chemistry Letters* **1**, 379 (2009).

27. E. P. Barrett, L. G. Joyner, P. P. Halenda, The Determination of Pore Volume and Area Distributions in Porous Substances. I. Computations from Nitrogen Isotherms. *Journal of the American Chemical Society* **73**, 373 (1951).

28. S. J. Gregg, K. S. W. Sing, *Adsorption, surface area and porosity*. (Academic Press, 1991), vol. 2, illustrated, pp. 10 - 15.

29. D. G. Kurth, T. Bein, Thin Films of (3-Aminopropyl)triethoxysilane on Aluminum Oxide and Gold Substrates. *Langmuir* **11**, 3061 (1995).

30. W. Yoshida, R. P. Castro, J.-D. Jou, Y. Cohen, Multilayer Alkoxysilane Silylation of Oxide Surfaces. *Langmuir* **17**, 5882 (2001).

31. D. G. Kurth, T. Bein, Monomolecular layers and thin films of silane coupling agents by vapor-phase adsorption on oxidized aluminum. *The Journal of Physical Chemistry* **96**, 6707 (1992).

32. F. Zhang *et al.*, Chemical vapor deposition of three aminosilanes on silicon dioxide: surface characterization, stability, effects of silane concentration, and cyanine dye adsorption. *Langmuir* **26**, 14648 (Sep 21, 2010).

33. S. Fiorilli *et al.*, Vapor-phase self-assembled monolayers of aminosilane on plasma-activated silicon substrates. *Journal of Colloid and Interface Science* **321**, 235 (2008).

34. E. Asenath Smith, W. Chen, How To Prevent the Loss of Surface Functionality Derived from Aminosilanes. *Langmuir* **24**, 12405 (2008).

35. N. Crampton, W. A. Bonass, J. Kirkham, N. H. Thomson, Formation of Aminosilane-Functionalized Mica for Atomic Force Microscopy Imaging of DNA. *Langmuir* **21**, 7884 (2005).

36. Y.-Y. Yu, W.-C. Chien, T.-W. Tsai, H.-H. Yu, Synthesis of soluble polyimide/silica–titania core–shell nanoparticle hybrid thin films for anti-reflective coatings. *Materials Chemistry and Physics* **126**, 962 (2011).

37. H. Ye, J. Li, Y. Lin, J. Chen, C. Chen, Synthesis of polyimides containing fluorine and their pervaporation performances to aromatic/aliphatic hydrocarbon mixtures. *Journal of Macromolecular Science, Part A: Pure and Applied Chemistry* **45**, 172 (2008).

4

Inorganic – polyimide hybrid membranes by sequential molecular grafting of porous alumina with proliferated surface functionalization

Abstract

Inorganic materials have, in general, superior thermal and mechanical stability, and do not suffer from plasticization and swelling. Organic materials allow for versatile molecular selectivity. We aim to construct hybrid materials in which an organic oligomer is confined in the pore structure of a porous ceramic, aiming at moderated molecular dynamics of the oligomer and accordingly a reduced propensity to swelling and plasticization. The approach is based on sequential molecular grafting of aromatic polyimide precursors inside meso-porous γ-alumina membranes. The selected precursors are hexafluoroisopropylidenediphthalic anhydride and hexafluoroisopropylidene dianiline. Particular focus is on proliferated initial amino functionalization of the surface, using a polyhedral oligomeric silsequioxane. N_2-sorption data reveal that each sequential grafting step causes an increase in the amount of organic species, manifested by a decrease in the amount of N_2-gas sorption, surface area and pore diameter, until the material is no longer meso-porous. Fourier Transform Infrared Spectroscopy confirms the presence of the various grafting agents in the pores of the ceramic material. Single gas permeance of N_2, CH_4 and CO_2 (100 °C, p_{av} = 4 bar) decreases with the number of grafting steps, further substantiating the incremental increases in organic concentration. For CO_2 the reduction in permeance is significantly lower, due to the affinity of this gas for the fluorine groups in the polyimide. The permselectivity of CO_2 over the other gases shows a maximum with temperature. Up to 60 °C confinement induced reduction in molecular dynamics impedes transport of CO_2. At 100 °C, augmented chain movements allow an increase of CO_2 transport. At 150 °C the

amplified chain mobility causes a large increase in transport of all three gases, resulting in lower selectivity.

Keywords: POSS, polyimides, surface modification, γ-alumina, meso-porous oxide, vapor phase grafting, liquid phase grafting

4.1 Introduction

In recent years novel materials have emerged with improved properties for a variety of applications. Examples include hybrid materials that consist of at least two different species, with significantly improved physico-chemical properties. Such materials can find application in many fields such as catalysis (*1*), membrane separation (*2*), sensors (*3*), biology (*4*), optics (*5*), electronics (*6*), tissue regeneration, and drug delivery. In membrane applications, hybrid materials may combine the advantages of their inorganic and organic species. Inorganic materials have, in general, superior thermal and mechanical stability and do not suffer from plasticization and swelling. Organic materials allow for versatile molecular selectivity and are less expensive, but suffer from plasticization and swelling at elevated pressures and temperatures. We aim to construct hybrid materials in which an organic oligomer is confined in the porous structure of an inorganic matrix, resulting in moderated molecular dynamics and accordingly a reduced propensity to swelling and plasticization.

Polyimides (such as P84®, Matrimid®, etc.) currently receive much attention from academia and industry, for application in solvent resistant nanofiltration and membrane gas separation (*7-10*). The relationship between chemical structure and gas permeability of polyimides has been extensively investigated by several groups (*11-14*). Particularly, the presence of the hexafluoroisopropylidene structure in the core structure of a polyimide appears to increase gas permeability, without significant loss of permselectivity for CO_2 over CH_4 (*15, 16*). Imide oligomers confined in the porous γ–alumina membrane may exhibit

similar separation performance, with moderated propensity to swelling and plasticization, allowing application in more demanding conditions.

Different approaches enable the accommodation of organic moieties on the internal pore surface of an inorganic material. One approach is via “sol-gel”, in which organic groups can be introduced directly into the matrix of the inorganic material, by using precursors such as bridged polysilsesquioxanes (*17, 18*). Another approach is “post synthetic grafting”, which involves covalent attachment of organic functional groups to the pore walls of a porous inorganic material (*19-21*). In the present study we focus on post synthetic grafting.

In a previous study (*22*), we discussed the influence of the initial surface functionalization on sequential grafting of imides inside meso-porous γ–alumina, using a linker molecule with a single nucleophile primary amine group for covalent attachment of the organic moieties. In the present study, we functionalize the surface with a polyhedral oligomeric silsesquioxane (POSS) decorated with eight primary amine groups: Octaaminophenyl POSS (OAPS, Figure 1), aiming at increased concentration of nucleophile sites for subsequent covalent polymer attachment.

The chemical structure of the silsesquioxane family of compounds is defined as $R_nSi_nO_{1.5n}$, (sesqui means ‘one and a half’), generating structures consisting of an inner inorganic framework of silicon and oxygen atoms, externally covered by organic groups (R). “R” can be hydrogen, amine, alkyl, alkene, aryl, arylene, halogen, or almost any other functional group (*23*). Cage-like silsesquioxanes are referred to as polyhedral oligosilsesquioxanes or polyhedral oligomeric silsesquioxanes (POSS) (*23*). POSS molecules have a regular three-

dimensional shape (since polyhedra are multi-faceted three dimensional entities) formed by a few units, each containing silsesquioxane ($SiO_{1.5}$). The most common structure has an inner inorganic framework of molecular silica comprised of 8 silicon atoms, 12 oxygen atoms and 8 organic groups (R) (Figure 1a). POSS molecules are thermally and mechanically robust, and can be incorporated in to polymers to form hybrid inorganic–organic copolymers with improved thermal, mechanical and physical properties (*23*). Each POSS molecule can contain up to eight functional groups. For OAPS, these are eight nucleophile primary amine groups, each of which can react with an appropriate functional group of an organic monomer (Figure 1). When the organic monomer contains more than one functional group (e.g., the dianhydride 6FDA, Figure 1), cross-linking of OAPS cages can occur. The resulting dense cross-linked network contains amic acid groups that can be transformed into imide groups by cyclization at elevated temperature.

Cross-linking of functionalized POSS with organic polymeric monomers has been investigated in many research groups, typically in order to prepare thermally stable organic-inorganic nanocomposites (*24-27*). In the present study fluoropolymers (6FDA, 6F*p*DA) will be grafted in sequential manner over an OAPS functionalized γ–alumina porous surface. Aim is to obtain an imide oligomer confined in, and filling up, the pores of the ceramic host, with moderated molecular dynamics and hence a lower propensity to swelling and plasticization.

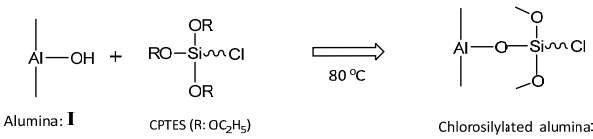

Alumina: **I** CPTES (R: OC_2H_5) Chlorosilylated alumina: **II**

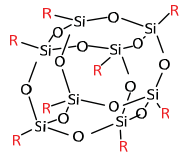

OAPS: R = NH_2

OAPS grafting over chlorosilylated alumina: **III**

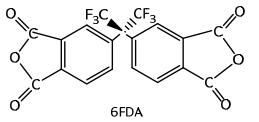

6FDA

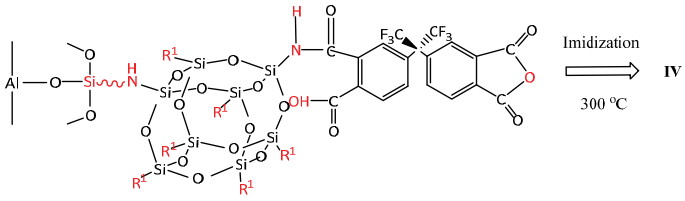

Sequential grafting of 6FDA over OAPS grafted alumina via amic acid formation (R^1 = NH)

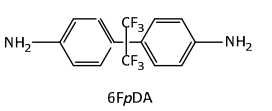

6F*p*DA

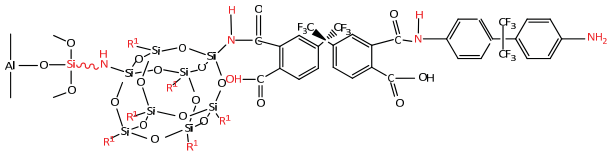

Sequential grafting of 6FpDA over 6FDA via amic acid formation with second anhydride group of 6FDA

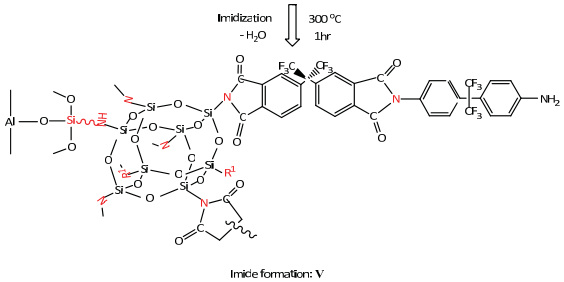

Imide formation: **V**

Figure 1: Schematic representation of sequential grafting of dianhydrides and diamines over OAPS functionalized γ-alumina, followed by thermal imidization.

4.2 Experimental

4.2.1 Materials

3-Chloropropyltriethoxsilane (CPTES, 97 % purity), toluene (anhydrous 99.8 %), tetrahydrofuran (THF) (anhydrous 98 %), 4,4` hexafluoroisopropylidinedipthalic anhydride (6FDA), hexafluoroisopropylidinedianiline (6F*p*DA), dimethylacetamide (DMAc) were obtained from sigma-Aldrich. High purity (98 %) ethanol was obtained from Merck. Octaaminophenyl polyhedral oligomeric silsesquioxane (OAPS) was obtained from hybrid plastics, USA.

4.2.2 Synthesis of meso-porous γ-alumina

Meso-porous γ-alumina flakes were prepared from a boehmite sol that was dried and subsequently calcined at 600 °C in air for 1 hr at a heating and cooling rate of 1 ˚C/min, as described in detail elsewhere (*19*). A sufficiently large quantity of powder was synthesized to allow use of the same batch of powder for all experiments in this chapter, in order to minimize the influence of variations in γ-alumina powder on the properties of samples obtained after sequential grafting experiments.

4.2.3 Sequential-grafting

4.2.3.1 Grafting CPTES linker by vapor phase grafting

Powders: CPTES liker was grafted on to meso-porous γ-alumina as described previously (*28*). In short, pre-treated γ-alumina powders were placed in one of the two round bottom flasks, connected to each other by a horizontal glass tube (see Figure 4 in Chapter 1, the lower image). Toluene and CPTES (2.5 wt %) were added to one RB flask (denoted as RB I) and the γ-alumina powders were taken in second RB flask (denoted as RB II). The CPTES vapors produced in RB I were allowed to pass through the horizontal tube to react with the porous material. Equal temperatures (80 ^{o}C) were maintained in the two RB flasks and the reaction was carried out for 3 hrs. All chemicals were added inside the glove box, prior to the start of the reaction.

Flat supported membranes: As shown in the schematic in Figure 2 (bottom) the precursor CPTES was added to toluene in a RB flask and the round disc shaped (39 mm diameter) γ-alumina porous supported membrane was placed upside down in a rack at the top of the RB flask (see the magnified part in Figure 4 in Chapter 1, upper image). The CPTES vapors produced were allowed to react with the porous surface of the membranes. All reaction conditions were similar to those mentioned above for the powders. After the reaction completed the powders and membranes were soaked in toluene (~10 hrs) and then in ethanol (~10 hrs). Finally, the chlorosilylated γ-alumina porous materials were annealed at 100 ^{o}C for 2 hrs. Reproducibility of the method has been checked by repeating the experiments at least three times. The vapor phase grafting method developed in this thesis

has recently been used by several colleagues in the group Inorganic Membranes of the University of Twente, without any reproducibility problems (*29, 30*).

4.2.3.2 Grafting OAPS on to chlorosilylated γ-alumina

Chlorosilylated γ-alumina powders were taken in a RB flask containing 50 ml THF and 0.1 g of OAPS was added to the reaction mixture. After 3 hrs of reaction at 60 ^{o}C under reflux, the filtered powders were overnight soaked in 30 ml THF solvent and then annealed at 100 ^{o}C for 3 hrs.

4.2.3.3 Sequential grafting of dianhydrides and diamines

An OAPS grafted flat membrane, or 0.3 g OAPS grafted powder, was placed in a flask containing 20 ml dimethylacetamide (DMAc). Next, 1.5 g 6FDA was added to the solution and allowed to react at room temperature under N_2 atmosphere (powder: 16 hrs, flat membrane: 2 hrs). The samples were separated from the reaction mixture (powders by filtering over filter paper, Millipore grade 101) and placed/soaked in 20 ml DMAc to remove physically adsorbed 6FDA. Subsequently, 0.26 g 6F*p*DA was added to a flask containing 20 ml dimethylacetamide (DMAc) and the mixture was allowed to react again (powders: 16 hrs, flat membranes: 2 hrs). This way, the sequential grafting steps were repeated based on required numbers of grafting steps.

4.2.3.4 Thermal imidization

After sequential grafting the powders/flat membranes were soaked in DMAc overnight, and then heated to 300 ^{o}C in air for 1 hr, to convert the amic acid groups to imide groups, as schematically represented in Figure 1.

4.2.4 Materials characterization

4.2.4.1 Fourier Transform Infrared Spectroscopy

Surface chemistry of the material was characterized with Attenuated Total Reflectance Fourier Transform Infrared Spectroscopy (ATR-FTIR), using a Bruker optics tensor 27 model equipped with a diamond crystal.

4.2.4.2 N_2- physisorption

The pore morphology of the material was investigated with N_2-gas physisorption at –196 ^{o}C on a Micromeritics (model Gemini) apparatus. Prior to the sorption experiments, all samples were degassed at 100 ^{o}C for 12 hrs. Pore size distributions were estimated from the desorption branch of the isotherm by the Barrett-Joyner-Halenda (BJH) method (*31, 32*). The total surface area (S_{BET}) was obtained using the standard Brunauer-Emmett-Teller method for adsorption data (*33*). The pore volume (V_p) was calculated from the amount of N_2 adsorbed at a relative pressure of 0.95.

4.2.4.3 Scanning electron microscopy

Scanning electron microscopy images were taken on a field emission scanning electron microscope (model Merlin, Carl-Zeiss, Germany).

4.2.4.4 Gas permeance

Single gas permeance through the disc shape membranes was measured in a pressure controlled dead-end mode. Measurements were performed at a maximum operating temperature of 150 ^{o}C and a trans membrane pressure of 4 bar (ambient pressure at permeate side). The membrane was placed with the grafted polyimide layer directed towards the gas feed side. For each gas, adequate time was given until a stable gas flow was observed. The gases were measured in the following order: N_2, CO_2, and CH_4. All measurements were repeated for at least two identical membranes. Each sequential grafting step was performed on a membrane that was not used for permeance measurements.

4.3 Results & discussion

4.3.1 Unsupported membranes: N_2-physisorption

Figure 2a depicts the N_2-adsorption and desorption isotherms of a meso-porous γ–alumina powder prior to and after (sequential) grafting. The corresponding pore size distribution curves are shown in Figure 2b. The derived BET surface area, pore size, and pore volume are listed in Table 1.

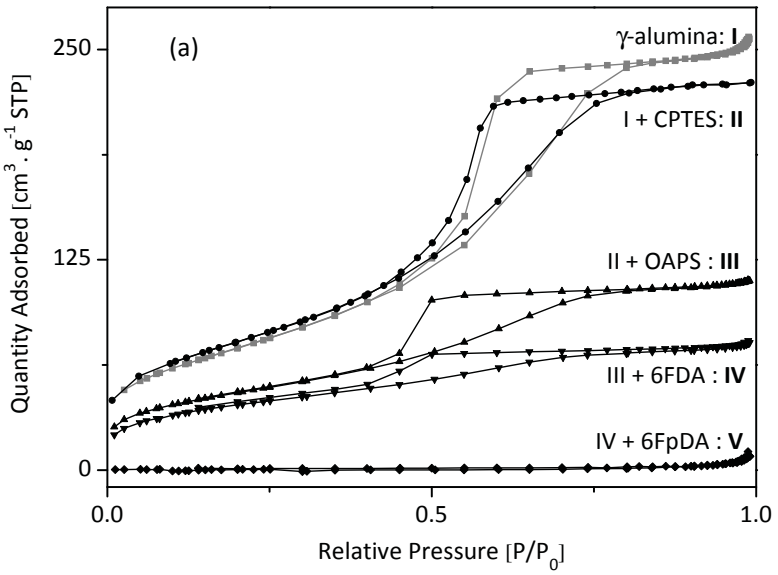
(a)
γ-alumina: I
I + CPTES: II
II + OAPS : III
III + 6FDA : IV
IV + 6FpDA : V
Quantity Adsorbed [cm3 . g-1 STP]
Relative Pressure [P/P0]
250
125
0
0.0
0.5
1.0

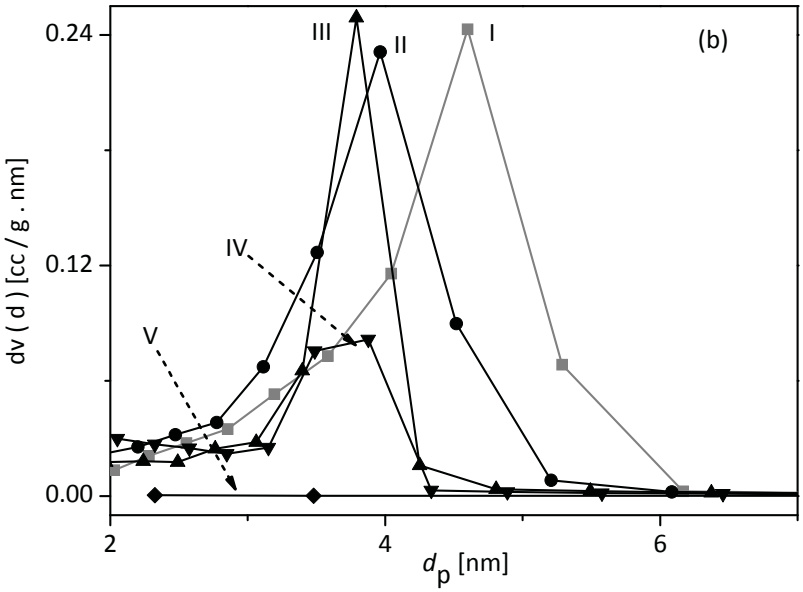
(b)
I
II
III
IV
V
dv (d) [cc / g . nm]
dp [nm]
0.24
0.12
0.00
2
4
6

Figure 2: (a) N_2-sorption isotherms after sequential grafting steps; (b) the corresponding pore size distribution curves. All the samples have been heated to 300 ^{o}C for thermal imidization.

All isotherms, except for the one obtained after grafting the diamine 6F*p*DA (**V**) are representative of a meso-porous material (*34*).

Prior to functionalization, γ–alumina shows a high quantity of gas sorption (~250 cm^3g^{-1}) corresponding to a surface area ~250 m^2g^{-1}, an average pore diameter of 4.6 nm, and a porosity of ~30 %. This is in agreement with other studies presented in literature (*19*) as well as our previous work (*28, 35*). The slight reduction in N_2-sorption after CPTES vapor phase grafting (~220 cm^3g^{-1}) indicates monolayer functionalization of the surface. This is also reflected by the reduction in pore size that is in agreement with the order of length of the silane molecules, ~0.3 nm (*28*). Sequential grafting of OAPS substantially reduces the quantity of N_2-sorption (~110 cm^3g^{-1}), and the surface area (~166 m^2g^{-1}). This indicates intrusion of OAPS molecules (~1.4 nm) into the pores, as is also evident from the reduction in average pore diameter (3.6 nm).

Material	S_{BET} [m^2g^{-1}]	V_P [cm^3g^{-1}]	d_P [nm]
γ–alumina : **I**	256	0.36	4.6
I + CPTES : **II**	225	0.29	4
II + OAPS : **III**	166	0.18	3.6
III + 6FDA : **IV**	140	0.11	3.4
IV + 6F*p*DA : **V**	1.2	0.01	——

Table 1: Structural properties of polyimides grafted on to γ-alumina material by using CPTES as linker deposited by VPG method. All the samples have been heated to 300 °C for thermal imidization. S_{BET}: BET-surface area obtained between 0.05 – 0.2 P/P_0. V_P and d_p: Meso-pore volume and pore diameter respectively, calculated by BJH method. The same batch of γ-alumina powder was used in order to minimize the error contribution from powder synthesis.

An additional grafting step, with 6FDA, results in reduction of the amount of N_2-sorption (~70 cm^3g^{-1}, Figure 2a). This suggests successful grafting of 6FDA onto OAPS functionalized porous γ–alumina. After a next grafting step, with 6F*p*DA, the shape of the isotherm is no longer type IV, and only a very limited sorption of N_2 (Figure 2a) is observed. This suggests that a negligible amount of, accessible, meso-pores remains in the material, which is in contrast with a previous study in which POSS has not been used for the surface functionalization (Chapter 3) and powders retained meso-porous characteristics.

4.3.2 Unsupported membranes: FT-IR analysis

Figure 3 depicts the FT-IR characterization of meso-porous γ-alumina prior to and after functionalization with CPTES and OAPS. The native γ-alumina is characterized by a broad band between 3700 and 3000 cm^{-1} that can be attributed to the presence of physisorbed water on the γ-alumina hydroxyls. A clear and elaborative description is provided in a previous study (*28, 35*).

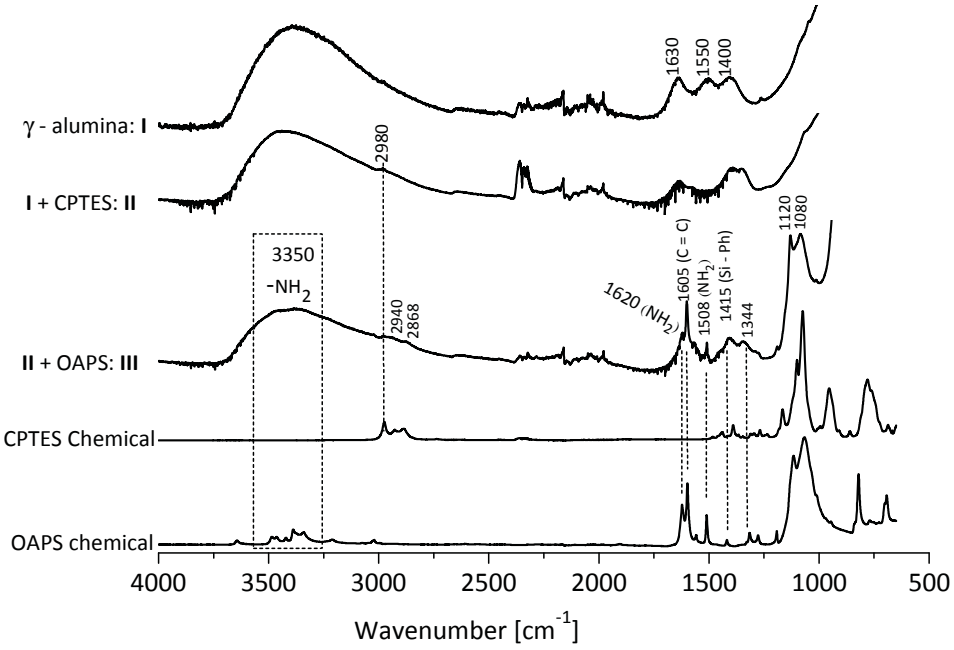

Figure 3: FT-IR spectra of sequentially grafted OAPS on to chlorosilynated meso-porous γ–alumina. All the samples have been heated to 300 °C for thermal imidization.

After reaction with CPTES a very small peak emerges around 2950 cm^{-1}, attributed to C-H stretching of the alkyl groups present in propyl chain. The unconvincing small change in the

spectrum is due to the low concentration (mono layer) of CPTES on the surface of the γ-alumina, as is evident from the N_2-sorption characterization. Similar observations have been made for vapor phase grafting of (3-aminopropyl)-trimethoxysilane onto meso-porous γ-alumina. For an extensive analysis, the readers are referred to chapter 2 (*28*).

The electrophilic chlorine group of a CPTES molecule can react with one of the eight nucleophilic amine groups of the OAPS. The presence of OAPS after grafting is clearly evident from the FT-IR spectrum, which reveals similar peaks as pure OAPS. The peak around 3350 and 1620 cm^{-1} is due to stretching vibrations and in plane bending vibrations of primary amine groups attached to the phenyl ring in OAPS (*26, 36*). The sharp intensive peaks at 1080 and 1140 cm^{-1} are symmetric and asymmetric stretching vibrations of Si–O (*36*) and confirm the presence of the silica structure of OAPS. The peak at 1415 cm^{-1} is attributed to Si–Ph bonds deformation, and the peak at 1605 cm^{-1} is attributed to stretching vibrations of C=C bonds (*36*).

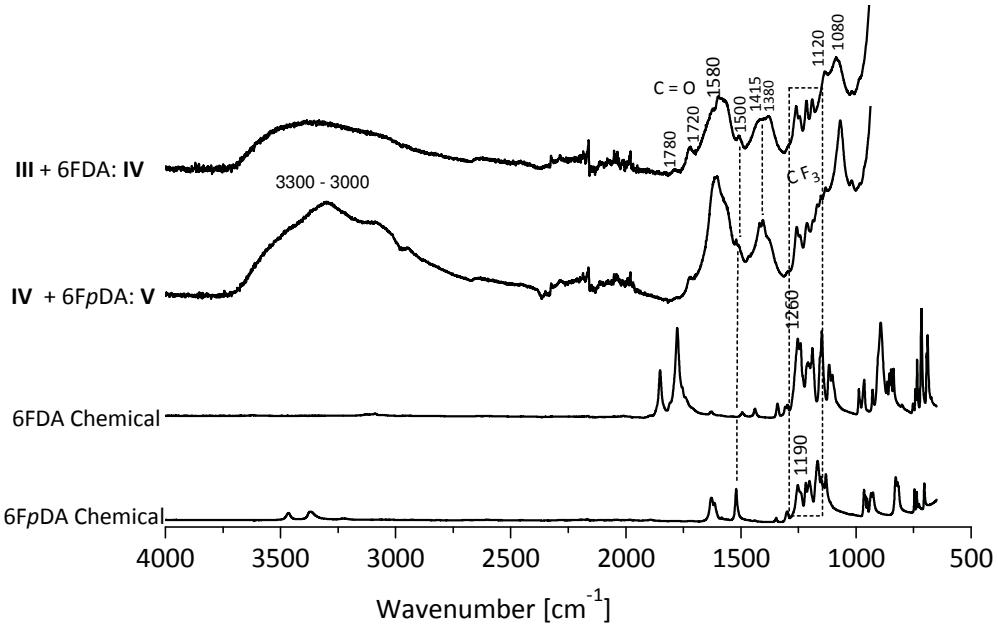

Figure 4: FT-IR spectra of sequentially grafted polyimides (6FDA–6F*p*DA) on to OAPS functionalized meso-porous γ–alumina, all materials have been treated at elevated temperature (300 °C) to induce thermal imidization.

Grafting of the 6FDA on to OAPS functionalized γ–alumina results in the appearance of new peaks in the FTIR spectrum (Figure 4). New peaks observed around 1250 cm^{-1} represent the characteristic fluorine groups of 6FDA. The peaks observed at 1720 and 1780 cm^{-1} are assigned to C=O symmetric and asymmetric stretching of the imide group (O=C–N–C=O), respectively (*37, 38*). The band at 1380 cm^{-1} is assigned to C-N stretching of the imide group (*24, 25*). The broad peak between 1620 – 1600 cm^{-1} is assigned to unreacted amine ($-NH_2$) groups and C=C bonds. The unreacted amine groups may be inaccessible because of steric hindrance.

In order to confine more fluorinated oligomer inside the meso-porous structure of γ–alumina, 6F*p*DA is sequentially grafted over 6FDA. In Figure 5 the intensity of the broad peak between 1620 – 1600 cm^{-1} has increased after sequential grafting with 6F*p*DA. This indicates an increase in the number of amine groups, associated with unreacted amines of 6F*p*DA.

4.3.3 Supported membranes: SEM analysis

Figure 5 depicts scanning electron microscopy images of the cross section of a supported γ-alumina layer, prior to functionalization (Figure 5a) and after six sequential grafting steps: 3 times 6FDA and 6F*p*DA (Figure 5b and 5c). For both the treated and untreated samples a clear distinction is visible between the α-alumina support and the γ-alumina layer. For the grafted sample, the top surface is homogeneously covered with organic material. The images obtained at higher magnification indicate that imide oligomer is present inside the pores of the γ-alumina, over the entire thickness of the γ-alumina layer.

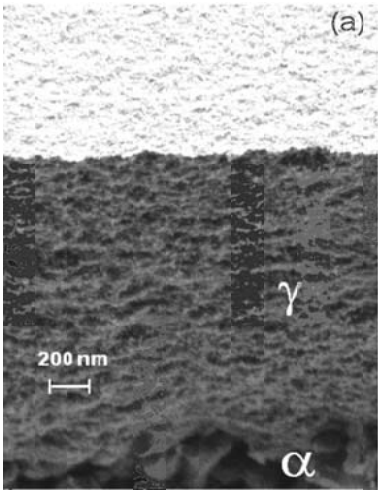

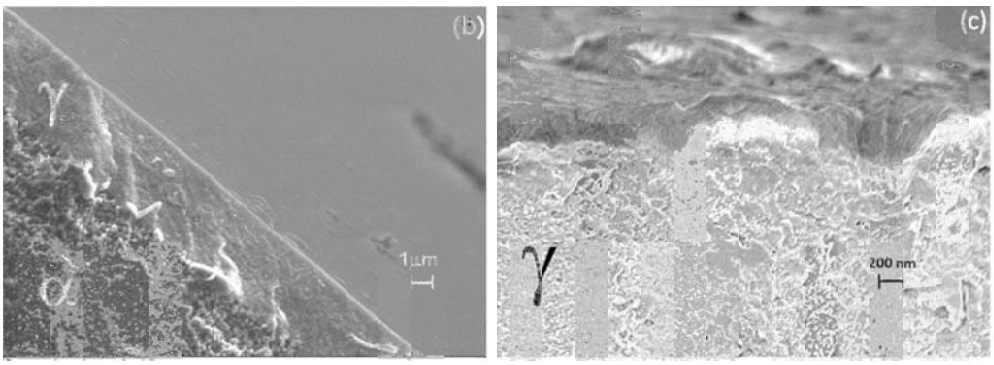

Figure 5: SEM images of supported γ–alumina membranes, untreated (a) and sequentially grafted three times with 6FDA-6F*p*DA: corresponding to material IX in the following Figure 6 (b and c).

4.3.4 Supported membranes: gas permeation

Figure 6 depicts the variation in the single gas dead-end permeance of CH_4, N_2 and CO_2, as a function of the number of sequential grafting steps, at 100 ^{o}C and Δp = 4 bar. After grafting OAPS on to chlorosilylated γ-alumina membranes, a moderate reduction in permeance of the three gases is observed, which is consistent with the reduced pore dimensions observed in the N_2-sorption analysis. OAPS functionalized membranes exhibit Knudsen selectivity, as is expected at these experimental conditions for a meso-porous material that does not have strong affinity for the respective gases.

After subsequent grafting with alternating 6FDA and 6F*p*DA, as the number of sequential grafting steps increases, a monotonic decrease in permeation of all gases is observed. This indicates either filling of pores with imide groups or closing of a few pores. The decrease is more pronounced for N_2 and CH_4, as compared to CO_2, which is due to the interactions of CO_2 with the $–(CF_3)_2$ and C = O groups in 6FDA (*11, 39*). The strong quadrupole moment of

the CO_2 molecule induces specific interactions between CO_2 and the polar groups ($–(CF_3)_2$, C = O) in the 6FDA-6F*p*DA imide groups (*39*). Alessandro *et al.* (*40*) discussed the differences in the electronic properties (quadrupolar moment and polarization) of the gases: CO_2 has a large quadrupole moment (13.4×10^{-40} cm^2) compared to N_2 (4.7×10^{-40} cm^2) and CH_4 is non-polar; the polarizabilities of respective gases are in the following order; CO_2 (26.3×10^{-25} cm^3) > CH_4 (26.0×10^{-25} cm^3) > N_2 (17.6×10^{-25} cm^3). 6FDA based polyimide membranes have been extensively explored with respect to their potential application for CO_2 separation in natural gas processing (*39, 41-49*). In the following, literature related to our observations is reviewed.

Gas separation in polyimide-based membranes has been shown to occur by the solution – diffusion mechanism (*39, 47, 48, 50-53*). Many research groups investigated the structure-property relationships between polyimides and transport of various gases (O_2, N_2, CO_2, and CH_4 etcetera). The general conclusion is that 6FDA based polyimides exhibit a good balance between high CO_2 permeability and CO_2/CH_4 selectivity (*47, 48, 50-52*). In the molecular design of polyimides, the main factors affecting the gas transport properties are: (1) the spatial linkage configurations, (2) the type of bridging groups, and (3) the bulkiness and polarity of pendant groups comprised in the polymer (*47*). Polymer chain rigidity is considered to, in particular, affect the permselectivity. The inter-chain spacing and chain mobility are considered to influence permeability (*47*).

Coleman *et al.* (*16*) investigated the gas transport properties based on the difference between two types of isomeric (*meta* and *para*) polyimides, with hexafluoroisopropylidene

moieties in the dianhydride and diamine monomers (6FDA and 6F*p*DA). They found that the CO_2 permeability of the *para* connected polyimide (6FDA-6F*p*DA) is 12 times higher than the *meta* connected polyimide (6FDA-6F*m*DA). The CO_2/CH_4 permselectivity is 37% lower in the *para* versus the *meta* connected polyimide. The difference in these two materials is mainly due to the differences in diffusivities, because of a more dense chain packing and more restricted rotational freedom in the *meta* versus the *para* connected material (*16, 47*). Similar observations were reported by Stern *et al.* (*48*) on a different polyimide pair, 6FDA-ODA. Okomoto *et al*. investigated the influence of carbonyl groups (C = O) on CO_2/CH_4 separation performance of polyimide membranes. They found a ~2.5 fold improvement in CO_2/CH_4 selectivity by increasing the quantity of carbonyl groups and concluded this improvement is because of interaction between CO_2 and carbonyl groups in the anhydride moieties.

One of the extensively investigated approaches to increase the CO_2 solubility is to introduce functional groups into the polymer via copolymer synthesis (*47, 54*). Authors investigated gas transport properties of PEO/polyimide block copolymers, and observed a significant increase in CO_2 permeability. This has been attributed to the increase in CO_2 solubility upon introducing PEO functional group in the polyimide. Smaihi *et al.* (*54*) have reported on the gas transport properties of poly(imide siloxane) copolymers. They have found a decrease in CO_2 permeability as the silica proportion is increased. This suggests a lower availability of polyimide groups, with affinity for CO_2, which reduces the solubility of CO_2. These

observations support the importance of interactions between CO_2 molecules with particular groups in polyimides, consistent with our observations.

The interactions between CO_2 and the organic groups introduced upon sequential grafting cause increased sorption of CO_2 in the material, and hence a more pronounced flux for this gas. After multiple grafting steps the permeability of the membrane is reduced dramatically for N_2 and CH_4. The dramatic reduction is in accordance with the N_2-sorption analysis that indicates that after a certain number of sequential grafting steps, a negligible amount of unfilled meso-pores remains. In comparison to N_2 and CH_4, the permeance of CO_2 through these membranes reduces less. This is due to two combined effects: (1) affinity of CO_2 for the $(CF_3)_2$ and C=O groups in the fluoro imides (*11, 39, 55*), in combination with (2) smaller molecular size of CO_2 (kinetic diameter, 3.3 Å (*56*)) as compared to the two other gases, N_2 and CH_4 (kinetic diameters: 3.64 Å (*40, 56*), 3.72 Å (*56*) respectively). This results in an increase in permselectivity of CO_2 over the other gases, with an increasing number of grafting steps (Figure 6).

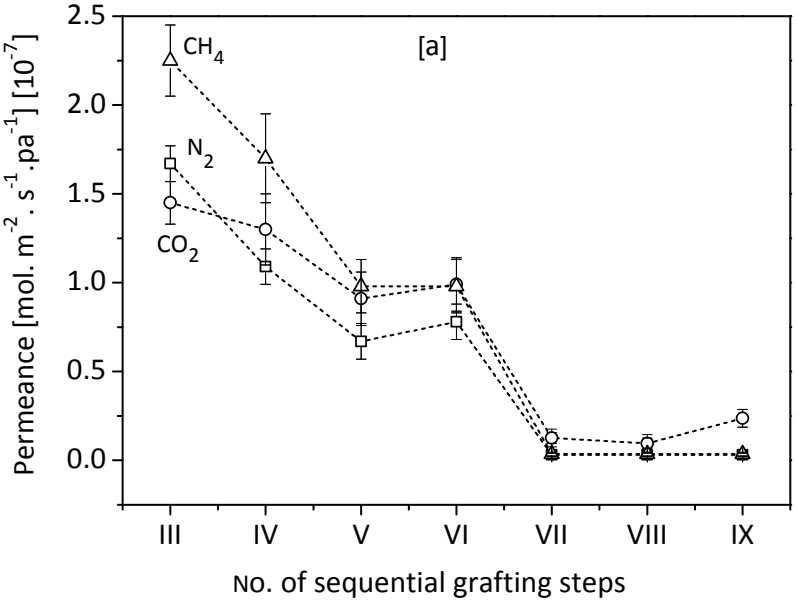
[a]
CH4
N2
CO2
Permeance [mol. m-2 . s-1 .pa-1] [10-7]
2.5
2.0
1.5
1.0
0.5
0.0
III
IV
V
VI
VII
VIII
IX
No. of sequential grafting steps

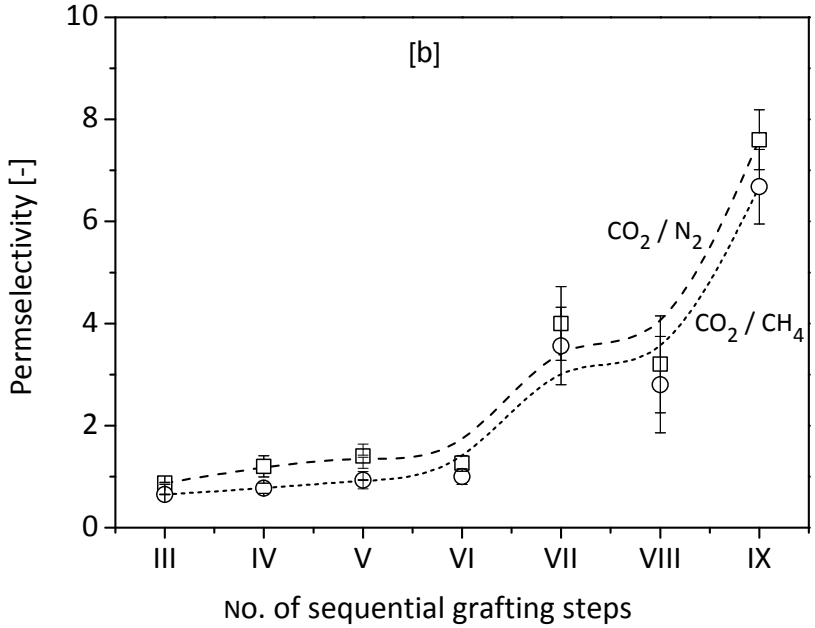
[b]
CO2 / N2
CO2 / CH4
Permselectivity [-]
10
8
6
4
2
0
III
IV
V
VI
VII
VIII
IX
No. of sequential grafting steps

Figure 6: Single gas dead-end (a) permeance and (b) permselectivity for 6FDA-6F*p*DA sequentially grafted meso–porous γ–alumina. Temperature =100 ^{o}C, the lines are guides to the eye.

The gas permeation measurements are performed at elevated temperatures up to 150 ^{o}C that can be considered relatively high for organic gas separation membranes. For instance, typical analysis of CO_2 separation based on the Robeson plot (*41, 49*) involves permeance measurements at 35^{o}C. At such low temperatures the grafted membranes, with substantial porefilling, show only very limited permeance.

For a membrane synthesized by sequential grafting of 6FDA-6F*p*DA precursors, the evolution of the permeance with temperature is displayed in Figure 7. In the temperature range up to 60 ^{o}C minor permeance of N_2 and CH_4 is observed, while the permeance of CO_2 is significantly higher because of favorable interactions between CO_2 and the grafted species and the small kinetic diameter of CO_2. At 100 ^{o}C, no remarkable change in permeance is observed for N_2 and CH_4, while an increase is observed for CO_2. This increase is related to increased macromolecular dynamics of the confined grafted organic species, resulting in a pronounced increase in mobility of CO_2 because of relatively small kinetic diameter of CO_2 (3.3 Å) compared to CH_4 (3.72 Å) and N_2 (3.64 Å) in combination with favorable interactions between strong the quadrupole moment of CO_2 with polar groups (–$(CF_3)_2$, C = O) in the 6FDA-6F*p*DA polyimide (*11, 39, 40, 48*). However, a further increase in temperature to 150 ^{o}C results in a continued rise in CO_2 permeance, combined with a significant rise in permeance of the other two gases, CH_4 and N_2. The result is a drastic reduction in permselectivity. This indicates that at 150 ^{o}C, despite the length scale confinement of the grafted organic species, macromolecular dynamics have increased to such an extent that all

three gases have become relatively mobile, which is consistent with observations at 100 ^{o}C. The increase in permeabilities with temperature occurs as diffusion through polymeric groups is an activated process; the diffusion coefficient increases exponentially with temperature (*57*). The mobility increases because at increasing temperature the probability that a molecular jump can occur across a particular energy barrier is larger, but also because the heights of energy barriers are reduced by enhanced thermal motions of the polymer matrix. The weak correlation between temperature and transport, up to 100 ^{o}C, suggests a limited enhancement in the thermal motions of the polyimide material. This is because of its confinement in the pores, and the covalent attachment to the pore walls (*58, 59*), of the rigid porous ceramic support. A number of research groups have reported on the thermal-mechanical properties of inorganic-organic composite materials, such as silsequioxane-polymer nanocomposites (*24, 55, 58-62*). Iyer *et al.* (*60*) reported a gradual increase in the glass transition temperature (T_g) of a polyimide from 300 ^{o}C to ~320 ^{o}C by incorporation of silsesquioxanes in the matrix. They have concluded that the shift in T_g to higher temperatures is due to restricted segmental chain mobility, because of chemical interactions between the flexible polymer segments and the rigid inorganic silsesquioxane. In an another study (*55*) the same group reported a significant improvement in the permselectivity of CO_2/CH_4, as a function of OAPS loading (0 - 20 wt%) in a fluoro polyimide (6FDA-MDA). The increase was attributed to the favorable interactions between amine groups in OAPS and CO_2. Kulkarni *et al.* (*58*) reported gas permeation studies at elevated temperature (60 ^{o}C) and showed a significant increase in CO_2/CH_4 permselectivity in silsesquioxane-polyimide mixed matrix membrane, as compared to a fully organic polyimide

membrane. This was explained by the restriction in mobility of the polymer segments induced by the silsesquioxane. Supporting the above report, Yani *et al.* (*61*) have reported molecular dynamics simulation studies showing the increase in T_g of polyimide ~20 ^{o}C by blending silsesquioxane into a polyimide matrix. Tamaki *et al.* used OAPS (octaaminophenyl) silsesquioxane as building blocks to form OAPS-polyimide nanocomposites with enhanced thermal-mechanical properties, such as the glass transition temperature (T_g), and the thermal expansion coefficient (*25, 63*). The high reactivity of octafunctional POSS was used to form a continuous POSS network within the polyimide. Choi *et al.* (*59*) reported improved physical, thermal, and mechanical properties of inorganic-imide composite material formed from aminophenylsilsesquioxanes and polyimides. They mentioned that improved thermal, mechanical properties were achieved, due to stability induced by cross-linking between OAPS and polyimides, and the uniform dispersion of OAPS silica particles in the polyimide matrix.

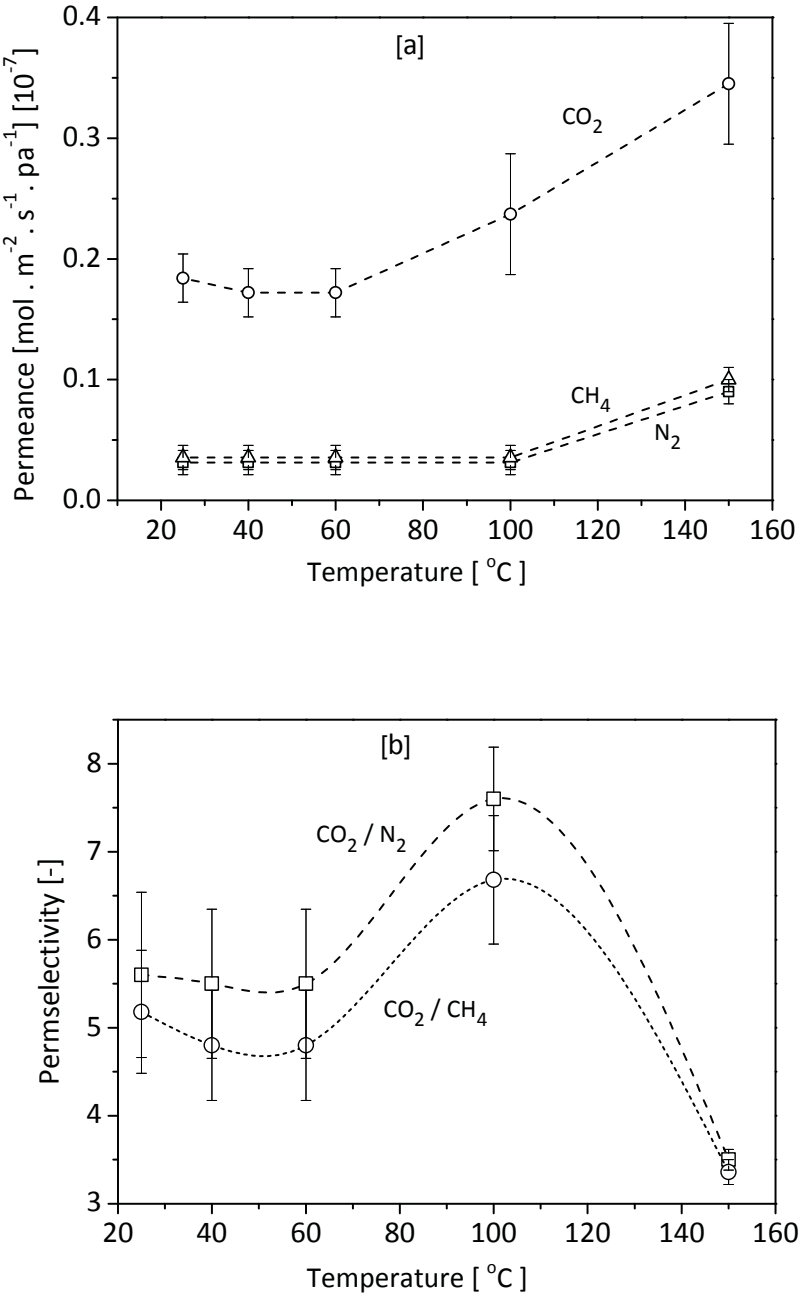

Figure 7: Single gas dead-end (a) permeance and (b) permselectivity for 6FDA-6F*p*DA sequentially grafted meso–porous γ–alumina membrane as a function of temperature, lines provide a guide to the eye.

In accordance with these studies, the thermal evolution of the permeance of samples observed in this chapter suggests a distinct thermal-mechanical behavior of the organic material, due to the confinement inside the nanopores of the ceramic. Based on the current data, a quantitative analysis of the confinement effect is not feasible. Such a quantitative assessment would require a far more elaborate performance study, involving a much larger sample collection and a much broader process parameter space. In particular, the process conditions should include much higher CO_2 pressures, as it is well-known that such conditions can cause plasticization of an organic material. In addition to direct confinement-performance studies, indirect measurements of thermal-mechanical properties should be conducted. In particular, changes in the glass transition temperature (T_g) can be exploited. The value of T_g is an indication for the temperature above which cooperative motions of polymer chains transform the material from a glassy to a liquid state. More flexible polymers would have a lower T_g, where as a rigid polymer would have a relatively higher T_g. The conventional techniques for T_g analysis include differential scanning calorimetry (DSC) and dynamic mechanical analysis (DMA) (*24, 58-60*). These techniques cannot be used in a straightforward manner to determine the T_g of the grafted samples synthesized in this chapter. DMA will probe the mechanical properties of the inorganic host, rather than those of the confined organic part. The interpretation of DSC data will be complicated by the fact that imides are typical high-T_g polymers. The confinement of the organic oligomers will further deprive the covalently attached oligomers from attaining liquid like mobility, up to

the temperature of chemical degradation. For direct characterization of the thermal-mechanical features of the grafted samples, dielectric spectroscopy (DRS) is a potentially very interesting technique. This technique allows direct probing of macromolecular mobility, and has been extensively applied to study the combined effects of length-scale confinement and temperature on polymer relaxation (*64-67*).

4.4 Conclusions

Sequential molecular grafting of aromatic polyimide precursors (6FDA and 6F*p*DA) onto aminofunctionalized meso-porous γ-alumina membranes causes an incremental increase of the amount of organic species in the meso-porous material. The initial amino functionalization of the surface with OAPS, covalently bound to vapor phase grafted CPTES molecules, allows effective sequential grafting until the material has lost its meso-porous characteristics. With increasing number of grafting steps, single gas permeance of CH_4, N_2 and CO_2 (100 ºC, Δp= 4 bar) decreases. For CO_2 the reduction in permeance is significantly lower, due to the affinity of this gas with the fluorine groups in the imide oligomer. The observed maximum permselectivity of CO_2 over the other gases, at 100 ºC, may be explained from a severe length scale confinement induced reduction in oligomer molecular dynamics at lower temperatures, and amplified chain mobility at higher temperatures.

References

1. C. W. Jones, Zeolites go organic. *Science* **300**, 439 (2003).

2. M. Dalwani *et al.*, Ultra-thin hybrid polyhedral silsesquioxane-polyamide films with potentially unlimited 2D dimensions. *Journal of Materials Chemistry* **22**, 14835 (2012).

3. C. Rottman, G. Grader, Y. De Hazan, S. Melchior, D. Avnir, Surfactant-Induced Modification of Dopants Reactivity in Sol−Gel Matrixes. *Journal of the American Chemical Society* **121**, 8533 (1999/09/01, 1999).

4. C. Sanchez *et al.*, Designed hybrid organic-inorganic nanocomposites from functional nanobuilding blocks. *Chemistry of Materials* **13**, 3061 (2001).

5. B. Lebeau, S. Brasselet, J. Zyss, C. Sanchez, Design, Characterization, and Processing of Hybrid Organic−Inorganic Coatings with Very High Second-Order Optical Nonlinearities. *Chemistry of Materials* **9**, 1012 (1997/04/01, 1997).

6. T. D. d. Morais, F. Chaput, K. Lahlil, J.-P. Boilot, Hybrid Organic–Inorganic Light-Emitting Diodes. *Advanced Materials* **11**, 107 (1999).

7. O. C. David, D. Gorri, K. Nijmeijer, I. Ortiz, A. Urtiaga, Hydrogen separation from multicomponent gas mixtures containing CO, N_2 and CO_2 using Matrimid ® asymmetric hollow fiber membranes. *Journal of Membrane Science* **419-420**, 49 (2012).

8. F. Li, Y. Li, T. S. Chung, S. Kawi, Facilitated transport by hybrid POSS®-Matrimid®-Zn2+ nanocomposite membranes for the separation of natural gas. *Journal of Membrane Science* **356**, 14 (2010).

9. P. Vandezande, X. Li, L. E. M. Gevers, I. F. J. Vankelecom, High throughput study of phase inversion parameters for polyimide-based SRNF membranes. *Journal of Membrane Science* **330**, 307 (2009).

10. K. Vanherck, P. Vandezande, S. O. Aldea, I. F. J. Vankelecom, Cross-linked polyimide membranes for solvent resistant nanofiltration in aprotic solvents. *Journal of Membrane Science* **320**, 468 (2008).

11. K. Tanaka, M. Okano, H. Kita, K.-i. Okamoto, S. Nishi, Effects of trifluoromethyl side groups on gas permeability and permselectivity in polyimides. *Polymer Journal* **26**, 1186 (1994).

12. Y. Hirayama *et al.*, Relation of gas permeability with structure of aromatic polyimides I. *Journal of Membrane Science* **111**, 169 (1996).

13. Y. Hirayama *et al.*, Relation of gas permeability with structure of aromatic polyimides II. *Journal of Membrane Science* **111**, 183 (1996).

14. L. M. Robeson, C. D. Smith, M. Langsam, A group contribution approach to predict permeability and permselectivity of aromatic polymers. *Journal of Membrane Science* **132**, 33 (1997).

15. T.-H. Kim, W. J. Koros, G. R. Husk, Advanced gas separation membrane materials: Rigid aromatic polyimides. *Separation Science and Technology* **23**, 1611 (1988).

16. M. R. Coleman, W. J. Koros, Isomeric polyimides based on fluorinated dianhydrides and diamines for gas separation applications. *Journal of Membrane Science* **50**, 285 (1990).

17. K. J. Shea, D. A. Loy, Bridged polysilsesquioxanes. Molecular-engineered hybrid organic-inorganic materials. *Chemistry of Materials* **13**, 3306 (2001).

18. D. A. Loy *et al.*, Dialkylene carbonate-bridged polysilsesquioxanes. Hybrid organic-inorganic sol-gels with a thermally labile bridging group. *Chemistry of Materials* **11**, 3333 (1999).

19. H. L. Castricum, A. Sah, M. C. Mittelmeijer-Hazeleger, J. E. ten Elshof, Hydrophobisation of mesoporous γ-Al_2O_3 with organochlorosilanes—efficiency and structure. *Microporous and Mesoporous Materials* **83**, 1 (2005).

20. A. Stein, B. J. Melde, R. C. Schroden, Hybrid Inorganic–Organic Mesoporous Silicates—Nanoscopic Reactors Coming of Age. *Advanced Materials* **12**, 1403 (2000).

21. A. Sah, H. L. Castricum, A. Bliek, D. H. A. Blank, J. E. ten Elshof, Hydrophobic modification of γ-alumina membranes with organochlorosilanes. *Journal of Membrane Science* **243**, 125 (2004).

22. V. G. P. Sripathi *et al.*, Sequential grafting strategy for hybrid meso-porous polyimide-alumina. *manuscript in preparation*, (2013).

23. C. Hartmann-Thompson, *Applications of polyhedral Oligomeric Silsesquioxanes*. J. Matisons, Ed., Advances in Silicon Science (Springer Sciences+Business Media B.V., 2011), vol. 3

24. J.-c. Huang *et al.*, Polyimide/POSS nanocomposites: interfacial interaction, thermal properties and mechanical properties. *Polymer* **44**, 4491 (2003).

25. R. Tamaki, J. Choi, R. M. Laine, A Polyimide Nanocomposite from Octa(aminophenyl)silsesquioxane. *Chemistry of Materials* **15**, 793 (2003/02/01, 2003).

26. F. Huang, Z. Rong, X. Shen, L. Du, Z. Li, Organic/inorganic hybrid bismaleimide resin with octa(aminophenyl) silsesquioxane. *Polymer Engineering and Science* **48**, 1022 (2008).

27. J.-H. Choi *et al.*, Preparation of polymer/POSS nanocomposites by radiation processing. *Radiation Physics and Chemistry* **78**, 517 (2009).

28. V. G. P. Sripathi, B. L. Mojet, A. Nijmeijer, N. E. Benes, Vapor phase versus liquid phase grafting of alumina. *Microporous and Mesoporous Materials* **172**, 1 (2013).

29. A. F. d. M. Pinheiro, Development and charecterization of polymer-grafted ceramic membranes for solvent nanofiltration. *Ph.D. thesis, University of Twente*, (2013).

30. Velianti, M. Sc. thesis, Inorganic Membranes Group, University of Twente (2010).

31. E. P. Barrett, L. G. Joyner, P. P. Halenda, The Determination of Pore Volume and Area Distributions in Porous Substances. I. Computations from Nitrogen Isotherms. *Journal of the American Chemical Society* **73**, 373 (1951/01/01, 1951).

32. N. Gartmann, C. Schütze, H. Ritter, D. Brühwiler, The Effect of Water on the Functionalization of Mesoporous Silica with 3-Aminopropyltriethoxysilane. *The Journal of Physical Chemistry Letters* **1**, 379 (2010/01/07, 2009).

33. S. Brunauer, P. H. Emmett, E. Teller, Adsorption of Gases in Multimolecular Layers. *Journal of the American Chemical Society* **60**, 309 (1938/02/01, 1938).

34. S. J. Gregg, K. S. W. Sing, *Adsorption, surface area and porosity*. (Academic Press, 1991), vol. 2, illustrated, pp. 10 - 15.

35. V. G. P. Sripathi, B. L. Mojet, A. Nijmeijer, N. E. Benes, Sequential grafting strategy for hybrid meso-porous polyimide-alumina. *Manuscript under preparation*, (2013).

36. M. Bhagiyalakshmi, R. Anuradha, S. D. Park, H. T. Jang, Octa(aminophenyl)silsesquioxane fabrication on chlorofunctionalized mesoporous SBA-15 for CO_2 adsorption. *Microporous and Mesoporous Materials* **131**, 265 (2010).

37. T. Suzuki, Y. Yamada, Characterization of 6FDA-based hyperbranched and linear polyimide–silica hybrid membranes by gas permeation and 129Xe NMR measurements. *Journal of Polymer Science Part B: Polymer Physics* **44**, 291 (2006).

38. J. Ren, R. Wang, T.-S. Chung, D. F. Li, Y. Liu, The effects of chemical modifications on morphology and performance of 6FDA-ODA/NDA hollow fiber membranes for CO_2/CH_4 separation. *Journal of Membrane Science* **222**, 133 (2003).

39. S. A. Stern, Y. Liu, W. A. Feld, Structure/permeability relationships of polyimides with branched or extended diamine moieties. *Journal of Polymer Science, Part B: Polymer Physics* **31**, 939 (1993).

40. D. M. D'Alessandro, B. Smit, J. R. Long, Carbon Dioxide Capture: Prospects for New Materials. *Angew. Chem. Int. Ed.* **49**, 6058 (2010).

41. L. M. Robeson, Correlation of separation factor versus permeability for polymeric membranes. *Journal of Membrane Science* **62**, 165 (1991).

42. A. Bos, I. G. M. Pünt, M. Wessling, H. Strathmann, CO_2-induced plasticization phenomena in glassy polymers. *Journal of Membrane Science* **155**, 67 (1999).

43. A. Bos, High pressure CO_2/CH_4 separation with glassy polymer membranes. *Ph.D. thesis, University of twente, The Netherlands*, (1996).

44. A. Bos, I. G. M. Pünt, M. Wessling, H. Strathmann, Plasticization-resistant glassy polyimide membranes for CO_2/CH_4 separations. *Separation and Purification Technology* **14**, 27 (1998).

45. A. Bos, I. Pünt, H. Strathmann, M. Wessling, Suppression of gas separation membrane plasticization by homogeneous polymer blending. *AIChE Journal* **47**, 1088 (2001).

46. T. Visser, Mixed gas plasticization phenomena in asymmetric membranes. *Ph.D. thesis, University of twente, The Netherlands*, (2006).

47. Y. Xiao, B. T. Low, S. S. Hosseini, T. S. Chung, D. R. Paul, The strategies of molecular architecture and modification of polyimide-based membranes for CO_2 removal from natural gas-A review. *Progress in Polymer Science (Oxford)* **34**, 561 (2009).

48. S. A. Stern, Y. MI, H. Yamamoto, Structure / permeability relationships of polyimide membranes. Applications to the seperation of gas mixtures. *journal of polymer science: Part B: Polymer physics* **27**, (1989).

49. L. M. Robeson, The upper bound revisited. *Journal of Membrane Science* **320**, 390 (2008).

50. W.-H. Lin, R. H. Vora, T.-S. Chung, Gas transport properties of 6FDA-Durene/1,4-phenylenediamine (pPDA) copolyimides. *Journal of polymer science: Part B: Polymer physics* **38**, (2000).

51. S.L.Liu *et al.*, Effect of diamine composition on the gas transport properties in 6FDA-durene/3,3' -diaminodiphenyl sulfone copolyimides. *Journal of Membrane Science* **202**, (2002).

52. S.-X. Cheng, T.-S. Chung, R. Wang, R. H. Vora, Gas-sorption properties of 6FDA-Durene/1,4-Phenylenediamine (pPDA) and 6FDA-durene/1,3-Phenylenediamine (mPDA) copolyimides. *Journal of Applied Polymer Science* **90**, (2003).

53. R. W. Baker, *Membrane Technology and Applications,* . (A John Wiley & Sons, Ltd., Publications, ed. 3, 2012).

54. M. Smaihi, J. C. Schrotter, C. Lesimple, I. Prevost, C. Guizard, Gas separation properties of hybrid imide - siloxane copolymers with various silica contents. *Journal of Membrane Science* **161**, (1999).

55. P. Iyer, G. Iyer, M. Coleman, Gas transport properties of polyimide-POSS nanocomposites. *Journal of Membrane Science* **358**, 26 (2010).

56. D. W. Breck, *Zeolite Molecular Sieves: structure, chemistry, and use*. (Wiley & Sons: New York., 1974).

57. W.-H. Lin, T.-S. Chung, Gas permeability, diffusivity, solubility, and aging charecteristics of 6FDA-durene polyimide membranes. *Journal of Membrane Science* **186**, 183 (2001).

58. P. P. Kulkarni, Effect of Polyhedral Oligomeric Silsesquioxane on Gas transport Properties of Polyimide *PhD Thesis, University of Toledo*, (2007).

59. J. Choi, R. Tamaki, S. G. Kim, R. M. Laine, Organic/Inorganic Imide Nanocomposites from Aminophenylsilsesquioxanes. *Chemisry of Materials* **15**, 3365 (2003).

60. P. Iyer, M. R. Coleman, Thermal and mechanical properties of blended polyimide and amine functionalized poly(orthosilsesquioxane) composites. *Journal of Applied Polymer Science* **108**, 2691 (2008).

61. Y. Yani, M. H. Lamm, Molecular dynamics simulation of mixed matrix nanocomposites containing polyimide and polyhedral oligomeric silsesquioxane (POSS). *Polymer* **50**, 1324 (2009).

62. M. L. Chua, L. Shao, B. T. Low, Y. Xiao, T.-s. Chung, Polyetheramine-polyhedral oligomeric silsesquioxane organic-inorganic hybrid membranes for CO_2/H_2 and CO_2/N_2 separation. *Journal of Membrane Science* **385**, 40 (2011).

63. R. Tamaki, Y. Tanaka, M. Z. Asuncion, J. Choi, R. M. Lain, Octa(aminophenyl)slsesquioxane as a nanoconstruction site. *J. Am. Chem. Soc.* **123**, 1241 (2001).

64. J. Schuller, Y. B. M. nichenko, R. Richert, E. W. Fischer, Dielectric studies of the glass transitionn in porous media. *Phys. Rev. Lett.* **73**, 2224 (1994).

65. M. Arndt, R. Stannarius, H. Groothues, E. Hempel, F. Kremer, Length scale of cooperativity in the dynamic glass transition. *Phys. Rev. Lett.* **79**, 2077 (1997).

66. G. Barut, P. Pissis, R. Pelster, G. Nimtz, Glass transition in liquids: Two versus three-dimentional confinement. *Phys. Rev. Lett.* **80**, 3543 (1998).

67. K. Fukao, Y. Miyamoto, Glass transitions and dynamics in thin polymer films: Dielectric relaxation of thin films of polystyrene. *Physical Review E* **61**, 1743 (2000).

5

Polyether-alumina hybrid membranes by sequential molecular grafting

Abstract

Hybrid polyether-alumina membranes have been prepared by sequential grafting of a diamine (Jeffamine®) and tri (ethylene glycol) bis (chloroformate) onto chloro-functionalized meso-porous γ-alumina. Aim is to construct membranes with low molecular weight ether oligomers, confined to the pores of the meso-porous ceramic material. Length-scale confinement of the oligomeric ether molecules is anticipated to affect the molecular selectivity of these membranes. N_2- physisorption and FTIR confirm the sequential grafting of the γ-alumina powder. The grafting becomes less effective with an increasing number of grafting steps, and obtaining a fully non-porous structure via this approach appears to be impracticable. For supported thin film γ-alumina membranes, sequential grafting results in a thin polyether layer on top of the external surface of the γ-alumina layer, while inside the γ-alumina material open nanometer size pores persist. Permeance data at 100 ^{o}C reveal that the thin polyether layer acts as a barrier for N_2 and CH_4, while for CO_2 transport, the solution-diffusion mechanism is apparent. The low permeance of N_2 and CH_4 at the relatively high temperature is due to the moderated dynamics of the nano-confined organic species and its covalent attachment to the surface of the thermo-mechanically stable ceramic material. The distinct transport rate of CO_2 is due to the favorable interactions of the quadrupolar CO_2 with polar ethers.

5.1 Introduction

The molecular separation of carbon dioxide (CO_2) from mixtures of gases is important in many industrial fields. In this respect, membrane technology can be considered promising, because of the associated high energy and separation efficiency. Membranes for CO_2 removal typically posses a higher affinity towards CO_2 than to the other gases, from which it is to be separated. Several organic materials are known for exhibiting such enhanced affinity for CO_2. Examples include fluorinated polyimides and polyethylene oxides (PEO). In the last materials family the affinity for CO_2 is considered to originate from interactions between the quadrupole moment of the CO_2 and the polar ether oxygen atoms (*1-3*). Hydrophilic PEO based block copolymers, such as PEBAX®, are currently used in many applications on an industrial scale (*2, 4-6*). Kusuma *et al.* (*7-9*) and Reijerkerk *et al.* (*2, 4, 5, 10*) reported extensive investigations aiming at further optimization of poly (ethylene oxide) based membranes for separation of CO_2 from light gases. In particular, investigations have been devoted to moderating the tendency of PEO to crystallize (*11-14*). Approaches include the use of block co-polymers containing PEO and various types of hard and soft segments (e.g., polyamides (*15-17*), polyimides (*18*), PDMS (*9*), (*19*)). The incorporated segments should provide mechanical stability and/or inhibit crystallization of PEO. Lin *et al.* proposed (*1*) that crystallization can be controlled in cross-linked PEO if the molecular weight between the cross-linkers is lower than 1500 Dalton. Freeman and co-authors reported the fabrication of cross-linked network materials, formed from PEO acrylates and diacrylates, exhibiting superior separation performance (*20-23*).

Here we propose a distinct method for moderating the propensity of ethylene oxide to crystalize. The approach is aimed at confining low molecular weight PEO in the pores of a meso-porous inorganic material. The construction of such a hybrid organic-inorganic material is to be achieved by sequential chemical grafting of a polyether diamine (Jeffamine®) and tri (ethylene glycol) bis (chloroformate) (TEBC), inside the porous structure of meso-porous γ-alumina (see Figure 1). Jeffamine® can be covalently bonded to the γ-alumina surface by using chloropropyltriethoxysilane (CPTES) as primer. The hydrolysable alkoxy groups of CPTES react with the hydroxyl groups of γ-alumina, leaving the chlorine groups available for a condensation reaction with the Jeffamine®. Subsequently, unreacted primary amines of the Jeffamine® can react with the chlorine groups in TEBC. The reaction with Jeffamine® and TEBC can be repeated in a sequential fashion, to further fill up the pores of the alumina. This process will terminate when the remaining amount of open pore space is too low to allow an appreciable rate of mass transport of the grafting molecules, or until the reactive groups are no longer accessible for a reaction.

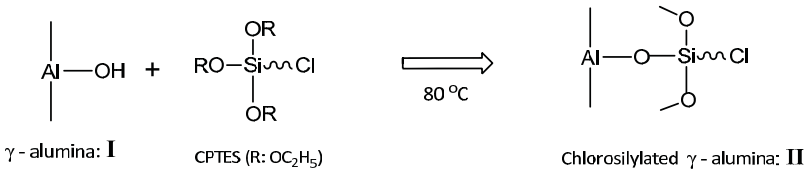

γ - alumina: **I** CPTES (R: OC_2H_5) Chlorosilylated γ - alumina: **II**

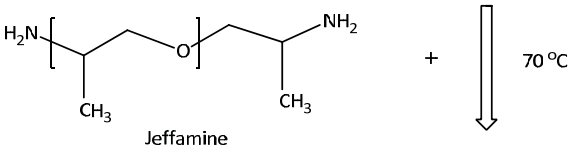

Jeffamine

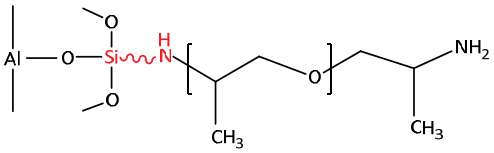

Jeffamine grafting over chlorosilylated γ - alumina: **III**

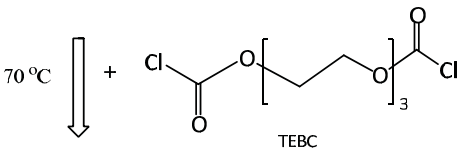

TEBC

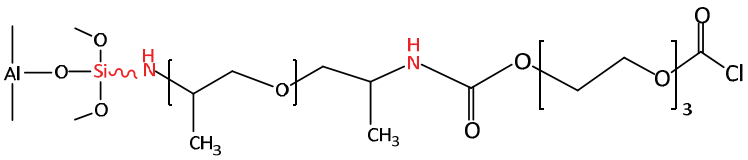

Sequential grafting of TEBC over ethoxylated γ - alumina: **IV**

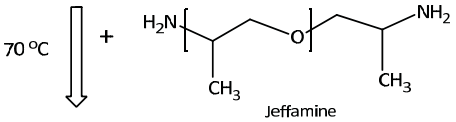

Jeffamine

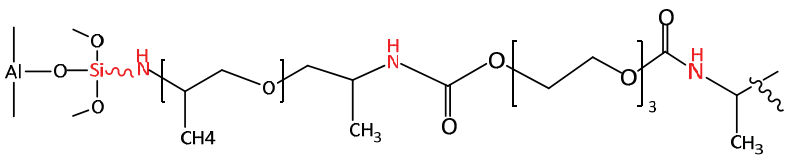

Sequential grafting of jeffamine over TEBC functionalized γ - alumina: **V**

Figure 1: Schematic representation of sequential grafting of PEO over chlorosilylated meso-porous γ-alumina.

5.2 Experimental

5.2.1 Materials

Chloropropyltriethoxysilane (CPTES, 97 % purity), toluene (anhydrous 99.8 %) and tri(ethyleneglycol) bis(chloroformate) (TEBC), were obtained from Sigma-Aldrich. Jeffamine® D-400 polyether amine and high purity (98%) ethanol were obtained from Merck.

5.2.2 Synthesis of meso-porous γ-alumina

Meso-porous γ-alumina flakes were prepared from a boehmite sol that was dried and subsequently calcined at 600 ^{o}C in air, as described in detail elsewhere (*24*). A sufficiently large quantity of powder was synthesized to allow use of the same batch of powder for all experiments in this chapter, in order to limit the influence of variations in γ-alumina powder properties on sequential grafting experiments.

5.2.3 Sequential grafting

5.2.3.1 Grafting CPTES linker by vapor phase grafting

Powders: CPTES was grafted on to meso-porous γ-alumina as described previously (*25, 26*). Briefly, toluene and CPTES (2.5 wt %) were added to a round bottom flask RB I, and were allowed to pass through a horizontal tube to react with γ-alumina powder in round bottom flask RB II (Figure 4 (lower), Chapter 1). Equal temperatures (80 ^{o}C) were maintained in the two RB flasks and the reaction was carried out for 3 hrs. All chemicals were added inside a glove box prior to the start of the reaction.

Flat supported membranes: CPTES and toluene were added to a triple neck flask, on top of which a glass tube was connected (Figure 4 (top), Chapter 1). In this glass tube a disc shaped flat supported γ-alumina membrane (39 mm diameter, 2 mm thick α-alumina coated with 2 μm γ-alumina, for details see (*27*) was placed upside down as shown in the magnified part in Figure 4 (*28*), chapter 1. CPTES vapor, produced upon heating to 80 °C, was allowed to react with the top γ-alumina layer of ceramic membrane. All reaction conditions were similar to those used for the powders (see above).

After the reaction was completed, the powders and membrane were soaked in 30 ml toluene and in 30 ml ethanol for ~10 hrs each. Finally the chlorosilylated γ-alumina porous materials were annealed at 100 °C for 2 hrs.

5.2.3.2 Sequential grafting onto chlorosilylated γ-alumina

Chlorosilylated γ-alumina powder (600 mg) or a chlorosilylated flat membrane was placed in a RB flask containing 50 ml toluene. Subsequently, 179 μl Jeffamine® was added. After 3 hrs reaction time at 70 °C under reflux, the membranes were soaked in toluene overnight, and then annealed at 100 °C for 3 hrs.

Jeffamine® grafted powder (250 mg) or a γ-alumina disk shaped membrane was placed in a RB flask containing 50 ml toluene. Subsequently, 415 μl of TEBC was added and the reaction was allowed to proceed for 3 hrs at 70 °C under reflux conditions. Finally, the membrane was soaked in 30 ml toluene overnight, and annealed at 100 °C for 2 hrs.

Sequential grafting was done by repeating these two steps, intermittingly rinsing the samples with toluene.

5.2.4 Characterization

5.2.4.1 N_2-physisorption

Pore morphology of the powders was investigated with N_2-gas physisorption at -196 °C in a Micromeritics Gemini device. Prior to the sorption experiments, all samples were degassed at 100 ^{o}C for 12 hrs. The pore size distributions were estimated from desorption branch of the isotherm by the Barrett-Joyner-Halenda (BJH) method (*29, 30*). The total surface area (S_{BET}) was obtained using the standard Brunauer-Emmett-Teller method for adsorption data (*31*). The total pore volume (V_p) was calculated from the amount of N_2-adsorbed at a relative pressure of 0.95.

5.2.4.2 Fourier transform infrared spectroscopy

Surface chemistry of the material was characterized with Attenuated Total Reflection Fourier Transform Infrared Spectroscopy (ATR-FTIR), using a Bruker optics tensor 27 model equipped with a diamond crystal.

5.2.4.3 Scanning electron microscopy

Scanning electron microscopy images of supported membranes were taken on a field emission scanning electron microscope (model Merlin, Carl-Zeiss, Germany).

5.2.4.4 Gas permeance

Single gas permeance through supported membranes was measured in pressure controlled dead-end mode. Measurements were performed at a maximum operating temperature up to 100 ^{o}C, and a trans membrane pressure of 4 bar with ambient pressure at the permeate side. Membranes were placed with γ-alumina layer directed towards the gas feed side. For

each gas, adequate time (5 - 12 hrs) was given until a stable gas flow was observed. The gases were measured in the following order: N_2, CO_2, and CH_4. All measurements were repeated for at least two identical membranes. Each sequential grafting step was performed on a membrane that was not used for permeance measurements.

5.3 Results & discussion

5.3.1 N_2-physisorption

Figure 2 depicts the N_2-adsorption-desorption isotherms of sequentially grafted porous γ-alumina. The corresponding pore size distribution curves are shown in Figure 2b. Morphological characteristics are listed in Table I.

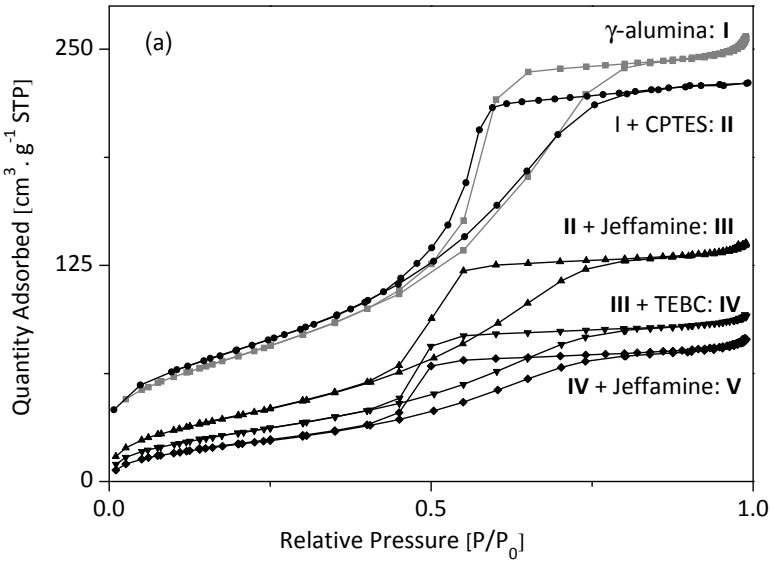

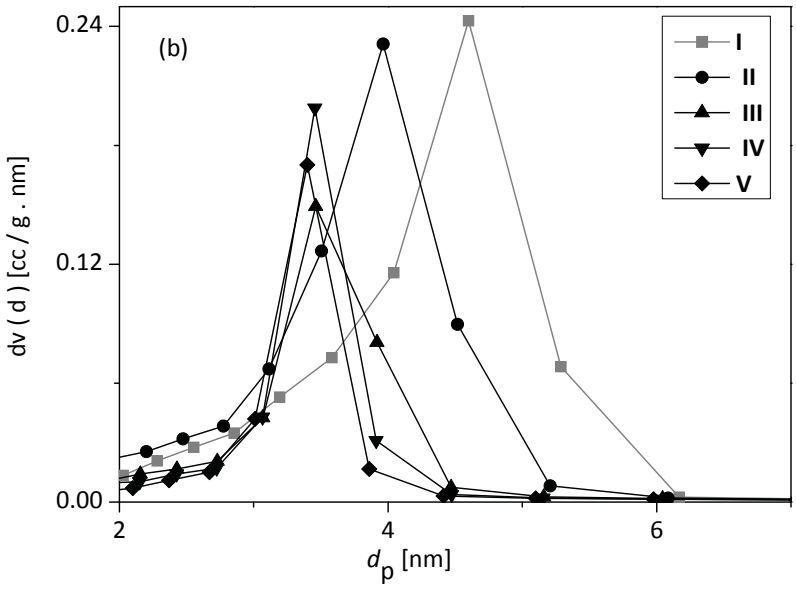

Figure 2: N_2-physisorption analysis of meso-porous γ-alumina, sequentially grafted with Jeffamine® and TEBC; (a) isotherms and (b) corresponding pore size distribution curves.

Vapor phase grafting of CPTES onto γ-alumina surface results in a small reduction in the amount of N_2-sorption. The pore size of the grafted material has shifted to a slightly lower value (from 4.6 to 4.1 nm) that corresponds well with the molecular dimensions of CPTES. These data suggest that the vapor phase grafting results in monolayer coverage of the internal pore surface of the porous ceramic material by CPTES. Similar observations have been made previously for vapor phase functionalization of γ-alumina with 3aminopropyltrimethoxysilane (3APTMS) (*23, 32-37*), more extensive details are discussed in chapter 2 of this thesis. These findings can be rationalized by the fact that oligomers of the precursor molecules have a relatively low vapor pressure, and hence low concentration

in the vapor phase. Consequently, reactions between single precursor molecules and the pore surface are predominant (*5*).

Material	S_{BET} [m^2g^{-1}]	V_p, BJH [cm^3g^{-1}]	d_p, BJH [nm]
γ–alumina : **I**	256	0.36	4.6
I + CPTES : **II**	225	0.3	4.1
II + Jeffamine: **III**	121	0.16	3.5
III + TEBC: **IV**	104	0.16	3.4
IV + Jeffamine: **V**	81	0.12	3.4

Table 1: Structural properties of γ-alumina powder after vapor phase functionalization with CPTES and sequential grafting with polyethylene oxides. S_{BET}: BET-surface area obtained between 0.05 – 0.2 P/P_0. V_P and d_p: Meso-pore volume and pore diameter respectively, calculated by BJH method. Same batch of γ-alumina powder is used for all experiments in this chapter in order to minimize the error contribution from powder synthesis.

After grafting of Jeffamine® onto the chloro-functionalized surface an additional reduction in N_2-gas sorption is observed, the surface area reduces from 225 to 121 m^2g^{-1}, the pore volume reduces from 0.3 to 0.16 cm^3g^{-1}, and the average pore size reduces from 4.1 to 3.5 nm. The sorption isotherm remains characteristic of a meso-porous material (*38*). This gradual reduction in pore size indicates that the Jeffamine® is intruding inside the pores of the γ-alumina powder, but the remaining pore size is still sufficiently large to allow transport of the monomers, and subsequent grafting. This is confirmed by the further reduction in N_2-gas sorption and surface area (121 to 104 m^2g^{-1}) after grafting with TEBC. No change in

average pore diameter after TEBC sequential grafting is observed, which suggests very limited intrusion of TEBC molecules inside the pores. This is most likely because of the large size of the TEBC, ~2 nm. The change is less compared to the pore-size reduction upon grafting (for the first time) with Jeffamine®. In addition, the decrease in pore volume and decrease in pore size are within the experimental error. This indicates that this second grafting step is less effective than the first one. Due to the second grafting step more organic molecules are present in the material, but still a meso-porous structure persists, allowing for an additional grafting step with Jeffamine®. This grafting step causes a further reduction in surface area (104 to 81 m^2/g), and insignificant changes in pore volume and pore size. These observations indicate that the effectiveness of grafting becomes less with an increasing number of grafting steps, and obtaining a fully non-porous structure via our approach appears to be impracticable.

5.3.2 Surface analysis by FT-IR

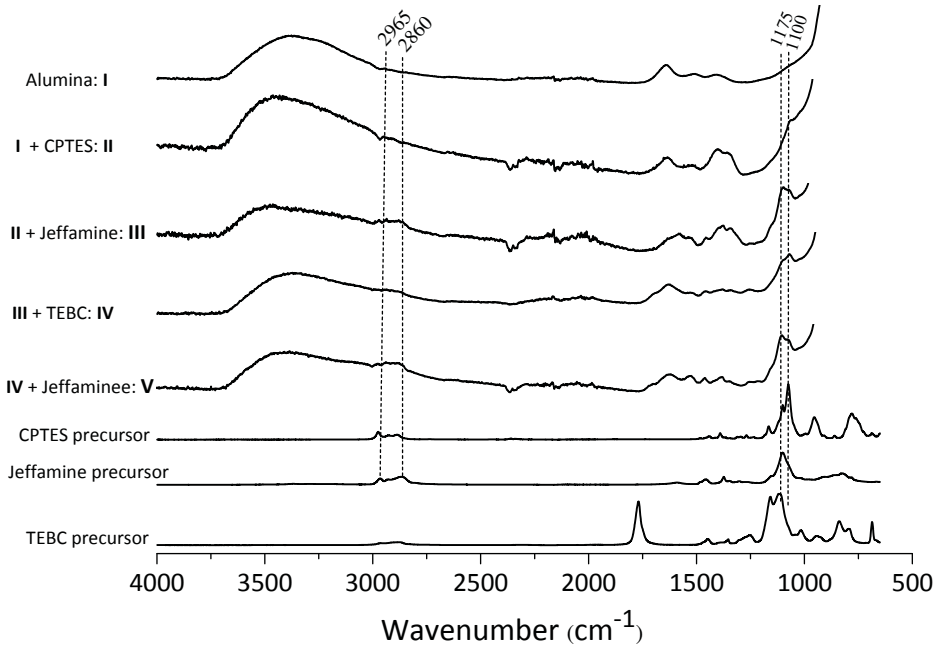

Figure 3: FT-IR characterization of CPTES functionalized meso-porous γ–alumina sequentially grafted with Jeffamine® and TEBC.

Figure 3 depicts infrared spectra of porous γ–alumina, before and after sequential grafting with polyethers. As reported previously, the γ–alumina powder is characterized by a broad band between 3700 – 3500 cm^{-1} that can be attributed to the presence of physisorbed water on γ–alumina hydroxyls. The sharp band at 1630 cm^{-1}, representing the bending mode of adsorbed water, further confirms this. The broad band at 1550 cm^{-1} has been attributed in literature to stretching vibrations of Al-OH bond, and the band at 1415 cm^{-1} probably corresponds to residual nitrates or organic groups, such as polyvinyl alcohol (*39, 40*) used in the preparation of the γ-alumina.

The reaction of CPTES with porous γ–alumina generates weak bands between 3000 – 2800 cm^{-1} that are assigned to C-H stretching of the propyl chain in CPTES. As discussed in Chapter 4, the persistence of a broad band at 3400 cm^{-1} indicates that some of the surface hydroxyl groups are still present. It is known that only single and geminal hydroxyl groups are able to react with silanes, whereas hydrogen bonded hydroxyl groups are inaccessible for such a reaction (*41, 42*).

The reaction of Jeffamine® with the chlorosilylated γ–alumina results in new bands, resembling those of the Jeffamine® precursor molecule. The bands around 1100 cm^{-1} are assigned to C-O stretching (*43, 44*), bands around 2965 and 2860 cm^{-1} are attributed to C-H stretching (*45*).

Further sequential grafting with TEBC does not result in major changes in the spectra, except for the change in shape of the band at 1100 cm^{-1} and emergence of a new shoulder at 1175 cm^{-1}, corresponding to a band of the TEBC precursor. Also, another shoulder emerges at around 1700 cm^{-1}, probably corresponding to the shifted distinct peak observed for the TEBC precursor at 1750 cm^{-1}.

Further sequential grafting of Jeffamine® over TEBC resulted in no major changes in spectra. The minor changes in spectra upon sequential grafting are consistent with the decrease in effectiveness of the surface modification with an increasing number of grafting steps, as has been observed in the N_2-physisorption experiments.

5.3.3 Supported membranes: SEM analysis

Figure 4 shows SEM images of a supported γ-alumina membrane after sequential grafting (step V). At lower magnification (25.000×) in Figure 4b, the α–alumina and γ-alumina layers can be distinguished. The image at higher magnification (462.000×) in Figure 4c, reveals a layer on top of the γ-alumina membrane. The thickness of this layer cannot be resolved quantitatively from the image. Clearly, the organic material does not completely fill all the pores of the γ-alumina.

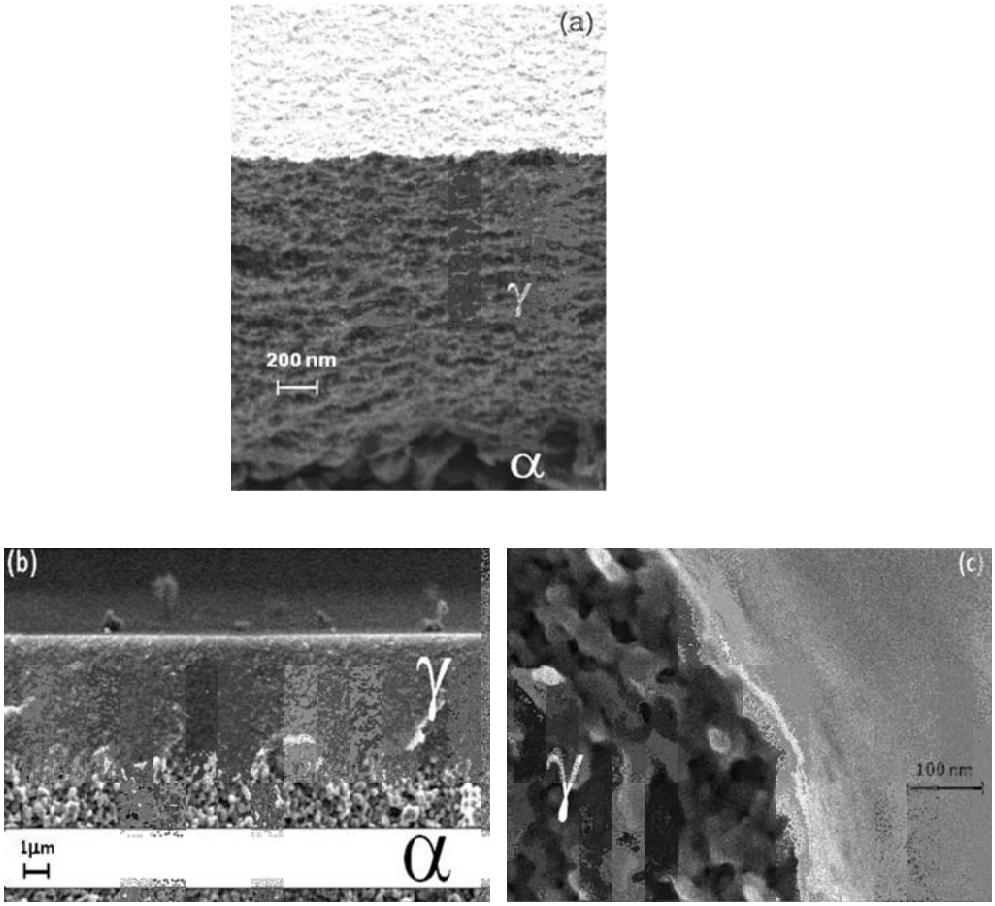

Figure 4: SEM images of supported γ–alumina membranes, unreacted (a) and sequentially grafted with polyethylene oxides: corresponding to material V (b & c).

5.3.4 Gas permeation

Figure 5 depicts data for dead-end gas permeance of N_2, CH_4, and CO_2 through γ-alumina membranes, as a function of the number of grafting steps.

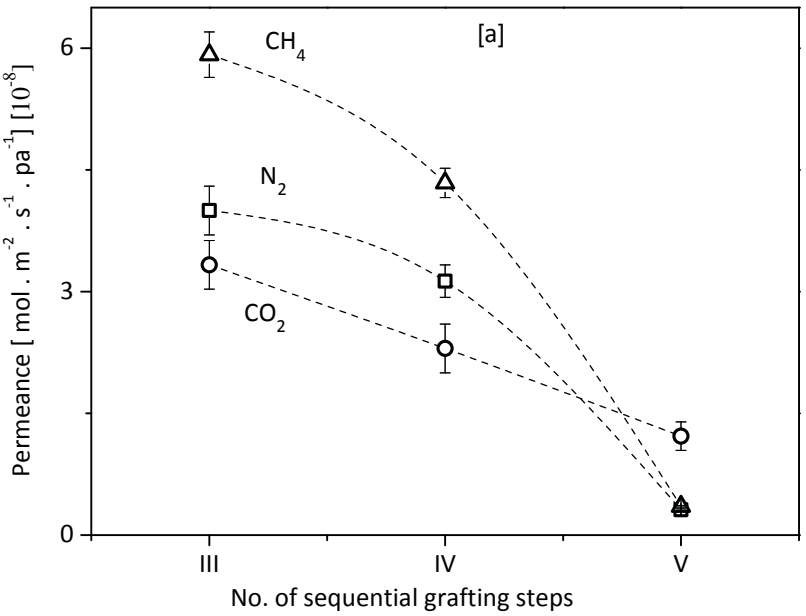

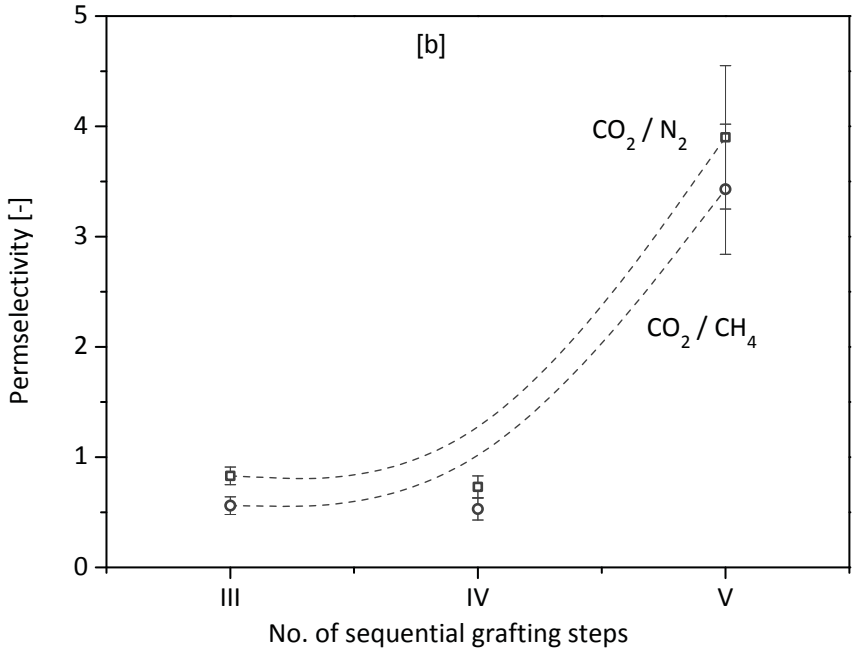

Figure 5: Single gas dead-end (a) permeance and (b) permselectivity of porous γ-alumina sequentially grafted with etheroxides. Temperature: 100 °C, trans-membrane pressure 4 bar, atmospheric pressure at permeate side, lines provide a guide to the eye.

For the chlorosyliated membrane, the permeance is comparable to that of an untreated γ-alumina membrane (*46*), and the selectivity of the gases complies with the square root of molar mass dependence typical for Knudsen diffusion. This indicates that, in the porous material, the translational degrees of freedom of the molecules remain similar to those of a gas, and affinity between the porous material and the gas molecules is not apparent.

After grafting with Jeffamine® (for the first time) the permeance of all three gases decreases and the selectivity remains unaltered. This indicates that the pore volume in the material

has reduced upon grafting, but the pore size is still sufficient to allow gas (Knudsen) like translation of the permeating molecules. This is further substantiated the fact that the ratio of permeances of N_2 and CH_4 remains similar to the square root of ratio of their molar masses.

After grafting with TEBC the permeance of all gases reduces further. The low permeance of N_2 and CH_4 indicate that for these gases the membrane has become a barrier which has almost no percolating open pore structure, that severely impedes the transport rate of these gases. SEM images reveal that the pores of the γ-alumina layer are not filled upon grafting, suggesting that the barrier properties of the grafted membrane arise from the thin layer covering the γ-alumina layer. As compared to the other gases, the reduction in permeance is less pronounced for CO_2. This is due to the affinity or favorable interactions of the quadrupolar CO_2 with polar ethers in the organic material, i.e., the ethylene oxide, which allows more extensive sorption of CO_2 in the organic material, facilitating transport. The favorable interactions between quadrupolar CO_2 and ether groups in polyethylene oxide have been extensively reported, as can be seen in the following literature (*1, 2, 23, 47-50*). The rate of transport of CO_2 is not very high, which can be rationalized from the small extent of sorption expected at the temperature of the permeation experiment (100 ^{o}C).

In contrast to the behavior of polymeric polyether membranes sequentially grafted membranes are able to perform at 100 ^{o}C. This can be explained by the covalent bonding between the PEO monomers (jeffamine – TEBC – Jeffamine) and the surface of the thermo-

mechanically stable ceramic material (*7, 8, 18, 19, 51-53*). Ethylene oxide moieties confined at the pore entrance can also have reduced mobility.

Physical or geometric confinement of liquids within small pores does affect the physical properties of respective liquids or polymers as shown by different experimental techniques and theoretical approaches (*54-57*). Schuller *et al.* (*54*) investigated the behavior of liquid polypropylene glycol and its oligomers inside the pores (diameter ~ 10 nm) of porous glass as a function of temperature by dielectric spectroscopy. They found that pore confinement results in retardation and broadening of the inherent α relaxation, which indicates an increase in glass transition temperature (T_g) of around 4.5 °C. Barut *et al.* (*56*) investigated the confinement of polypropylene liquid in 2D and 3D pores with the pore diameters of 2-20 nm and 7-11 nm, respectively. They found a significant influence of pore confinement on the molecular dynamics of the glassy liquids. Apparently, 3D pore confinement effects seem to be more pronounced than 2D pore confinement. Schuller *et al.* (*58*) reported the dielectric relaxation of glass forming liquid N-methyl caprolactum confined in meso-porous glass. They observed three distinct relaxation peaks for the confined liquid: a broadened α process with slightly modified temperature dependence compared to bulk relaxation, an intermediate peak originates from Maxwell-Wagner polarization of heterogeneous system, and a extremely slow process associated with the layer attached to the pore surface. The fundamental change in the properties of the polymeric solutions, particularly glass transition temperature (T_g) by pore confinement, has been reported in the following literature (*59-61*). The above mentioned literature suggests the changes in the fundamental properties of the polymers by pore confinement as well as composite materials synthesized

by blending or combining with thermo-mechanically stable inorganic counter parts. This literature is in agreement with findings and the main hypothesis of this thesis.

5.4 Conclusions

Successful sequential covalent grafting of polyethylene oxides onto meso-porous γ-alumina is demonstrated. The grafting involves layer-by-layer covalent attachment of a diamine (Jeffamine®) and a bis(chloroformate) (TEBC) onto a chloro-functionalized γ-alumina surface. For powders, N_2-physisorption and FT-IR reveals that the method only permits partial filling-up of the meso-pores by the organic groups. For supported membranes SEM images also indicate that the pores are not completely filled upon sequential grafting. For N_2 and CH_4, barrier properties of the grafted membranes are observed, resulting from a thin film covering the outer surface of the γ-alumina layer. The reduction in permeance of CO_2 is relatively less pronounced compared to other two gases due to the favorable interactions of the quadrupolar CO_2 with polar ethers in the organic material. In contrast to the behavior of polymeric polyether membranes sequentially grafted membranes are able to perform at 100 ^{o}C because of the covalent bonding between the PEO monomers (jeffamine – TEBC – Jeffamine) and the surface of the thermo-mechanically stable ceramic material, and the nano confinement.

References

1. H. Lin, B. D. Freeman, Materials selection guidelines for membranes that remove CO_2 from gas mixtures. *Journal of Molecular Structure* **739**, 57 (2005).

2. S. R. Reijerkerk, M. H. Knoef, K. Nijmeijer, M. Wessling, Poly(ethylene glycol) and poly(dimethyl siloxane): Combining their advantages into efficient CO_2 gas separation membranes. *Journal of Membrane Science* **352**, 126 (2010).

3. S. R. Reijerkerk, A. Arun, R. J. Gaymans, K. Nijmeijer, M. Wessling, Tuning of mass transport properties of multi-block copolymers for CO_2 capture applications. *Journal of Membrane Science* **359**, 54 (2010).

4. S. R. Reijerkerk, Polyether based block copolymer membranes for CO_2 separation. *Ph.D. thesis, university of twente*, (2010).

5. S. R. Reijerkerk *et al.*, Subambient temperature CO_2 and light gas permeation through segmented block copolymers with tailored soft phase. *ACS Applied Materials and Interfaces* **2**, 551 (2010).

6. Arkema, PEBAX. *URL:http:// www.pebax.com*.

7. V. A. Kusuma, B. D. Freeman, M. A. Borns, D. S. Kalika, Influence of chemical structure of short chain pendant groups on gas transport properties of cross-linked poly(ethylene oxide) copolymers. *Journal of Membrane Science* **327**, 195 (2009).

8. V. A. Kusuma, B. D. Freeman, S. L. Smith, A. L. Heilman, D. S. Kalika, Influence of TRIS-based co-monomer on structure and gas transport properties of cross-linked poly(ethylene oxide). *Journal of Membrane Science* **359**, 25 (2010).

9. V. A. Kusuma, S. Matteucci, B. D. Freeman, M. K. Danquah, D. S. Kalika, Influence of phenoxy-terminated short-chain pendant groups on gas transport properties of cross-linked poly(ethylene oxide) copolymers. *Journal of Membrane Science* **341**, 84 (2009).

10. S. Sridhar, R. Suryamurali, B. Smitha, T. M. Aminabhavi, Development of crosslinked poly(ether-block-amide) membrane for CO_2/CH_4 separation. *Colloids and Surfaces A: Physicochemical and Engineering Aspects* **297**, 267 (2007).

11. V. Barbi, S. S. Funari, R. Gehrke, N. Scharnagl, N. Stribeck, SAXS and the gas transport in polyether-block-polyamide copolymer membranes. *Macromolecules* **36**, 749 (2003).

12. D. Husken, T. Visser, M. Wessling, R. J. Gaymans, CO_2 permeation properties of poly(ethylene oxide)-based segmented block copolymers. *Journal of Membrane Science* **346**, 194 (2010).

13. N. P. Patel, M. A. Hunt, S. Lin-Gibson, S. Bencherif, R. J. Spontak, Tunable CO_2 transport through mixed polyether membranes. *Journal of Membrane Science* **251**, 51 (2005).

14. A. C. Ijzer *et al.*, Synthesis and properties of hydrophilic segmented block copolymers based on poly(ethylene oxide)- ran-poly(propylene oxide). *Journal of Applied Polymer Science* **117**, 1394 (2010).

15. V. I. Bondar, B. D. Freeman, I. Pinnau, Gas sorption and characterization of poly(ether-b-amide) segmented block copolymers. *Journal of Polymer Science Part B: Polymer Physics* **37**, 2463 (1999).

16. V. I. Bondar, B. D. Freeman, I. Pinnau, Gas transport properties of poly(ether-b-amide) segmented block copolymers. *Journal of Polymer Science Part B: Polymer Physics* **38**, 2051 (2000).

17. G. Chatterjee, A. A. Houde, S. A. Stern, Poly(ether urethane) and poly(ether urethane urea) membranes with high H_2S/CH_4 selectivity. *Journal of Membrane Science* **135**, 99 (1997).

18. K.-i. Okamoto *et al.*, Gas permeation properties of poly(ether imide) segmented copolymers. *Macromolecules* **28**, 6950 (1995/09/01, 1995).

19. H. B. Park, C. K. Kim, Y. M. Lee, Gas separation properties of polysiloxane/polyether mixed soft segment urethane urea membranes. *Journal of Membrane Science* **204**, 257 (2002).

20. H. Lin *et al.*, in *ACS National Meeting Book of Abstracts*. (2004), vol. 228, pp. POLY-447.

21. H. Lin, T. Kai, B. D. Freeman, S. Kalakkunnath, D. S. Kalika, The effect of cross-linking on gas permeability in cross-linked poly(ethylene glycol diacrylate). *Macromolecules* **38**, 8381 (2005).

22. H. Lin, B. D. Freeman, Gas and vapor solubility in cross-linked polyethylene glycol diacrylate. *Macromolecules* **38**, 8394 (2005).

23. H. Lin, B. D. Freeman, Gas permeation and diffusion in cross-linked poly(ethylene glycol diacrylate). *Macromolecules* **39**, 3568 (2006).

24. H. L. Castricum, A. Sah, M. C. Mittelmeijer-Hazeleger, J. E. ten Elshof, Hydrophobisation of mesoporous γ-Al_2O_3 with organochlorosilanes—efficiency and structure. *Microporous and Mesoporous Materials* **83**, 1 (2005).

25. V. G. P. Sripathi, A. Nijmeijer, N. E. Benes, Inorganic - polimide hybrid membranes by sequential molecular grafting with proliferated surface functionalization. *manuscript In preparation*, (2013).

26. V. G. P. Sripathi, B. L. Mojet, A. Nijmeijer, N. E. Benes, Vapor phase versus liquid phase grafting of alumina. *Microporous and Mesoporous Materials* **172**, 1 (2013).

27. A. Nijmeijer, *Hydrogen - selective silica membranes for use in membrane steam reforming*. Ph.D. thesis, University of twente, The Netherlands (1999).

28. R. D. Lowe, M. A. Pellow, T. D. P. Stack, C. E. D. Chidsey, Deposition of dense siloxane monolayers from water and trimethoxyorganosilane vapor. *Langmuir* **27**, 9928 (2011).

29. E. P. Barrett, L. G. Joyner, P. P. Halenda, The Determination of Pore Volume and Area Distributions in Porous Substances. I. Computations from Nitrogen Isotherms. *Journal of the American Chemical Society* **73**, 373 (1951/01/01, 1951).

30. N. Gartmann, C. Schütze, H. Ritter, D. Brühwiler, The Effect of Water on the Functionalization of Mesoporous Silica with 3-Aminopropyltriethoxysilane. *The Journal of Physical Chemistry Letters* **1**, 379 (2010/01/07, 2009).

31. S. Brunauer, P. H. Emmett, E. Teller, Adsorption of Gases in Multimolecular Layers. *Journal of the American Chemical Society* **60**, 309 (1938/02/01, 1938).

32. D. G. Kurth, T. Bein, Thin Films of (3-Aminopropyl)triethoxysilane on Aluminum Oxide and Gold Substrates. *Langmuir* **11**, 3061 (1995/08/01, 1995).

33. D. G. Kurth, T. Bein, Monomolecular layers and thin films of silane coupling agents by vapor-phase adsorption on oxidized aluminum. *The Journal of Physical Chemistry* **96**, 6707 (1992/08/01, 1992).

34. F. Zhang *et al.*, Chemical Vapor Deposition of Three Aminosilanes on Silicon Dioxide: Surface Characterization, Stability, Effects of Silane Concentration, and Cyanine Dye Adsorption. *Langmuir* **26**, 14648 (2010/09/21, 2010).

35. S. Fiorilli *et al.*, Vapor-phase self-assembled monolayers of aminosilane on plasma-activated silicon substrates. *Journal of Colloid and Interface Science* **321**, 235 (2008).

36. E. Asenath Smith, W. Chen, How To Prevent the Loss of Surface Functionality Derived from Aminosilanes. *Langmuir* **24**, 12405 (2008/11/04, 2008).

37. N. Crampton, W. A. Bonass, J. Kirkham, N. H. Thomson, Formation of Aminosilane-Functionalized Mica for Atomic Force Microscopy Imaging of DNA. *Langmuir* **21**, 7884 (2005/08/01, 2005).

38. S. J. Gregg, K. S. W. Sing, *Adsorption, surface area and porosity*. (Academic Press, 1991), vol. 2, illustrated, pp. 10 - 15.

39. M. K. Naskar, Hydrothermal Synthesis of Petal-Like Alumina Flakes. *Journal of the American Ceramic Society* **92**, 2392 (2009).

40. H. Vigué, P. Quintard, T. Merle-Méjean, V. Lorenzelli, An FT–IR Study of the Chlorination of γ-Alumina Surfaces. *Journal of the European Ceramic Society* **18**, 305 (1998).

41. S. Kim, J. Ida, V. V. Guliants, Y. S. Lin, Tailoring Pore Properties of MCM-48 Silica for Selective Adsorption of CO_2. *The Journal of Physical Chemistry B* **109**, 6287 (2005).

42. X. S. Zhao, G. Q. Lu, A. K. Whittaker, G. J. Millar, H. Y. Zhu, Comprehensive Study of Surface Chemistry of MCM-41 Using 29Si CP/MAS NMR, FTIR, Pyridine-TPD, and TGA. *The Journal of Physical Chemistry B* **101**, 6525 (1997/08/01, 1997).

43. P. Wang, K. L. Tan, E. T. Kang, K. G. Neoh, Plasma-induced immobilization of poly(ethylene glycol) onto poly(vinylidene fluoride) microporous membrane. *Journal of Membrane Science* **195**, 103 (2002).

44. S. Zalipsky, C. Gilon, A. Zilkha, Attachment of drugs to polyethylene glycols. *European Polymer Journal* **19**, 1177 (1983).

45. M. Ulbricht, H. Matuschewski, A. Oechel, H.-G. Hicke, Photo-induced graft polymerization surface modifications for the preparation of hydrophilic and low-proten-adsorbing ultrafiltration membranes. *Journal of Membrane Science* **115**, 31 (1996).

46. S. H. Hyun, S. Y. Jo, B. S. Kang, Surface modification of γ-alumina membranes by silane coupling for CO_2 separation. *Journal of Membrane Science* **120**, 197 (1996).

47. B. A. Car, C. Stropnik, W. Yave, K.-V. Peinemann, Tailor-made polymeric membranes based on segmented block copolymers for CO_2 separation. *Adva. Funct. Mater* **18**, 2815 (2008).

48. S. R. Reijerkerk, A. Arun, R. J. Gaymans, K. Nijmeijer, M. Wessling, Tuning of mass transport properties of multi-block copolymers for CO_2 capture applications. *Journal of Membrane Science* **359**, 54 (2010).

49. H. Lin, E. V. Wagner, R. Raharjo, B. D. Freeman, I. Roman, High performance polymer membranes for natural gas sweetening. *Advanced Materials* **18**, 39 (2006).

50. H.Lin, B. D. Freeman, Gas solubility, diffusivity and permeability in poly(ethylene oxide). *Journal of Membrane Science* **239**, 105 (2004).

51. H. Lin *et al.*, Transport and structural characteristics of crosslinked poly(ethylene oxide) rubbers. *Journal of Membrane Science* **276**, 145 (2006).

52. J. J. Richards *et al.*, Relation between structure and gas transport properties of polyethylene oxide networks based on crosslinked bisphenol A ethoxylate diacrylate. *Chemical Engineering Science* **64**, 4707 (2009).

53. X. Chen, D. Rodrigue, S. Kaliaguine, Diamino-organosilicone APTMDS: A new cross-linking agent for polyimides membranes. *Separation and Purification Technology* **86**, 221 (2012).

54. J. Schuller, Y. B. M. nichenko, R. Richert, E. W. Fischer, Dielectric studies of the glass transitionn in porous media. *Phys. Rev. Lett.* **73**, 2224 (1994).

55. M. Arndt, R. Stannarius, H. Groothues, E. Hempel, F. Kremer, Length scale of cooperativity in the dynamic glass transition. *Phys. Rev. Lett.* **79**, 2077 (1997).

56. G. Barut, P. Pissis, R. Pelster, G. Nimtz, Glass transition in liquids: Two versus three-dimentional confinement. *Phys. Rev. Lett.* **80**, 3543 (1998).

57. K. Fukao, Y. Miyamoto, Glass transitions and dynamics in thin polymer films: Dielectric relaxation of thin films of polystyrene. *Physical Review E* **61**, 1743 (2000).

58. J. Schüller, R. Richert, E. W. Fischer, Dielectric relaxation of liquids at the surface of a porous glass. *Physical Review B* **52**, 15232 (1995).

59. J. Zhang, G. Liu, J. Jonas, Effects of confinement on the glass transition temperature of molecular liquids. *The Journal of Physical Chemistry* **96**, 3478 (1992/04/01, 1992).

60. J. Dubochet *et al.*, Glass-forming microemulsions: vitrification of simple liquids and electron microscope probing of droplet-packing modes. *The Journal of Physical Chemistry* **88**, 6727 (1984/12/01, 1984).

61. K. Hofer, E. Mayer, G. P. Johari, Glass-liquid transition and calorimetric relaxation of glassy aqueous solutions imbibed in poly(2-hydroxyethyl methacrylate); a comparison with bulk behavior. *The Journal of Physical Chemistry* **95**, 7100 (1991/09/01, 1991).

6

Surface functionalization of meso-porous BTESE by grafting: FTIR study

Abstract

Surface functionalization of a meso-porous hydrophobic sol-gel (1,2 bis(triethoxy)silane) derived powder has been performed by solution phase grafting as well as vapour phase grafting of 3APTMS in the presence of 500 and 5000 ppm water, followed by subsequent grafting with 6FDA. The powders have been characterized by FTIR. At low concentration of water (500 ppm), surface functionalization, via grafting with 3APTMS from the vapor phase, and subsequent grafting with 6FDA, does not result in any significant changes in the FTIR spectra. In contrast, when the surface functionalization at 500 ppm water is done via solution phase grafting, peaks emerge in the FTIR spectrum that correspond to amine, propyl, and imide groups, confirming that grafting has occurred. A higher water concentration (5000 ppm) does not affect functionalization from the solution phase, as similar FTIR spectra are obtained. For grafting from the vapor phase, a higher water concentration triggers successful surface functionalization. The observations can be rationalized by a low concentration of water on the surface of the fresh hydrophobic material, impeding the required hydrolysis of precursor molecules in the vicinity of the reactive surface hydroxyls. In particular for the vapor phase grafting, limited water and hydrolyzed precursor molecules are present in the vapor phase, and additional water is required for instigating hydrolysis of the precursor molecules before the reaction at the surface can occur.

6.1 Introduction

In affinity-based membrane separations, distinct permeation of particular species derives from differences in molecular-level interactions between species and the membrane material (*1*). In particular organic polymer membranes allow affinity-based selectivity, due to the versatility in physico-chemical properties of these materials. Drawbacks of using organic polymers as membrane materials include their susceptibility to swelling and plasticization (*2*), especially when in contact with penetrant molecules. Swelling and plasticization generally result in an enhanced permeation of all the species present in a mixture, causing the molecular selectivity to decrease.

Strategies to moderate swelling and plasticization include cross-linking of the polymer network, and incorporating 'hard' inorganic particles. In this chapter the approach is to confine an oligomeric material in the nano-sized pores of a ceramic host material, by post-synthetic grafting. Confinement of the oligomer in the inorganic material is expected to affect its molecular dynamics, in turn affecting the molecular selectivity and the propensity to swelling and plasticization. The approach described in this chapter is in analogy with those discussed in the previous chapters; functionalization of the inorganic porous material with a precursor that provides anchoring sites, followed by subsequent covalent attachment of other organic precursor molecules. The principal difference is the nature of the inorganic material.

In the previous chapters highly porous (~60%) hydrophilic γ-alumina has been used as host material. Here a hydrophobic meso-porous (2-5 nm pore size) hybrid organo-silica material is considered, that has recently been reported by Gruzien *et al* (*3*) and Na *et al* (*4*). The

porous material is derived from bis(triethoxysilyl)ethane (BTESE) and contains ethylene organic bridges within the silica network, ensuing superior hydrothermal and alkaline stability as compared to γ-alumina (*5, 6*). In addition, the hydrophobic characteristics of the material avoid condensation of water in its pores, which is beneficial in applications where the presence of water is currently to be avoided for this reason. Despite the beneficial properties of the BTESE derived material, it contains a minor amount of surface hydroxyl groups that are required for covalent attachment of the precursors used in our previous studies, complicating adequate grafting. Here, the effectiveness of surface functionalization of meso-porous silica with 3aminopropyltrimethoxysilane (3APTMS) subsequent grafting with 4,4-(hexafluoroisopropyldiene) diphthalic anhydride (6FDA), is explored. Particular focus is on the influence of water on the surface functionalization.

6.2 Experimental

6.2.1 Materials

1,2 bis(triethoxy)silane (BTESE, 97 % purity) obtained from ABCR, Pluronic® F127 obtained from BASF, Hydrochloric acid (32 %) and 1-butanol (99.5 % purity) were obtained from Merck. 3-aminopropyltrimethoxysilane (3APTMS, 97 % purity), 4,4-(hexafluoroisopropyldiene) diphthalic anhydride (6FDA, 99%), toluene (anhydrous, 99.8 %) and N,N-dimethyleacetamide (DMAc) were obtained from Aldrich. High purity (~98 %) ethanol was obtained from Merck. All chemicals were used as received.

6.2.2 Synthesis of meso-porous BTESE

Meso-porous BTESE was synthesized by hydrolysis and subsequent polycondensation of 1,2-bis(triethoxysilyl)ethane, in the presence of a structure directing agent (Pluronic® F127), under acidic conditions. First, 1.97 g of Pluronic® F127 was added to 70 g of deinonized water. Then, 1.86 g of butanol, followed by 3.8 g of HCl (32 %), was added under stirring. Stirring at room temperature was continued for 24 hrs, after which a transparent solution was observed. Subsequently, 3.4 ml of bis(triethoxysilyl)ethane (BTESE) precursor was added and the solution was kept at 35 ^{o}C for 20 hrs, followed by exposure to 100 ^{o}C in an air oven for 24 hrs. The obtained powder was neutralized by adding NaOH (1 mol/lit in water) basic solution until pH ~7. The neutralized powder was washed with ethanol and water (3 times) to remove excess pluronic® F127. The wet powder was dried overnight in oven at 70 ^{o}C. Finally the milled powders were heat treated at 300 ^{o}C for 2 hrs (heating and cooling rate, 0.5 ^{o}C/min). Before grafting, BTESE powders were pretreated by soaking in an ethanol/water (2:1) solution for 24 hrs at ambient temperature. The ethanol solution was removed from the wet powders by using a filter paper (Millipore filter paper, grade 101), followed by placing and drying the powder in a fume hood until a fluffy powder was obtained. The physically adsorbed moisture/water was removed by drying in an oven at 100 $^{\circ}$C for 2 hrs in air.

6.2.3 3APTMS grafting

Equal amounts 300 mg of BTESE powders were placed in two round bottom (RB) flasks, connected to each other by a thermally insulated horizontal glass tube (chapter 1, Figure 4, lower). Toluene and 3APTMS (2.5 wt %) were added to one RB flask (denoted as RB I). No

liquid was added to the second RB flask (denoted as RB II). The powder in RB I was in direct contact with the liquid solution (Solution Phase Grafting, SPG). The powder placed in RB II was only in contact with the aminosilane vapors produced in RB I (Vapor Phase Grafting, VPG). Equal temperatures (80 ^{o}C) were maintained in the two RB flasks and the reaction was carried out overnight. All chemicals were added to the RB flasks inside the glove box prior to the start of the reaction. Water (44 mg = 500 ppm, 444 mg = 5000 ppm) was thoroughly mixed with toluene under sonication for 20 min, prior to adding 3APTMS.

After the reaction, the powder present in RB I was separated from the solution by using a filter paper (Millipore, grade 101). Subsequently, the SPG and VPG derived powders were soaked in toluene for ~10 hrs, then in ethanol for ~10 hrs, to remove physically adsorbed 3APTMS. Finally, the powders were annealed at 100 ^{o}C for 2 hrs in air.

6.2.4 Sequential grafting of 6FDA

Aminosilylated BTESE powder (300 mg) was placed in a flask containing 20 ml dimethylacetamide (DMAc). 6FDA (2.35 g) was added to the solution; the reaction was performed at ambient temperature under nitrogen atmosphere for 16 hrs. Subsequently, the powders were soaked in DMAc overnight.

6.2.5 Imidization

Amic acid groups in the grafted alumina were converted to imides by thermal imidization, allowing ring closure via the removal of water. Grafted flakes were heated to 300 ^{o}C for 1 hr (heating/cooling rate of 1 ^{o}C/min) well above the onset temperature of imidization (~180 ^{o}C) (*7*).

6.2.6 Stability

The stability of the grafted amino functional groups was tested by intensive washing treatments, in the following manner. In the first step, 3APTMS treated powders were soaked in toluene overnight. In the second step, the powders were soaked again in toluene for 24 hrs. In the third step the powders were treated by 1 hr sonication in toluene.

6.3 Results & discussion

The effectiveness of grafting has been investigated with FTIR, for four different sets of circumstances of the amino functionalization:

- SPG in the presence of low concentration water (500 ppm)
- VPG in the presence of low concentration water (500 ppm)
- SPG in the presence of excess water (5000 ppm)
- VPG in the presence of excess water (5000 ppm)

6.3.1 Low water concentration (500 ppm)

SPG

Figure 1 depicts FTIR spectra meso-porous BTESE powders, before and after grafting of 3APTMS (by SPG) and 6FDA.

Prior to grafting the BTESE derived powder only shows distinct absorbance in the region below 1500 cm^{-1}. The pronounced broad band between 1100 to 1020 cm^{-1} corresponds to symmetric and asymmetric stretching of Si-O bands of the silica rich BTESE (*8-11*). The bands between 2930 – 2865 cm^{-1} are assigned to ethyl groups present in BTESE (*8, 11-13*). The very

weak band around 3500 cm^{-1} indicates the presence of a limited amount OH groups or physically adsorbed water molecules.

Upon amino functionalization with 3APTMS, in presence of 500 ppm water, the increase in the intensity of the bands around 2900 cm^{-1} is observed; bands at 2930 and 2865 cm^{-1} correspond to symmetric and asymmetric stretching of C– H groups of the propyl chain present in 3APTMS (*11-13*).

Subsequent 6FDA grafting of the amino functionalized BTESE results in new bands around 1715 and 1775 cm^{-1}. These bands correspond to symmetric and asymmetric stretching of the imide band (O=C–N–C=O) formed between amine groups and anhydride groups of 6FDA, followed by thermal imidization (*7, 14*).

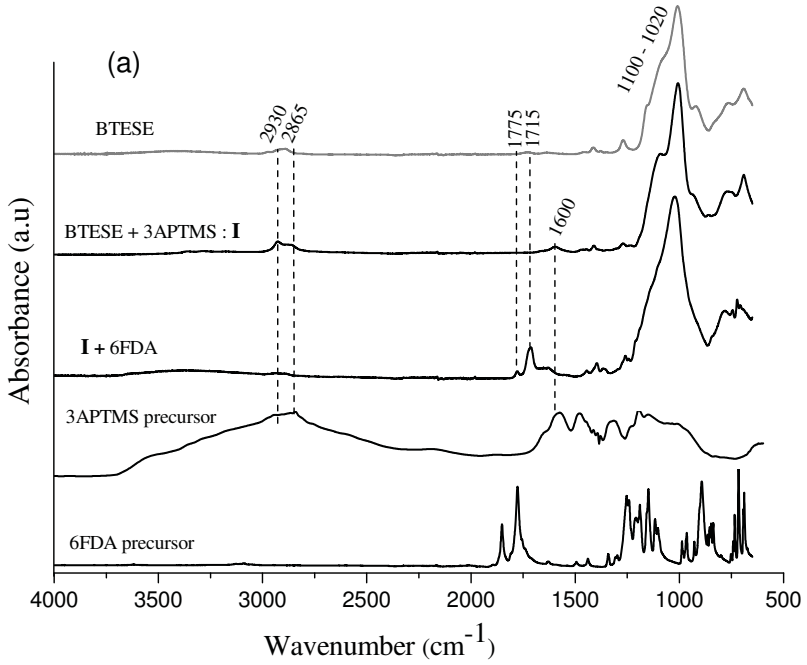

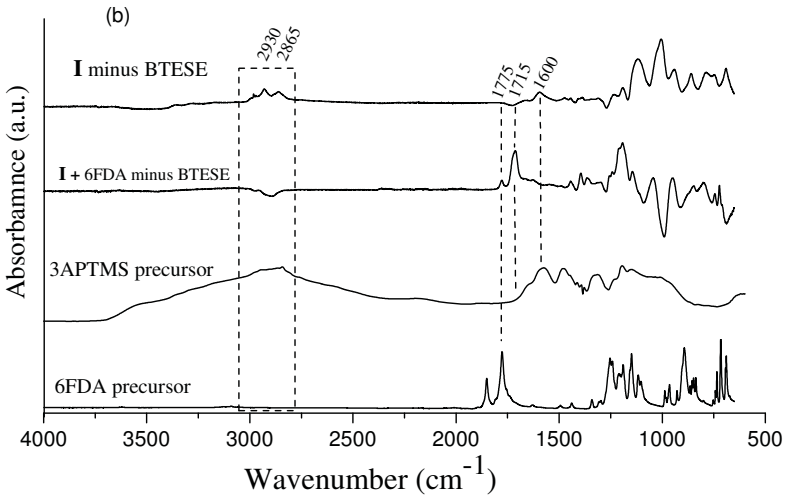

Figure 1: a) FTIR spectra of untreated BTESE powder, powders functionalized with 3APTMS from the solution phase (SPG) at low water concentration (500 ppm), and subsequently grafted with 6FDA. The spectra of the precursors have been added for reference. The spectra have been shifted along the *y*-axis for clarity. b) Corresponding difference FTIR spectra: original spectra minus the contribution of the BTESE derived powder.

In Figure 1b, the spectra corrected for the contribution of the BTESE derived powder are provided. The negative peak observed around 3500 cm^{-1} suggests the reaction of surface hydroxyl groups with 3APTMS, or physically adsorbed water. The peaks around 2900 cm^{-1} correspond to alkyl groups (*11-13*). This is further confirmed by the intensive imide peaks at 1716 and 1775 cm^{-1} after sequential grafting of 6FDA suggesting the imide bond formation between amines and anhydrides (*7, 14*).

VPG

Figure 2 shows FTIR spectra for powders that have been amino functionalized via VPG. Compared to the SPG functionalized powders the changes in the spectra, after the grafting

steps, are significantly less apparent. After 3APTMS treatment no major changes are observed, suggesting very limited or no 3APTMS is present in the powder. After subsequent grafting of 6FDA no clear distinct peaks are observed, which supports the absence of 3APTMS in powder. The difference spectra in Figure 2b confirm these observations.

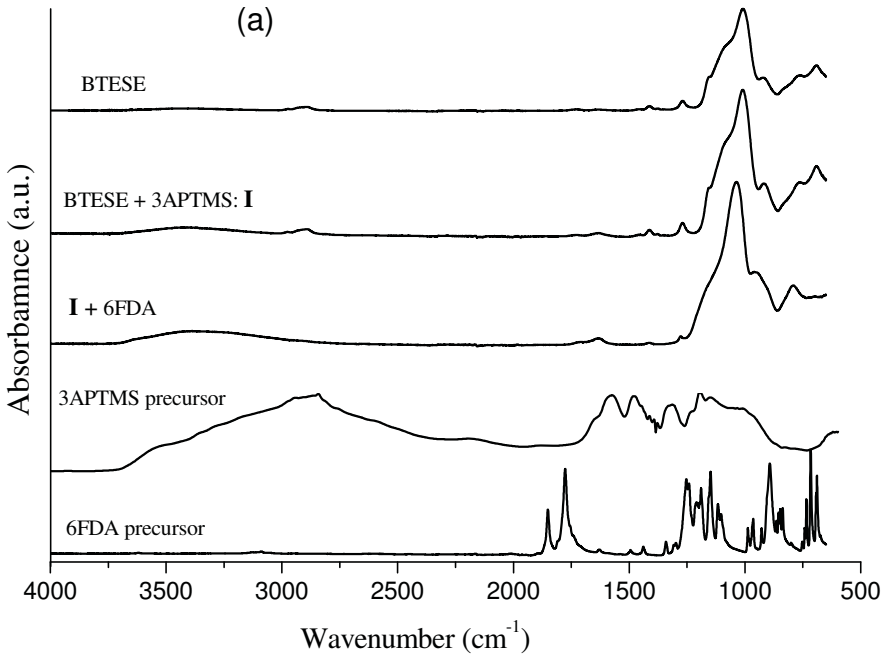

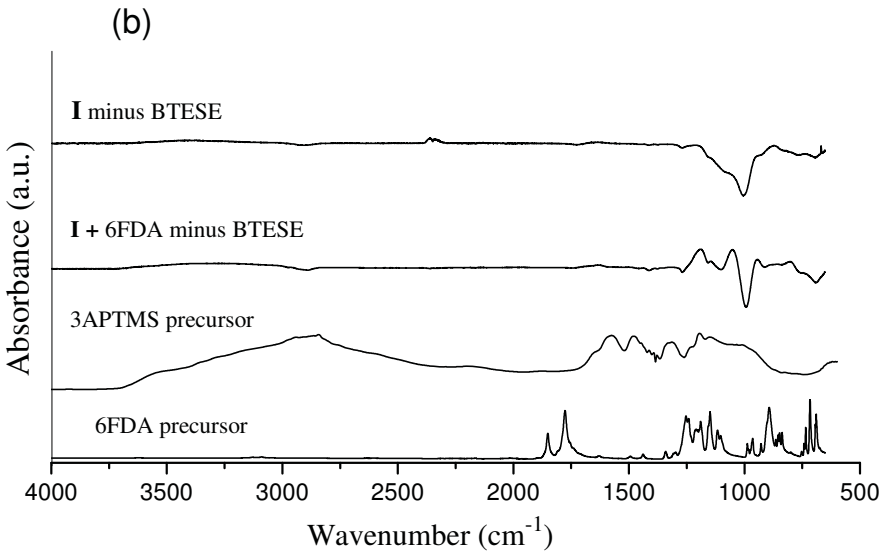

Figure 2: a) FTIR spectra of untreated BTESE powder, powders functionalized with 3APTMS from the vapor phase (VPG) at low water concentration (500 ppm), and subsequently grafted with 6FDA. The spectra of the precursors have been added for reference. The spectra have been shifted along the *y*-axis for clarity. b) Corresponding difference FTIR spectra: original spectra minus the contribution of the BTESE derived powder.

6.3.2 Excess water (5000 ppm)

SPG

Figure 3a shows spectra for powders that have been amino functionalized by SPG, in the presence of excess water (5000 ppm). The spectra are almost identical to those obtained for powder functionalized at low water concentration (Figure 1). Figure 3b shows difference spectra, confirming that the effect of water on the amino functionalization by SPG is not significant.

VPG

Figure 4a shows spectra for powders that have been amino functionalized by VPG, in the presence of excess water (5000 ppm). In contrast to the spectra obtained for the low concentration of water (Figure 2), the spectra show significant changes after amino functionalization and subsequent 6FDA grafting. After functionalization with 3APTMS, peaks are visible at 2970 cm^{-1} and 2880 cm^{-1}, which can be attributed to the ethyl groups of the precursor (*11-13*). This indicates that 3APTMS is present in the powder. In the subsequent grafting step, with 6FDA, new peaks emerge at 1780 and 1720 cm^{-1}. These peaks are associated with the imide group formed between the amine groups of the 3APTMS and the 6FDA, hence confirming the presence of, and reaction between amine groups and anhydride groups of 6FDA (*7, 14*). In the difference spectra in Figure 4b the changes are more readily identified. The distinct sharp bands at 2970 and 2880 cm^{-1} correspond to C-H stretching of the alkyl group of propyl chain (*11-13*). After sequential grafting with 6FDA peaks at 1780 cm^{-1} and 1720 cm^{-1} confirm imide formation. The band at 1860 cm^{-1} belongs to unreactive anhydride groups of 6FDA.

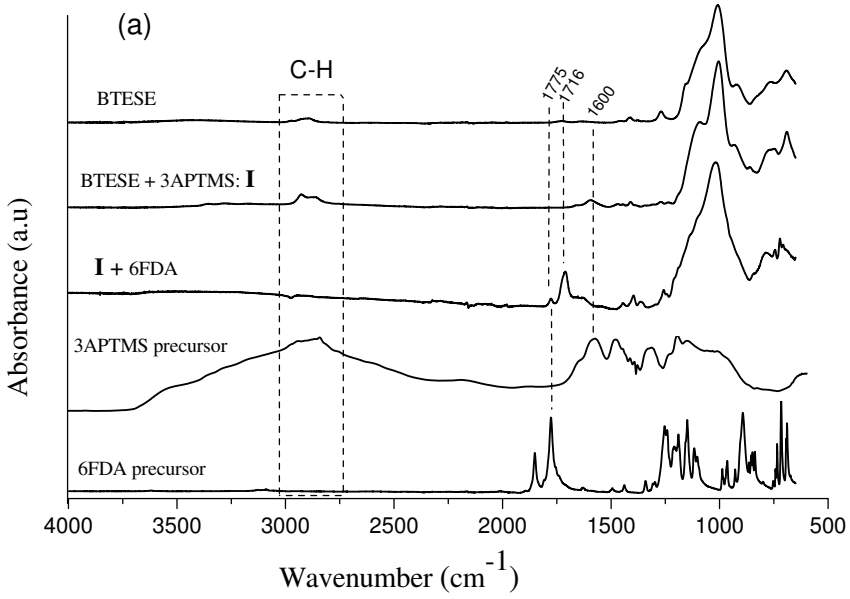
(a)
C-H
1775
1716
1600
BTESE
BTESE + 3APTMS: I
I + 6FDA
3APTMS precursor
6FDA precursor
Absorbance (a.u)
4000
3500
3000
2500
2000
1500
1000
500
Wavenumber (cm-1)

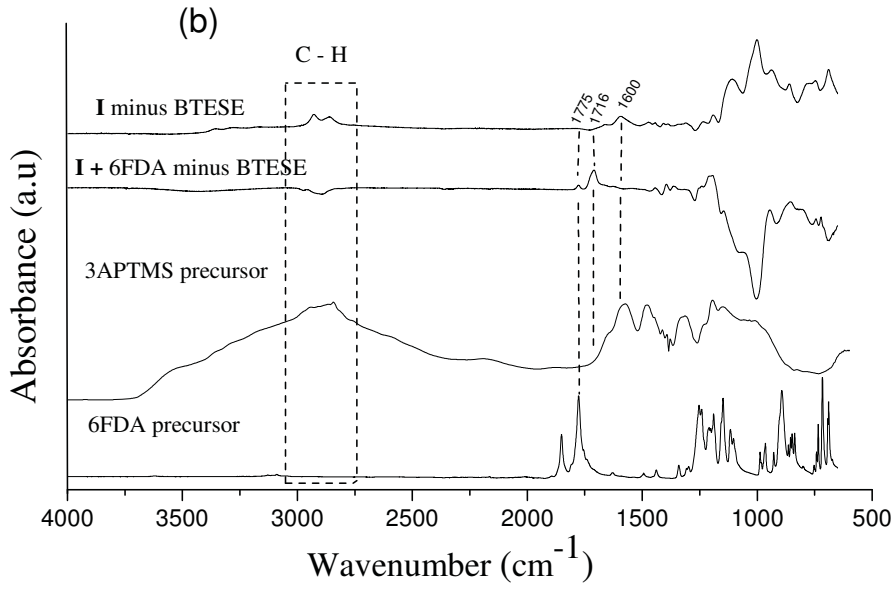
(b)
C - H
1775
1716
1600
I minus BTESE
I + 6FDA minus BTESE
3APTMS precursor
6FDA precursor
Absorbance (a.u)
4000
3500
3000
2500
2000
1500
1000
500
Wavenumber (cm-1)

Figure 3: a) FTIR spectra of untreated BTESE powder, powders functionalized with 3APTMS from the solution phase (SPG) at high water concentration (5000 ppm), and subsequently grafted with 6FDA. The Spectra of the precursors have been added for reference. The spectra have been shifted along the *y*-axis for clarity. b) Corresponding difference FTIR spectra: original spectra minus the contribution of the BTESE derived powder.

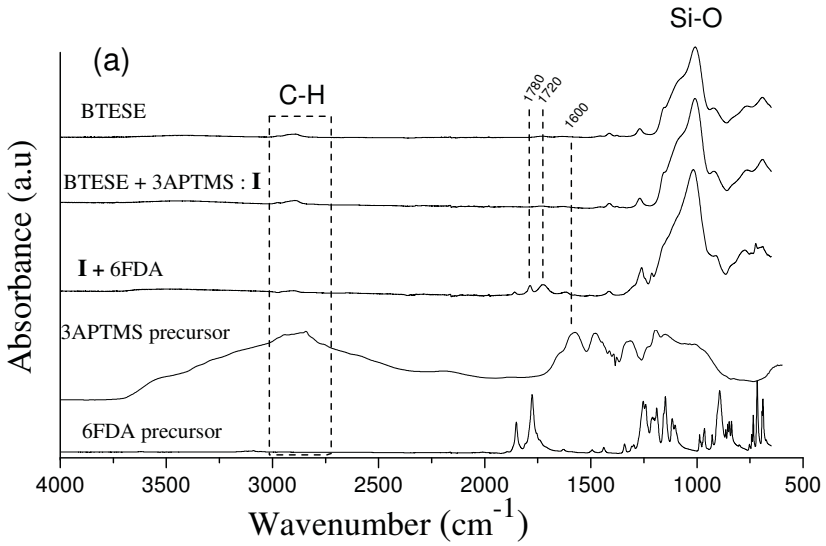

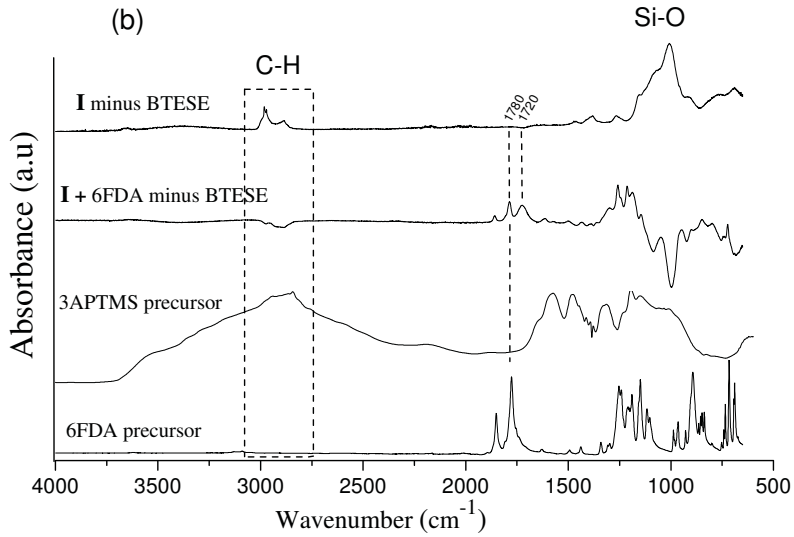

Figure 4: a) FTIR spectra of untreated BTESE powder, powders functionalized with 3APTMS from the vapor phase (VPG) at high water concentration (5000 ppm), and subsequently grafted with 6FDA. The Spectra of the precursors have been added for reference. The spectra have been shifted along the *y*-axis for clarity. b) Corresponding difference FTIR spectra: original spectra minus the contribution of the BTESE derived powder.

These observations can be rationalized by the role of water in the surface functionalization. The reaction between 3APTMS and surface hydroxyl groups requires a preceding hydrolysis of the precursor molecule. In the case of hydrophilic materials water will generally be present on the (pore) surface, allowing for hydrolysis of the precursor in close proximity of the reactive surface hydroxyl groups. On the surface of the hydrophobic material used in this study the concentration of water on the surface is very low and does not allow sufficient hydrolysis. In solution phase grafting, the water present in the liquid is sufficient to commence hydrolysis, already at relatively low water concentration. In vapor phase grafting, the water concentration and the concentration of hydrolyzed precursor molecules, in the vapor, will be relatively low as compared to the liquid phase. At lower water concentration this hinders the surface reaction, while at higher water concentration, hydrolysis of the 3APTMS is sufficient for the surface reaction to commence. These observations are in complete agreement with the extensive, fundamental in-depth investigations reported on various types of substrates (*15-21*), which is briefly discussed in the following. For a more extensive discussion readers are requested to refer chapter 1 and chapter 2 in this thesis.

The significance of water in self-assembly was first proposed by Sagiv *et al.* (*15*). They proposed that traces of water are needed for covalent attachment of silanes to surface hybdroxyl groups. Later Finklea *et al.* (*16*) discovered that organized OTS SAMs can also be

formed on substrate surfaces without hydroxyl groups. They proposed that self-assembly occurs on the water film adsorbed on the gold surface, where silanes form a 2D network of Si-O-Si bonds. This proposition of Finklea *et al.* has been supported by several authors (*17, 18, 20, 21*). Britt *et al.* (*19*) reported on the influence of the degree of hydration of a mica surface on layer formation with OTS. Deposition of 200 nm thick clusters, or islands, of OTS oligomers was observed after less than 10 seconds reaction time. As the reaction time prolonged to 40 seconds the thickness of the islands increased to 1 µm. Finally, in 300 seconds the surface was completely covered. In partially hydrated mica, the formation of uniformly distributed OTS clusters on the surface was observed from the beginning of the reaction and no large islands were observed. Tripp and Hair (*20*) reported that the adsorption of OTS species on silica is sensitive to the amount of water present on the silica surface, or in the solvent. They used in-situ infrared spectroscopy to show that in the absence of water molecules there is no reaction between the OTS and surface hydroxyl groups. In contrast, in the case of hydrated silica surface grafting is observed.

6.4 Conclusions

Surface functionalization of meso-porous hydrophobic BTESE has been performed by solution phase grafting as well as vapour phase grafting, in the presence of 500 and 5000 ppm water. At low concentration of water (500 ppm) surface functionalization, via grafting with 3APTMS from the vapor phase, does not result in any significant changes in the FTIR spectra of the powders. Also in the subsequent grafting step, with 6FDA, no new peaks emerge in the FTIR spectra. This indicates that grafting from the vapor phase, at low water

concentration, is not successful. In contrast, when the surface functionalization at 500 ppm water is done via solution phase grafting, peaks emerge in the FTIR spectrum that correspond to the amine and propyl groups of the 3APTMS precursor. Upon subsequent grafting, with 6FDA, peaks corresponding to the imide emerge. These observations indicate grafting from the solution phase, at low water concentrations, is feasible. When the concentration of water is increased to 5000 ppm, for grafting from the solution phase the changes in the FTIR spectra are similar to those observed at low water concentration. At high water concentration also surface functionalization by grafting from the vapor phase, and subsequent grafting with 6FDA, is successful, and new peaks emerge in the spectra that confirm the presence of the 3APTMS and the formation of imide bonds. The results can be rationalized by the low concentration of water on the surface of the hydrophobic material, not allowing the required hydrolysis of precursor molecules in the vicinity of the reactive surface hydroxyls. In particular for the vapor phase grafting, additional water is required for instigating hydrolysis of the precursor molecules, before the reaction at the surface can occur.

References

1. A. Javaid, M. P. Hughey, V. Varutbangkul, D. M. Ford, Solubility-based gas separation with oligomer-modified inorganic membranes. *Journal of Membrane Science* **187**, 141 (2001).

2. V. G. P. Sripathi, A. Nijmeijer, N. E. Benes, Inorganic - polimide hybrid membranes by sequential molecular grafting with proliferated surface functionalization. *manuscript In preparation*, (2013).

3. R. M. Grudzien, B. E. Grabicka, M. Jaroniec, Effect of organosilane/polymer ratio on adsorption properties of periodic mesoporous ethane-silica. *Colloids and Surfaces A: Physicochemical and Engineering Aspects* **300**, 235 (2007).

4. W. Na, Q. Wei, Z. C. Zou, Q. Y. Li, Z. R. Nie, Mesoporous organosilicas with ultra-large pores: Mesophase transformation and bioadsorption properties. *Journal of Colloid and Interface Science* **346**, 61 (2010).

5. G. G. Paradis, R. Kreiter, M. M. A. Van Tuel, A. Nijmeijer, J. F. Vente, Amino-functionalized microporous hybrid silica membranes. *Journal of Materials Chemistry* **22**, 7258 (2012).

6. G. G. Paradis, Novel concepts for microporous hybrid silica membranes. *PhD thesis*, (2012).

7. T. Suzuki, Y. Yamada, Characterization of 6FDA-based hyperbranched and linear polyimide–silica hybrid membranes by gas permeation and 129Xe NMR measurements. *Journal of Polymer Science Part B: Polymer Physics* **44**, 291 (2006).

8. H. L. Castricum *et al.*, Hydrothermally stable molecular separation membranes from organically linked silica. *Journal of Materials Chemistry* **18**, 2150 (2008).

9. Y.-F. Chen, Y.-H. Hu, Y.-I. Chou, S.-M. Lai, C.-C. Wang, Surface modification of nano-porous anodic alumina membranes and its use in electroosmotic flow. *Sensors and Actuators B: Chemical* **145**, 575 (2010).

10. S. Barrientos-Ramírez *et al.*, Surface modification of natural halloysite clay nanotubes with aminosilanes. Application as catalyst supports in the atom transfer radical polymerization of methyl methacrylate. *Applied Catalysis A: General* **406**, 22 (2011).

11. P. Yuan *et al.*, Functionalization of Halloysite Clay Nanotubes by Grafting with γ-Aminopropyltriethoxysilane. *The Journal of Physical Chemistry C* **112**, 15742 (2008).

12. C. P. Tripp, M. L. Hair, Reaction of methylsilanols with hydrated silica surfaces: The hydrolysis of trichloro, dichloro and monochloromethylsilanes and the effects of curing. *Langmuir* **11**, 149 (1995).

13. H. Azour, J. Derouault, P. Lauroua, G. Venzon, Fourier transform infrared spectroscopic charecterization of grafting of 3-aminopropyl silanol onto alumina substrate. *Spectrachemica Acta Part A* **56**, 1627 (2000).

14. J. Ren, R. Wang, T.-S. Chung, D. F. Li, Y. Liu, The effects of chemical modifications on morphology and performance of 6FDA-ODA/NDA hollow fiber membranes for CO_2/CH_4 separation. *Journal of Membrane Science* **222**, 133 (2003).

15. J. Sagiv, Organized monolayers by adsorption. 1. Formation and structure of oleophobic mixed monolayers on solid surfaces. *Journal of the American Chemical Society* **102**, 92 (1980).

16. H. O. Finklea *et al.*, Formation of an organized monolayer by solution adsorption of octadecyltrichlorosilane on gold: electrochemical properties and structural characterization. *Langmuir* **2**, 239 (1986).

17. D. L. Allara, A. N. Parikh, F. Rondelez, Evidence for a Unique Chain Organization in Long Chain Silane Monolayers Deposited on Two Widely Different Solid Substrates. *Langmuir* **11**, 2357 (1995).

18. P. Silberzan, L. Leger, D. Ausserre, J. J. Benattar, Silanation of silica surfaces. A new method of constructing pure or mixed monolayers. *Langmuir* **7**, 1647 (1991).

19. D. W. Britt, V. Hlady, An AFM Study of the Effects of Silanization Temperature, Hydration, and Annealing on the Nucleation and Aggregation of Condensed OTS Domains on Mica. *Journal of Colloid and Interface Science* **178**, 775 (1996).

20. C. P. Tripp, M. L. Hair, Direct Observation of the Surface Bonds between Self-Assembled Monolayers of Octadecyltrichlorosilane and Silica Surfaces: A Low-Frequency IR Study at the Solid/Liquid Interface. *Langmuir* **11**, 1215 (1995).

21. C. P. Tripp, M. L. Hair, An infrared study of the reaction of octadecyltrichlorosilane with silica. *Langmuir* **8**, 1120 (1992).

7

Conclusions and future perspectives

This chapter provides a discussion on the main conclusions of this thesis, and reflects on the implications and future perspectives.

7.1 Conclusions

This thesis presents a novel method of synthesizing hybrid inorganic – polymeric membranes by sequential grafting. The approach of confinement of the organic species within the nano-sized pores is expected to moderate the propensity of these membranes to plasticize and swell. As such, the approach can be beneficial for applications such as gas separation of carbon dioxide from other light gases, such as methane. The precursors of carbon dioxide selective polymers (polyimides, polyethers) have been chemically grafted inside the pores of meso-porous γ-alumina and meso-porous BTESE. In particular, the approach involves initial functionalization of the porous material with linker groups, followed by sequential grafting of precursors with alternating electrophile and nucleophile reactive groups.

Chapter 2 focused on functionalization of the pore surface of meso-porous γ-alumina. This step is expected to be crucial for the efficacy of the subsequent grafting steps, in which the organic species of choice can be build-up sequentially. For functionalization of the surface of inorganic materials, covalent grafting of functional alkoxysilanes is the most common approach. In this chapter, functionalization of meso-porous γ-alumina has been performed by grafting 3-aminopropyltrimethoxysilane (3APTMS) from the liquid phase (solution phase grafting, SPG) as well as from the vapor phase (vapor phase grafting, VPG). Depending on the grafting conditions, significant differences in morphology of the functionalized pores are observed. FT-IR characterization confirms the presence of Si-O bonds and primary amine groups after grafting. Grafting from the liquid phase is affected by oligomerization of the precursor molecules. The presence of oligomers in the liquid phase results in relatively non-

homogeneous grafting, and ultimately in pore blocking. This is more pronounced at higher reaction temperature and, especially, in the presence of water. A higher reaction temperature and presence of water cause the rate of oligomerization to increase. In contrast, when grafting occurs from the vapor phase a more homogeneous thin layer of grafted molecules is obtained, with a thickness similar to the length of the grafting molecule. Grafting from the vapor phase is relatively insensitive to the reaction temperature and the presence of water. This is explained by the low concentration of oligomers in the vapor phase, due to their relatively low vapor pressure. A higher rate of oligomeriziation results in more and larger oligomers in the liquid phase, but in the vapor phase the presence of unreacted precursor molecules prevails. As such, vapor phase grafting is preferable when the aim is to achieve thin mono-layer functionalization, allowing effective further sequential grafting inside the porous structure. Grafting from the liquid phase is more suitable when the aim is to obtain thick multi-layers. Elemental analysis by X-ray photo electron spectroscopy (XPS) on supported γ-alumina membranes revealed that, in SPG treated samples, no elemental band for aluminum (Al) on the external surface was found, indicating that the external surface is completely covered with an aminosilane layer. This can be explained by the deposition of oligomerized aminopropylsilanes; as the trifunctional silanes undergo self-condensation (*1, 2*). In contrast, for VPG treated membranes, an Al elemental band is apparent indicating a low concentration of aiminosilanes, i.e. no oligomerized aminosilanes on the external surface due to their low vapor pressure (*3, 4*), which is consistent with the results obtained for powders.

Chapter 3 demonstrates the sequential grafting of polyimides over aminosilylated meso-porous γ-alumina. The amino functionalization is done by the two distinct methods, SPG and VPG. The characteristic FT-IR peaks of polyimides around 1780 and 1720 cm^{-1}, observed after sequential grafting, suggests the chemical reaction between the anhydride groups of 6FDA and the amine groups of 3APTMS on the porous γ-alumina, which is also confirming the successful aminosilylation by SPG and VPG (the materials synthesized in chapter 2). Subsequent grafting of 6FDA and 6F*p*DA results in a gradual reduction in the quantity of nitrogen gas sorption, surface area, pore volume and average pore diameter indicating the presence/grafting of polymer groups on the porous γ-alumina, supporting the FT-IR observations. A gradual reduction in average pore diameter (in combination with the XPS results as presented in chapter 2) can suggest pore intrusion of polymer groups. In the case of VPG functionalization, a relatively high pore volume remains after the grafting step with 6F*p*DA, offering the possibility for subsequent grafting. In the case of SPG functionalization, less pore volume remains for subsequent grafting. For both approaches FT-IR analysis confirms imide bond formation between amines and anhydride groups, after thermal imidization at 300 ^{o}C.

Chapter 4 explores the effect of using a linker molecule with multiple functional groups, allowing for an increased amount of linker sites for subsequent grafting of imide precursors. In the FT-IR spectra of the obtained materials, bands at 1720 cm^{-1} suggest imide bond formation. Nitrogen sorption experiments reveal that grafting can lead to loss of the meso-porous characteristics of the initial inorganic powder. For supported thin γ-alumina layers, as the number of sequential grafting steps increases, single gas permeation of nitrogen,

methane and carbon dioxide decreases. For carbon dioxide the decrease in permeation is least pronounced due to favourable interactions of carbon dioxide with the grafted species in combination with the small kinetic diameter of carbon dioxide (*5-8*). A maximum is observed in the temperature dependence of permselectivity of carbon dioxide over other gases, at 100 ^{o}C. The maximum can be explained by length-scale confinement induced reduction in macromolecular dynamics at lower temperatures around 100 ^{o}C, and amplified polymer chain mobility at higher temperatures.

Chapter 5 presents sequential grafting of polyethylene oxides on chlorosilylated γ-alumina. Like in chapter 4, nitrogen gas sorption measurements reveal a gradual reduction in pore diameter, as sequential grafting proceeds. The presence of PEO groups is confirmed by FT-IR analysis. SEM images reveal that the pores of the γ-alumina layer are not filled upon grafting, suggesting that the barrier properties of the grafted membrane arise from the thin layer covering the γ-alumina layer. Single gas permeation of nitrogen and methane at 100 ^{o}C, decreases with increasing number of sequential grafting steps. However, for carbon dioxide the decrease in permeance is less pronounced compared to methane and nitrogen due to affinity or favourable interactions of the quadrupolar CO_2 with polar ethers in the organic material, i.e., the ethylene oxide, which allows more extensive sorption of CO_2 in the organic material, facilitating transport.

Porous γ-alumina has limited hydrothermal and alkaline stability. In **chapter 6** the feasibility of sequential grafting of a novel hydrophobic hybrid meso-porous material is explored. The hybrid material is prepared by the sol-gel technique, using BTESE as precursor, and has pores in the range of 2 - 5 nm. Initial functionalization of the material with 3APTMS is

performed via SPG as well as VPG. The hybrid silica material contains a low concentration of surface hydroxyl groups, hence, the influence of external water on grafting is investigated. In the case of functionalization via SPG, FT-IR reveals the characteristic peaks [2900 cm^{-1} of C-H alkyl groups & 1780 cm^{-1}, 1720 cm^{-1} of O=C–N–C=O imide groups] corresponding to the precursor molecules (3APTMS and 6FDA) when the process is conducted at low as well as high water concentration. In contrast, at low water concentration, functionalization via VPG does not reveal new peaks in the FT-IR spectra. However, VPG functionalization is successful at high water concentration. The necessity of the presence of water is associated with the increased rate of hydrolysis of the precursor molecules, which is a required reaction step before the desired reaction with surface hydroxyl groups can occur.

7.2 Future perspectives

7.2.1 Effects of confinement

The presented hybrid membranes can be operated at elevated temperature (100 ^{o}C), but do not exhibit excellent separation performance. The observed fluxes of carbon dioxide through the membranes are low to moderate, and the selectivity is below that of existing membranes. For industrial application of these membranes major improvements in their performance would be required. Yet, membranes obtained by “confining the oligomer segments inside a thermo-mechanically stable porous ceramic support” do reveal separation characteristics that are distinct from those observed for ‘normal’ polymers. In particular, for the hybrid membranes the selectivity of carbon dioxide over other small gases is observed to increase with temperature up to 100 ^{o}C, while for the corresponding ‘regular’ polymers the opposite trend is typical. The distinct trend for the hybrid membranes is

considered related to the reduced mobility of the short oligomer segments, due to their covalent attachment to a surface of a very rigid material. Such length-scale induced effects have been reported extensively for polymer materials (*9-12*). With increasing temperature the mobility of the constrained segments will increase, and the diffusion mobility of penetrant molecules will increase accordingly. The effect is most pronounced for carbon dioxide, as compared to nitrogen and methane, because this species has favourable interactions with the organic oligomers. For too high temperatures (150 ^{o}C) the effect of higher affinity is less pronounced, and the molecular dynamics of the oligomers become relatively fast. The combination of these effects causes selectivity to decrease. Although the data in this thesis are in favour of such a hypothesis, they are insufficient proof. Additional experiments should be performed. The changes in molecular dynamics will be revealed by a shifting glass transition temperature that may be studied by thermal methods such as differential scanning calorimetry. Also the degradation temperature of the organic material may be affected by the confinement. Choi *et al* (*13*) reported an increase in thermal stability of OAPS/Pyromellitic dianhydride nanocomposites by TGA analysis, attributed to increased thermal stability of the organic species in the presence of the inorganic species. In analogy, Huang *et al* (*14*) reported a decomposition temperature of OAPS/ polyimide of 551 ^{o}C, which is highercompared to the original decomposition temperature of the polyimide of 513 ^{o}C. Techniques that probe the molecular dynamics in a more direct fashion would include NMR and dielectric relaxation (*12, 15-17*). Also, the free volume of the oligomer can be different compared to regular polymers and could be probed, for instance, using Positron Annihilation Lifetime Spectroscopy (*18, 19*).

Gas permeation at high pressure measurements: In chapter 4 the CO_2 selective permeation of the membranes is relatively significant; it will be interesting to check the membrane performance at high pressures (10 – 50 bar) where non-confined polymeric membranes undergo swelling or plasticization.

7.2.2 Alternative materials chemistry

The work in this thesis has focused on a selected number of precursor molecules, and two inorganic host materials. The approach, however, is generic in nature and would allow other choices. Other precursor molecules could be selected, aiming at oligomers with different chemical features. Another obvious change in the procedure would be the use of a ceramic host with larger pore size. This would allow a larger amount of polymer inside the pores, at least relative to the concentration of linker molecules, and a larger molecular weight of the oligomer. In addition, the large pore size would allow the use of larger building blocks, i.e., pre-oligomerized precursors can be accommodated inside the pore space, reducing the number of required sequential grafting steps. It seems reasonable to assume the length-scale induced effects will to a large extent persist for pores found in typical macro-porous ceramics (the α-alumina supports used in this study have pores ~10^{-7} m). For thin polymer films 1-D length-scale effects are observed for layers with thickness < ~10^{-7} m; the 3-D geometry of the pores will likely amplify such effects.

In particular for larger pore sizes, increasing the concentration of functional linking groups on the pore surface is probably crucial, considering the observations of Chapter 4. The same strategy may be adopted as is used in that chapter, grafting POSS molecules. In addition to changing the amount of anchoring sites, also the nature of the sites could be altered. For

this, incorporating the nucleophile or electrophile functional groups directly within the material surface during the sol-gel process would be particularly interesting. This would help to avoid one grafting step, but would also prevent the formation of hydrolysable bonds inherent to the use of alkoxy silanes. Such an approach could be very beneficial for the hybrid hydrophobic silica material studied in chapter 6, because of the intrinsic low concentration of surface hydroxyl groups. Various studies have been reported on the synthesis of meso-porous materials with inbuilt surface functional groups (*20*). Hu *et al*. reported direct functionalization of meso-porous silica material by using TEOS and aminopropyltriethoxysilane (*21*). Athens *et al*. reported an extensive review on functionalization of ordered meso-porous materials by a co-condensation method (*22*).

7.2.3 Alternative applications

In this thesis the emphasis is on the use of the hybrid materials as selective membranes. The obtained results may, however, be beneficial outside this application field. The sequential approach could for instance aid devising controlled drug carrier systems, by controllable surface functionalization of a porous structure by VPG, and subsequent filling of these pores with a selected drug that is bound to the functionalized surface by triggerable bonds. Via SPG, the outer surface of such a porous system could be covered with grafted layers that do excessively infiltrate the pores. Such a system is in analogy with that presented by Aznar *et al* (*23*), who reported a temperature triggered controlled drug carrier system.

References

1. A. Y. Fadeev, T. J. McCarthy, Self-Assembly Is Not the Only Reaction Possible between Alkyltrichlorosilanes and Surfaces: Monomolecular and Oligomeric Covalently Attached Layers of Dichloro- and Trichloroalkylsilanes on Silicon. *Langmuir* **16**, 7268 (2000).

2. A. Sah, H. L. Castricum, A. Bliek, D. H. A. Blank, J. E. ten Elshof, Hydrophobic modification of γ-alumina membranes with organochlorosilanes. *Journal of Membrane Science* **243**, 125 (2004).

3. D. G. Kurth, T. Bein, Monomolecular layers and thin films of silane coupling agents by vapor-phase adsorption on oxidized aluminum. *The Journal of Physical Chemistry* **96**, 6707 (1992).

4. D. G. Kurth, T. Bein, Thin Films of (3-Aminopropyl)triethoxysilane on Aluminum Oxide and Gold Substrates. *Langmuir* **11**, 3061 (1995).

5. S. A. Stern, Y. MI, H. Yamamoto, Structure / permeability relationships of polyimide membranes. Applications to the seperation of gas mixtures. *journal of polymer science: Part B: Polymer physics* **27**, (1989).

6. D. M. D'Alessandro, B. Smit, J. R. Long, Carbon Dioxide Capture: Prospects for New Materials. *Angew. Chem. Int. Ed.* **49**, 6058 (2010).

7. K. Tanaka, M. Okano, H. Kita, K.-i. Okamoto, S. Nishi, Effects of trifluoromethyl side groups on gas permeability and permselectivity in polyimides. *Polymer Journal* **26**, 1186 (1994).

8. S. A. Stern, Y. Liu, W. A. Feld, Structure/permeability relationships of polyimides with branched or extended diamine moieties. *Journal of Polymer Science, Part B: Polymer Physics* **31**, 939 (1993).

9. S. Napolitano, A. Pilleri, P. Rolla, M. Wübbenhorst, Unusual deviations from bulk behavior in ultrathin films of poly(tert-butylstyrene): Can dead layers induce a reduction of Tg? *ACS Nano* **4**, 841 (2010).

10. S. Napolitano, V. Lupaşcu, M. Wübbenhorst, Temperature dependence of the deviations from bulk behavior in ultrathin polymer films. *Macromolecules* **41**, 1061 (2008).

11. M. Wübbenhorst, G. J. Klap, J. C. Jansen, H. Van Bekkum, J. Van Turnhout, Glass transition of one-dimensional molecular chains of p-nitroaniline confined in AlPO4-5 nanopores revealed by dielectric spectroscopy. *Journal of Chemical Physics* **111**, 5637 (1999).

12. M. Wübbenhorst, V. Lupascu. (2005), vol. 2005, pp. 87-90.

13. J. Choi, R. Tamaki, S. G. Kim, R. M. Laine, Organic/Inorganic Imide Nanocomposites from Aminophenylsilsesquioxanes. *Chemistry of Materials* **15**, 3365 (2003/08/01, 2003).

14. J. C. Huang *et al.*, Polyimide/POSS nanocomposites: Interfacial interaction, thermal properties and mechanical properties. *Polymer* **44**, 4491 (2003).

15. S. Napolitano, M. Wübbenhorst, Dielectric signature of a dead layer in ultrathin films of a nonpolar polymer. *Journal of Physical Chemistry B* **111**, 9197 (2007).

16. J. Schüller, R. Richert, E. W. Fischer, Dielectric relaxation of liquids at the surface of a porous glass. *Physical Review B* **52**, 15232 (1995).

17. J. Schuller, Y. B. M. nichenko, R. Richert, E. W. Fischer, Dielectric studies of the glass transitionn in porous media. *Phys. Rev. Lett.* **73**, 2224 (1994).

18. Y. H. Huang *et al.*, Investigation of fine-structure of polyamide thin-film composite membrane under swelling effect by positron annihilation lifetime spectroscopy and molecular dynamics simulation. *Journal of Membrane Science* **417-418**, 201 (2012).

19. G. Q. Chen *et al.*, The thickness dependence of Matrimid films in water vapor permeation. *Chemical Engineering Journal* **209**, 301 (2012).

20. G. G. Paradis, R. Kreiter, M. M. A. Van Tuel, A. Nijmeijer, J. F. Vente, Amino-functionalized microporous hybrid silica membranes. *Journal of Materials Chemistry* **22**, 7258 (2012).

21. Z. Hu, D. Zhang, J. Wang, Direct Synthesis of Amine-functionalized Mesoporous Silica for CO2 Adsorption. *Chinese Journal of Chemical Engineering* **19**, 386 (2011).

22. G. L. Athens, R. M. Shayib, B. F. Chmelka, Functionalization of mesostructured inorganic–organic and porous inorganic materials. *Current Opinion in Colloid & Interface Science* **14**, 281 (2009).

23. E. Aznar *et al.*, Finely Tuned Temperature-Controlled Cargo Release Using Paraffin-Capped Mesoporous Silica Nanoparticles. *Angewandte Chemie - International Edition* **50**, 11172 (2011).

Summary

In this thesis, the synthesis of inorganic – polymeric hybrid membranes by sequential grafting is discussed, for application in gas separation.

At high pressures and temperatures, organic (polymer) membranes may suffer from swelling and plasticization. Generally, this causes a reduced molecular selectivity of organic membranes. Confining the organic in a thermo-mechanically stable porous material may aid moderating plasticization and swelling. Here, it is investigated if sequential chemical grafting of precursors in the pores of a meso-porous ceramic support will allow such confinement.

Chapter 1 presents a general introduction on membrane technology, in particular focussing on hybrid organic-inorganic membranes, in which the advantages of polymeric and inorganic species may be combined.

Chapter 2 focused on chemical functionalization of meso-porous γ-alumina with 3-aminopropyltrimethoxysilane (3APTMS). In literature, solution phase grafting (SPG) has been most commonly used for functionalization of inorganic materials with functional silanes. However, functional silanes are sensitive to the presence of water, and can undergo self-condensation reactions resulting in dense structures. Particularly, in case of porous materials this may lead to blocking of pores and pore entrances. Here, vapor phase grafting (VPG) is extensively investigated as an alternative method. This method allows more controlled functionalization of the internal pore surface of a meso-porous ceramic, resulting in thin layers of the functional precursors. For VPG nitrogen physisorption reveals a reduction in the pore diameter in the range of the length of precursor (3APTMS, 0.4 nm). FTIR investigation confirms differences between thick multi-layer formation in SPG and thin monolayer formation in VPG. The results are rationalized by the fact that cross-linked precursors form oligomers that do not readily vaporize, because of their low vapor pressure. In contrast to SPG, where oligomers can reacted with the ceramic material, in VPG the ceramic is exposed to predominantly non-cross-linked precursor molecules.

Chapter 3 deals with the sequential grafting with precursors of polyimides (6FDA, F*p*DA, and BADF) over aminofunctionalized γ-alumina described in chapter 2, followed by thermal imidization at 300 ^{o}C. Nitrogen physisorption reveals incremental pore filling with the number of grafting steps. The materials retain their meso-porous characteristics. FT-IR reveals clear imide bands, confirming covalent bonding of the polyimide oligomers and the primary amines of the functionalized γ-alumina. VPG derived materials showed lower imide concentration compared to SPG derived materials, because of lower linker (3APTMS) concentration in VPG.

Chapter 4 focuses on increasing the quantity of the confined imide monomers/oligomers in the hybrid porous material, by introducing a multi-functionalized octaaminophenyl silsesquioxane (OAPS). Each OAPS molecule contains eight amine groups, seven of which remain available for reaction with 6FDA monomers. FT-IR data confirm a increased concentration of amine groups after surface functionalization. Nitrogen physisorption reveals that the proliferation of the surface functional groups allows filling of pores until the meso-porous characteristics no longer persist. For supported thin films, sequentially grafted, single gas permeance of methane, nitrogen and carbon dioxide reduces incrementally with the number of grafting steps. For carbon dioxide, the reduction is lowest, because of the favourable interactions of this gas for the fluorine groups in imide oligomer as well as relatively small kinetic diameter of the CO_2 compared to other gases. Carbon dioxide permeance shows a maximum with temperature. Up to 100 ^{o}C the confinement induced reduction in molecular dynamics impedes transport of carbon dioxide, and increasing temperature results in augmented chain mobility and a corresponding increase in carbon dioxide transport. At 150 ^{o}C, amplified chain mobility results in increase in transport of all three gases, resulting in lower selectivity.

In chapter 5 polyethylene oxide – alumina hybrid membranes are synthesized, by sequential grafting of polyethylene oxides (Jeffamine® – TEBC) (TEBC: tri (ethylene glycol) bis (chloroformate)) chlorofunctionalized γ-alumina. FT-IR investigations confirm the presence

of ethylene oxide groups. Nitrogen physisorption indicates that achieving complete pore filling with this approach is impracticable. SEM images of supported γ-alumina membranes, obtained after grafting, show open pore structures with a thin ethylene oxide layer covering the external membrane surface. This thin layer acting as a barrier for nitrogen and methane gases, while carbon dioxide can transport through it by a solution diffusion mechanism.

The hydro-thermal and pH stability of γ-alumina is limited. In **chapter 6**, surface functionalization has been investigated on recently developed hydrophobic meso-porous (bis(triethoxysilyl)ethane) derived hybrid silica. This material has a low amount of surface hydroxyl groups for chemical functionalization. The influence of external water is investigated on the effectiveness of grafting with 3APTMS, by SPG and VPG. At low water concentrations, grafting via VPG is not determined. When water is present at higher concentration, FT-IR reveals presence of amine groups. Grafting is further substantiated by peaks corresponding to fluorine and imide groups, after sequential grafting of the amino functionalized material with 6FDA.

Samenvatting

In deze scriptie wordt de synthese van anorganisch-polymeer hybride membraan door middel van stapsgewijs graften, voor toepassing in gasscheiding, beschreven.

Organische polymeren kunnen onder invloed van hoge druk of temperatuur zwellen of plasticeren. Dit leidt normaal gesproken tot een gereduceerde moleculaire selectiviteit van het organische membraan. Door het organische materiaal in te sluiten in een thermomechanisch stabiel poreus materiaal kan het plasticeren en zwellen van het materiaal beperkt worden. Dit onderzoek richt zich op de vraag of deze beperking op het polymeer kan worden bereikt door stapsgewijs graften door middel van chemische additie in de poriën van een meso-poreus keramische drager.

Hoofdstuk 1 geeft een algemene introductie in membraantechnologie, specifiek gericht op hybride organisch-anorganische membranen waarin de voordelen van polymeer en anorganische bestanddelen kunnen worden gecombineerd.

Hoofdstuk 2 richt zich op het chemisch modificeren van meso-poreus γ-alumina met 3-aminopropyltrimethoxysilaan (3APTMS). In de recente literatuur wordt stapsgewijs graften voornamelijk met functionele silanen vanuit de vloeistof fase (SPG) uitgevoerd. Echter, deze functionele silanen zijn gevoelig voor de aanwezigheid van water doordat ze een condensatiereactie met andere silaangroepen kunnen ondergaan, wat uiteindelijk leidt tot dichte structuren. Vooral als ze gebruikt worden voor poreuze materialen kan dit leiden tot het blokkeren van poriën en porieopeningen. In dit onderzoek is stapsgewijs graften vanuit de gasfase (VPG) onderzocht als alternatief hierop. Deze methode, resulterend in dunne lagen van de functionele bestanddelen, staat meer controle toe op de modificatie van de interne poriestructuur van meso-poreus keramiek. Fysische stikstof adsorptie metingen laten zien dat er een reductie van de poriediameter plaats vindt in het bereik van de grootte van de reactant (3APTMS, 0.4 nm). FTIR resultaten bevestigen de verschillen tussen de dikke multi laag vorming met SPG en dunne mono laag vorming met VPG. Deze resultaten kunnen

beargumenteerd worden met het feit dat gecondenseerde bestanddelen niet snel zullen verdampen door hun lage dampspanning. In tegenstelling tot SPG, waar oligomeren kunnen reageren met de keramische laag, wordt de keramiek bij VPG alleen blootgesteld aan voornamelijk niet gecondenseerde bestanddelen.

Hoofdstuk 3 beschrijft het stapsgewijs graften van uitgangsstoffen voor de synthese van polyimides (6FDA, FpDA en BADF) aan amine-functioneel γ-alumina beschreven in hoofdstuk 2, gevolgd door imidizatie door middel van warmtebehandeling op 300 °C. Stikstof fysisorptie metingen laten zien dat de porie met toenemende mate gevuld worden bij elke opeenvolgende reactiestap. De materialen behouden hun meso-poreus karakter na elke behandeling. FTIR laat duidelijke imide absorptiebanden zien, wat een covalente binding tussen de imide oligomeren en de primaire amines van het gefunctionaliseerde γ-alumina bevestigd. VPG materialen laten een lagere concentratie imide bindingen zien vergelen met SPG bereidde materialen, wat veroorzaakt wordt door een lagere linker (3APTMS) concentratie in VPG.

Hoofdstuk 4 is gericht op het laten toenemen van de hoeveelheid imide monomeren en oligomeren in het hybride poreuze materiaal door introductie van een octaaminophenyl functioneel silsesquioxaan (OAPS). Ieder OAPS molecuul heeft acht amine groepen beschikbaar voor reactie met 6FDA monomeer. FTIR bevestigt een toename van concentratie amine groepen na oppervlakte functionalisering met OAPS. Stikstof fysisorptie metingen laten zien dat de grote toename van oppervlakte functionele groepen het mogelijk maakt om de poriën van een mesoporeus materiaal in zijn geheel te vullen. Voor gedragen dunne films van γ-alumina neemt gas permeatie van methaan, stikstof en koolstofdioxide af met het aantal stapsgewijze reacties. Voor koolstofdioxide is de reductie in permeatie het laagste vanwege de affiniteit van dit gas voor de fluorgroepen in het imide oligomeer. Koolstofdioxide permeatie vertoont een maximum als functie van temperatuur; tot 100 °C belemmert de functionalisering van de poriën transport van koolstofdioxide door gelimiteerde moleculaire dynamica. Verdere verhoging van de temperatuur resulteert in hogere ketenmobiliteit en een corresponderende toename in koolstofdioxide transport. Dit

wordt aangetoond door de lagere selectiviteit op 150 °C voor transport van de drie bovengenoemde gassen, veroorzaakt door de toegenomen ketenmobiliteit.

In **hoofdstuk 5** worden polyethyleenoxide - alumina hybride membranen gesynthetiseerd, door stapsgewijs graften van polyethyleenoxiden (Jeffamine ® - TEBC) (TEBC: tri (ethyleenglycol) bis (chloorformiaat)) chloor gefunctionaliseerd γ-alumina. FTIR spectra bevestigen de aanwezigheid van ethyleenoxidegroepen. Stikstof fysisorptie laat zien dat compleet opvullen van mesoporiën vanuit deze aanpak niet mogelijk is. SEM beelden van gedragen γ-alumina membranen, verkregen na stapsgewijs graften, laten een open poriestructuur zien met een dunne ethyleenoxide laag op het externe membraanoppervlak. Deze dunne laag, die als barrière voor de gassen stikstof en methaan werkt, transporteert koolstofdioxide door middel van het zogenaamde oplossing-difussiemechanisme. In tegenstelling tot polymeer membranen vertoonden deze membranen toenemende selectiviteit voor koolstofdioxide bij toenemende temperatuur, gemeten bij temperaturen tot 100 °C.

De hydro-thermische en pH stabiliteit van γ-alumina beperkt. In **hoofdstuk 6** is oppervlakte functionalisering van recent ontwikkeld hydrofoob meso-poreus (bis(triethoxysilyl)ethaan) afgeleid hybride silica onderzocht. Dit materiaal heeft een relatief lage hoeveelheid oppervlakte hydroxylgroepen voor chemische functionalisering. De invloed van de aanwezigheid van water op de doeltreffendheid van graften met 3APTMS door middel van SPG en VPG wordt onderzocht. Bij lage water concentraties is het graften via VPG niet effectief. Wanneer water aanwezig is in een hogere concentratie, wordt met FTIR de aanwezigheid van aminegroepen gemeten. Dit wordt verder bevestigd door pieken die overeenkomen met fluor en imidegroepen na graften van de amino gefunctionaliseerde stof 6FDA.

Acknowledgements

Finally, time has come to express my gratitude towards the people who contributed directly or indirectly to be able reach this stage in my life.

The last five years of journey (expedition) has been very special in my life. Although it involves many ups and downs, when I look back there are many things to cherish, learned many new things (scientific as well as real life), met many wonderful people, worked with few wonderful people, made new friends, etcetera.

First and foremost my professor Arian Nijmeijer, who believed in me and provided chance to work under his supervision in inorganic membranes group. Arian, thanks a lot for keeping the faith in me from the beginning, particularly at difficult times. It was very inspiring to see your immediate replies to the emails/draft corrections from various parts of the world in spite of busy schedules. Although, you were not available every day in utwente, I never felt that I had to wait for one week to know your opinion on any issue, once again thank you for that.

The next, equally important person is Nieck, I learned many scientific things from you, starting from weekly work planning, making the best presentation slides in power point, building the story in a systematic manner during writing etc., in every stage there was something to learn from you. You always encouraged me to look for completely new directions, particularly in the second year when we were choosing the research directions which resulted in introducing vapour phase grafting and poss. Your support during the writing was immense, since I wanted to finish as soon as possible, I worked day and nights, some times that made you to spend extra hours, thank you very much for that. That resulted in finishing the writing part in three months which I didn`t expected.

In the beginning, you were the only person stood by me to believe vapour phase grafting is a promising method, later FT-IR confirmations with Barbara Mojet boosted our confidence, now we have nice publication ☺ .

Your creative suggestions in presenting the scientific data, either it making a power point presentation or writing a piece of text always amazes me. There was always something new to learn from your corrections and your suggestions are based on the level of my text/slides. That way you always made me learn new things based on the standard level of my submission, thank you for that!

Our meeting in eindhoven was very crucial to me to rebuild my confidence; my hope to finish the thesis was boosted.

You are very special, great human being, you always thinks in student perspective, I always admire you as best guide a PhD student can get, once again THANK YOU for everything !!!!!!

Henny, you are being the senior most professors in the group and highly ranked scientist in the world, you are always very friendly, helpful. You were one of the members in the interview panel when I first attended the interview at ISPT office (DSTI in 2008) in Amersfoort. I take this opportunity to thank you for that. We had monthly meetings during the early stage of my PhD, your comments, questions, doubts were very helpful to rethink and confirm. I still remember the encouraging words you said before my presentation at carre building for energy/MESA^{+} cluster. I was very happy that you were convinced with my talk, that gave me extra confidence in the later stages, Thank you !!

Louis, Your co-operation for the project, together with Ana was very important. Particularly, in the early days, because grafting was something new to the group, we had to discuss to all kinds issues (experimental, literature etc..), you always spared time for us and encouraged to do our experiments. Your suggestions, remarks, over-views were very helpful.

I take this opportunity to thank colleagues at ECN, Jaap Vente, Rob Kreiter, Marcel den Exter and technical staff for their co-operation and suggestions, particularly in synthesis of meso-BTESE at ECN.

I greatly acknowledge the colleagues at ISPT, Menno Plantenga and others for the efforts put in to organize the project meetings and all kinds of support during the four years.

I worked closely with Ana Pinheiro: thank you Ana for the long conversations about grafting experiments, discussions about literature, FT-IR spectra analysis, sharing the set-ups etc.. It was fun working with you.

In the last few months, I closely worked with Michiel (Raaijmakers). Raaijmakers, thank you very much for being very sportive, for nice scientific discussions, particularly on imidization and your efforts to characterize thin layers on wafers made by vapour phase grafting. Special thanks for helping with translating the summery in to dutch version. Emiel (Kappert) also partly helped with this, I also thank Emiel for the helping hand. Michiel-Karin, thank you for the dinner and nice time we had at your house.

I would like to thank all IM group members. Thank you Susanne for helping with all kinds of administration work, particularly during the thesis submission period and also nice conversations. Mieke, Cindy, its great to have you both in the group, you are always helpful for any problem in the labs, I am greatful for all your help. Frank (Morssinkhof) for helping with the set-ups, equipment, particularly the repair of the Gemini equipment, it was very crucial in my research. Also very nice social conversations and your helping nature, thank you for being Morssinkhof.

Tan, Marcel, Emiel, Martin, Zou, Sushumna, Cheryl, Bas, Patrick, Chug-Yul, Hammad, Wei Chen, thank you all for excellent working atmosphere in the office and co-operating each other whenever needed. Thank you Wojciech, for helping in ellipsometry measurements, unfortunately they were never convincing because of extremely thin layers.

I would like to thank my previous office colleagues, Katja, Ikenna, Enver (Guler) for nice conversations, and excellent working place. All SFI and MTG members, Can, Elif, Antoine, Zandrie, Herman, Harmen, John, Greet, Anne Corine, Kareena, Olga, Alhadidi, Beata, Jeroen for friendly atmosphere.

Time at TU/e:

I take this opportunity to thank professor Emiel Hensen for accepting to be part of the defence committee. You encouraged me to complete the thesis as soon as possible and reminded me until it gets to the final stage. Your support has been very crucial at this period at TU/e. In addition, you found the possibilities for my stay in IMC. Thank you for everything !!!!!!!.

I thank Emma Eltink for her co-operation in administration related things. I thank my colleagues in IMC@TU/e, Nikolay, Michel, Aysegul Ciftci, Christiaan, Chou-chou, Chou chin, Esther, Gerhaard, Georgy and all other for the excellent working atmosphere and jovial coffee breaks. I also take this opportunity to thank our volleyball team: Guanna Li, Yi Ma, Xuefang, Kaituo, Xioming and all for being very sportive and enjoying the game which helped me to relax.

Kishore-Hema & little Samhitha, , Koti-Sandya, Ambati-Sangeatha, Jitu-lavanya, Srivatsa, Krishna-Gayathri, Jigar-Falguni, Mayur-Shradha, Kranthi-Jyothi, Chaki-Nandana, Vijay-Ranjani, Rajnikanth and all indian community, I thank you all for being like a family and the wonder full times we spent together. Particularly, Ambati and Jitu, special thanks for you both for your encouragement and helpful nature.

I would take this opportunity to thank all my teachers and lecturers in india who encouraged me whenever I met them, particularly, Mallikarjun sir, Venkanna sir, Laxma Reddy sir, Rajashekar Reddy sir, Ashok kumar sir. My friends, Prasad Rachamalla (mom), Kishore, Manohar, Nazeem, Rajagopal, Venkat kumar, you all motivated me whenever I talk with you, just because i am the only person pursuing PhD in our batch, Thank you all for that.

Santhosh, Chandramouli uncle and aunty you are all equal to my family members, I always cherish the help and encouragement you have given me, Santhosh I am grateful to have you as my best friend.

I thank my parents (Bapu, Amma) whole heartedly, without your support, encouragement, it wouldn`t be possible for me to reach this stage. You spent all your earnings on my education. You provided me the best possible education available, though it was expensive and single drive. Your aim for “good education for children” took me this stage today. You supported my decision to pursue higher education in Europe, still encouraging me to move forward in my chosen direction. I will surely miss you on the defence day, but I understand your concern for travelling long distance and health issues. Thank you Amma, Bapu for everything !!!!!

Raju, I am greatful to have a brother like you. I believe, we understand each other very closely, thank you for being the best younger brother. I take this opportunity to thank my in-laws (Varsha parents) for the love they shower on me and the encouragement to get the PhD degree, we miss you uncle, but I am sure your blessings are with us always. Naresh, Rajesh and Karthik, i am greatful to have you as my brothers. Your help during the difficult days was great, thank you all for everything.

How can I thank my wife, she has been equally sharing the journey (the expedition). You had to do many sacrifices to get to this stage in this expedition, you don`t go for sleep until I complete my work during writing, just to keep me active. You encouraged me during the difficult times, you reminds me everything and take care of our food. Thank you for everything !!!!!, you deserve every bit of mine.